

Theoretical and experimental studies on bound magnons in one-dimensional spin 1/2 anisotropic Heisenberg ferromagnets
by Ying Liu

A thesis submitted in partial fulfillment of the requirements for the degree Of Doctor of Philosophy in Physics
Montana State University
© Copyright by Ying Liu (1995)

Abstract:
Open problems about the bound magnon, a quantum non-linear magnetic excitation, in one-dimensional spin 1/2 anisotropic Heisenberg ferromagnets are discussed and answered positively by studying theoretical models and testing them in experiments. First, thresholds of intrachain and interchain exchange couplings for bound magnon effects are theoretically predicted and experimentally confirmed. Second, bound magnon excitations and corresponding thermodynamic properties affected by the spin canting, commonly occurring in spin chain systems, are considered and solved. Further, bound magnon excitations with effects of anisotropies, arising from the exchange anisotropy and the single-ion anisotropy, are discussed. Experimental results on several good one-dimensional spin 1/2 ferromagnets ranging from the Heisenberg to the Ising limit agree with theoretical expectations and confirm that bound magnons dominate susceptibility over the entire exchange anisotropy range and for magnetic fields up to 9 tesla.

Finally, while experiments have confirmed that bound magnons dominate the susceptibility over linear spin waves, classical non-linear excitation solitons are found in the bound magnon system and decrease the susceptibility of the system. The susceptibility can be decomposed into the separate contributions from bound magnons, magnons and solitons. The relations between bound magnons and solitons are presented in certain parameter ranges of the models.

THEORETICAL AND EXPERIMENTAL STUDIES ON BOUND MAGNONS IN ONE-DIMENSIONAL SPIN 1/2 ANISOTROPIC HEISENBERG FERROMAGNETS

by

Ying Liu

A thesis submitted in partial fulfillment
of the requirements for the degree

of

Doctor of Philosophy

in

Physics

MONTANA STATE UNIVERSITY
Bozeman, Montana

July 1995

D378
L744

APPROVAL

of a thesis submitted by

Ying Liu

This thesis has been read by each member of the thesis committee and has been found to be satisfactory regarding content, English usage, format, citations, bibliographic style, and consistency, and is ready for submission to the College of Graduate Studies.

7/18/95
Date

Chairperson, Graduate Committee

Approved for the Major Department

7-18-95
Date

Head, Major Department

Approved for the College of Graduate Studies

8/27/95
Date

Graduate Dean

THEORETICAL AND EXPERIMENTAL STUDIES ON BOUND MAGNONS IN ONE-DIMENSIONAL SPIN 1/2 ANISOTROPIC HEISENBERG FERROMAGNETS

Ying Liu

Advisor: John E. Drumheller

Montana State University
1995

ABSTRACT

Open problems about the bound magnon, a quantum non-linear magnetic excitation, in one-dimensional spin 1/2 anisotropic Heisenberg ferromagnets are discussed and answered positively by studying theoretical models and testing them in experiments. First, thresholds of intrachain and interchain exchange couplings for bound magnon effects are theoretically predicted and experimentally confirmed. Second, bound magnon excitations and corresponding thermodynamic properties affected by the spin canting, commonly occurring in spin chain systems, are considered and solved. Further, bound magnon excitations with effects of anisotropies, arising from the exchange anisotropy and the single-ion anisotropy, are discussed. Experimental results on several good one-dimensional spin 1/2 ferromagnets ranging from the Heisenberg to the Ising limit agree with theoretical expectations and confirm that bound magnons dominate susceptibility over the entire exchange anisotropy range and for magnetic fields up to 9 tesla.

Finally, while experiments have confirmed that bound magnons dominate the susceptibility over linear spin waves, classical non-linear excitation solitons are found in the bound magnon system and decrease the susceptibility of the system. The susceptibility can be decomposed into the separate contributions from bound magnons, magnons and solitons. The relations between bound magnons and solitons are presented in certain parameter ranges of the models.

STATEMENT OF PERMISSION TO USE

In presenting this thesis in partial fulfillment of the requirements for a doctoral degree at Montana State University, I agree that the Library shall make it available to borrowers under rules of the Library. I further agree that copying of this thesis is allowable only for scholarly purposes, consistent with "fair use" as prescribed in the U.S. Copyright Law. Requests for extensive copying or reproduction of this thesis should be referred to University Microfilms International, 300 North Zeeb Road, Ann Arbor, Michigan 48106, to whom I have granted "the exclusive right to reproduce and distribute my dissertation in and from microfilm along with the non-exclusive right to reproduce and distribute my abstract in any format in whole or in part."

Signature Ying Li

Date 8-10-95

ACKNOWLEDGMENTS

My deepest thanks go to my advisor Jack Drumheller, for his support, guidance, advice, and also for the confidence he gives to me as woman in physics. During later years, in his busy time as a university administrator, he was always there when his student needed him. Many thanks to professors Hugo Schmidt and George Tuthill for their encouragement and patience. Many thanks to my colleague Dan Teske for his help and cooperation in the lab. Many thanks to my husband Stuart Hutton for all of his help, support, and love. Special thanks go to the Physics Department for giving Chinese students an opportunity to study at MSU and for providing an excellent atmosphere for graduate studies. Without all of these, this thesis work would never been finished.

This work was supported by NSF Grant DMR-93-10967.

TABLE OF CONTENTS

page

1. INTRODUCTION 1

2. EFFECTS OF EXCHANGE COUPLINGS ON BOUND MAGNONS 6

2.1. Formation of bound magnons 7
2.2. Thermodynamics of bound magnon effects 13
2.3. Threshold of intrachain exchange for bound magnon effects 17
2.4. Threshold of interchain exchange for bound magnon existence 20
2.5. Experiments 24

3. EFFECTS OF ANISOTROPIES ON BOUND MAGNONS 39

3.1. Introduction 39
3.2. Effect of single-ion anisotropy on bound magnons 40
3.3. Effect of exchange anisotropy on bound magnons 55
3.4. Experiments 64

4. EFFECT OF SPIN CANTING ON BOUND MAGNONS 66

3.1. Introduction to spin canting 66
3.2. Spin canting effect on bound magnon excitation energies 68
3.3. Spin canting effect on thermodynamics 72
3.4. Threshold of spin canting effect on bound magnons 81
3.5. Comparison with spin canting effect on XY model 82
3.6. Experiment 84

5. COMPARISON OF BOUND MAGNONS AND SOLITONS 90

5.1. Soliton and bound magnon models 91
5.2. Relations between bound magnons and solitons 94
5.3. Thermodynamics of solitons and bound magnons 102
5.4. Experiment 104

6. CONCLUSIONS 112

REFERENCES 115

LIST OF TABLES

Table page

1. Spin 1/2 anisotropic Heisenberg ferromagnetic systems and their properties.....26

2. A summary of experimental results for thresholds of exchanges J and J'.....31

LIST OF FIGURES

Figure page

1. Simple pictures of a bound magnon, a spin wave and a soliton..... 11

2. Susceptibilities contributed from bound magnons and spin waves..... 16

3. Competition between bound magnons and spin waves..... 19

4. A threshold of J..... 21

5. A threshold of J'..... 23

6. Susceptibility of TMSO..... 32

7. Susceptibility of TMCuC..... 33

8. Susceptibility of TTMCuC..... 34

9. Susceptibility of TRIMER..... 35

10. Susceptibility of CHAB..... 36

11. Susceptibility of CuTAC..... 37

12. Susceptibility of DMSO..... 38

13. Single-ion anisotropy effect on BM energy..... 44

14. Two-magnon spectra with an easy-axis single-ion anisotropy..... 48

15. Two-magnon spectra with large single-ion anisotropy..... 50

16. Two-magnon spectra with an easy-plane single-ion anisotropy..... 53

17. Two-magnon spectra involving quartic exchange interaction..... 53

18. Exchange anisotropy effect on bound magnon energy..... 56

LIST OF FIGURES - Continued

Figure page

19. $\chi(T)$ as a function of exchange anisotropy....60

20. $C_h(T)$ as a function of exchange anisotropy....61

21. Bound magnon & spin wave dominance on susceptibility in H-γ space....62

22. Bound magnon & spin wave dominance on specific heat in H-γ space....63

23. Spin canting effect on bound magnon energy....73

24. Spin canting effect on susceptibility....79

25. Spin canting effect on specific heat....80

26. Spin canting effect on thermodynamics of 1D spin 1/2 XY-model....85

27. Susceptibility of CHAC with consideration of spin canting....89

28. Susceptibilities contributed from bound magnons , magnons and solitons....105

29. Susceptibility of CHAB with soliton contribution....108

30. Magnetization of CHAB....111

ABSTRACT

Open problems about the bound magnon, a quantum non-linear magnetic excitation, in one-dimensional spin 1/2 anisotropic Heisenberg ferromagnets are discussed and answered positively by studying theoretical models and testing them in experiments. First, thresholds of intrachain and interchain exchange couplings for bound magnon effects are theoretically predicted and experimentally confirmed. Second, bound magnon excitations and corresponding thermodynamic properties affected by the spin canting, commonly occurring in spin chain systems, are considered and solved. Further, bound magnon excitations with effects of anisotropies, arising from the exchange anisotropy and the single-ion anisotropy, are discussed. Experimental results on several good one-dimensional spin 1/2 ferromagnets ranging from the Heisenberg to the Ising limit agree with theoretical expectations and confirm that bound magnons dominate susceptibility over the entire exchange anisotropy range and for magnetic fields up to 9 tesla.

Finally, while experiments have confirmed that bound magnons dominate the susceptibility over linear spin waves, classical non-linear excitation solitons are found in the bound magnon system and decrease the susceptibility of the system. The susceptibility can be decomposed into the separate contributions from bound magnons, magnons and solitons. The relations between bound magnons and solitons are presented in certain parameter ranges of the models.

CHAPTER 1

INTRODUCTION

Interest in one-dimensional (1D) magnetic systems was for a long time focused on the possibility that their study would provide a better understanding of the theory of three-dimensional (3D) phase transitions and critical phenomena, while ignoring the physics peculiar to such systems. The situation has changed in recent years because a number of quasi-1D magnetic substances have been identified experimentally. The discovery of quasi-1D magnetic materials has given study of 1D magnetic systems direct physical significance so that 1D systems are no longer simply test systems for 3D theories, but are interesting in their own right.

In three dimensions all magnetic systems have an ordered phase at sufficiently low temperature. The critical region is always small, typically 0.9 to $1.1T_c$, where T_c is the phase transition temperature. However, this situation changes dramatically when reducing the dimensionality of the system to two. When the magnetic moments are coupled only in planes, the existence of a phase transition depends on the anisotropy of the system: in a Ising system there is a phase transition but in a Heisenberg system there is no phase transition for $T > 0$ since the magnetic entropy is removed smoothly as temperature is reduced to zero and a short range order is built up. Going down one step more in dimensionality to 1D, the system with magnetic moments coupled along chains has no

phase transition at all for T > 0. A 1D system removes its entropy by developing strong short range order when the temperature is reduced. It is therefore possible to study critical properties over a *wide temperature range* in such systems. The physics of 1D systems is clearly interesting for its own sake. The thermodynamics of 1D systems especially should show properties which do not exist in higher dimensions.

An example of 1D effects is observed in a type of non-linear magnetic excitations called bound magnons (BMs), which are responsible for a dramatic effect upon thermodynamic properties when the dimensionality is reduced to 1D. Experimental and theoretical studies have shown that the BMs play an important role in determining the low temperature thermodynamic properties of 1D ferromagnetic systems. The existence of bound magnons casts serious doubt on the validity of linear spin wave theory in 1D, which has been very successfully applied in higher dimensional systems.

Bethe[1] was the first to show that there exist excitations in the 1D ferromagnetic systems in addition to the elementary spin waves (magnons), in which a complex of two or more spin deviations travel together through the chain with energies split from the spin wave continuum. He called these excitations bound states of magnons, or bound magnons. The problem of the low-lying excitations of BMs in an isotropic Heisenberg chain with spin 1/2 was first formulated and analyzed by Bethe[1]. In a number of subsequent papers[2,3,4], Bethe's results were generalized to the case of an anisotropic Heisenberg ferromagnetic (AHF) chain. Lately, the energy spectrum of low-lying excitations of BMs was examined by a numerical

analytical technique by Reklis[5]. Finally, the complete energy spectrum of bound magnons of the AHF chains was obtained[6,7].

There are many theoretical methods that have been used to solve the BM problem. For example, the Bethe ansatz, the Wortis method, Green's function techniques, perturbation theory, numerical and approximate analytical methods, computer simulations, and low-T or high-T series expansions.

The developing stage of the BM study was to obtain the thermodynamic properties of the BM systems. Gaudin[8] obtained the free energy expression of the AHF system. Johnson and Bonner[9] performed low-temperature expansions of Gaudin's formalism[8] and derived analytical magnetic susceptibility and specific heat expressions in terms of bound magnon and spin wave contributions. They predicted that BMs have a dramatic influence on low temperature thermodynamics. For isotropic Heisenberg chains, Takahashi and Yamada[10] obtained expressions for free energy and susceptibility at low temperature and zero field by numerically solving the thermodynamic Bethe-ansatz integral equations. Schlottmann[11] obtained susceptibility expressions for both zero and finite field.

Progress was also made in the experimental investigation of the BM effect. Low excitations of BMs have been observed[12] by the methods of neutron and photon scattering. Observation of BM effects on thermodynamic properties was first initiated in the Drumheller lab, at Montana State University. The ac susceptibility[13] of the spin 1/2 1D Heisenberg ferromagnetic compound $(C_6H_{11}NH_3)CuCl_3$ (CHAC), where the intrachain exchange J is strong and the interchain J' is quite weak, was measured in the temperature

range 4.2K - 40K. The results[13] confirmed the existence of BMs in this system, and for the first time by experiment, proved that the susceptibility is dominated by the BM contribution and linear spin wave theory fails completely in this system. The results for $(CH_3)_4 NCuCl_3$ (TMCuC) which has a intermediate J value and very weak J', and for the Ising compound $[(CH_3)_3NH]FeCl_3.2H_2O$ (FeTAC) were similarly showing a clear dominance of BMs.[14,15,16]

Despite this flurry of activity, solutions of BM problems still remain incomplete for perhaps the best known model, the 1D spin 1/2 anisotropic Heisenberg model first studied in the 1930's[1]. For example, the thresholds for the existence of BMs and BM effects on thermodynamics are not solved. By including effects from the single-ion anisotropy, spin canting, etc., the behavior of the thermodynamic properties and the spectral excitations of the corresponding models are not completely known. Specifically, only partial information exists for the relation between bound magnons and magnetic solitons.

The aim of this thesis is to examine these BM problems that are still open by discussing in detail the theoretical and experimental results in the following model for 1D spin 1/2 anisotropic Heisenberg ferromagnets:

$$H = -J\sum_{i}^{N}[S_i^z S_{i+1}^z + \gamma(S_i^x S_{i+1}^x + S_i^y S_{i+1}^y)] - J'\sum_{\langle i,j\rangle}^{N} S_i S_j$$
$$+A\sum_{i}^{N}(S_i^x S_{i+1}^y - S_i^y S_{i+1}^x) - D\sum_{i}^{N}(S_i^z)^2 - g\mu_B h\sum_{i}^{N} S_i^z \qquad (1.1)$$

In this model, the first term is the exchange interaction and the exchange anisotropy along the chain; the second term is the interchain exchange coupling; the third term is the

antisymmetric part of the anisotropic exchange interaction and represents the spin canting along the chain; the fourth term is the single-ion (on-site) anisotropy; and the last term is the interaction with the applied magnetic field. The excitation energies of BMs and their effects on thermodynamic properties will be studied term by term in each chapter of this thesis. In Chapter 2 the effects of both intra- and inter-chain exchange interactions on BMs will be examined. In Chapter 3 effects of anisotropies including the exchange anisotropy and the single-ion anisotropy on BMs will be considered. In Chapter 4 the effects of the spin canting on BMs will be discussed. In Chapter 5 the relations between BMs and 1D solitons will be investigated. Finally, some conclusions are drawn in Chapter 6 and possible investigations for the future are indicated.

CHAPTER 2

EFFECT OF EXCHANGE INTERACTIONS ON BOUND MAGNONS

The 1D ferromagnet is composed of chains of localized spins. The i-th site of the chain is permanently occupied by a spin $\mathbf{S}_i$ experiencing both exchange coupling with neighbor magnetic ions and the local crystalline field. The crystal field does not act directly on the spin angular momentum, but indirectly interacts with the spin via the L-S coupling and causes single-ion anisotropy in the system. In this chapter only exchange coupling is considered. Crystal field effect will be discussed in the next chapter.

As far as exchange interactions are concerned, the ratio of the interaction between next nearest and nearest neighbors may be considered as arbitrarily small since the exchange interaction depends critically on the separation r of the spins by r^{-10} or even more rapidly. Therefore, the properties of the system are not essentially different from the nearest-neighbor model. The 1D anisotropic Heisenberg ferromagnet is described by the spin Hamiltonian of Eq.(1.1) without the terms for A and D:

$$H = -J\sum_{i}^{N}[S_i^z S_{i+1}^z + \gamma(S_i^x S_{i+1}^x + S_i^y S_{i+1}^y)] - J'\sum_{\langle i,j\rangle}^{N} \mathbf{S}_i \mathbf{S}_j - g\mu_B h\sum_{i}^{N} S_i^z , \qquad (2.1)$$

where J is the intrachain exchange, J' is the interchain exchange and γ represents the exchange anisotropy. The elementary excitations of this system are spin waves (magnons). The weakly excited states are usually described in the approximation of non-interacting

magnons. It is, however, clear that interaction among magnons exists and can lead to a substantial reconstruction of the elementary excitation spectrum, and in particular to the formation of BMs.

The exchange mechanisms must play an important role for the existence of BMs and their effects on thermodynamic properties, since the excitation energy of the adjacent spin deviations is lower by J than that of the non-adjacent ones, giving rise to an effective attractive interaction between magnons which lead to the formation of BMs. Whether a threshold of intrachain J exists above which J becomes a determining factor for BM effects should be understood. Also, the interchain exchange interaction J' has a dramatic effect on excitations of BMs and the threshold of J' for the existence of BMs must be determined. In this chapter, the effects of J and J' upon BM formation and their dominance in the thermodynamic properties will be discussed.

1. Formation of Bound Magnons

A. Interactions Between Magnons

The interactions between magnons which result in the formation of BMs is easier to see in the boson representation, instead of the coordinate representation. Therefore, the Hamiltonian (2.1) (with $J' = 0$) is transformed into the boson representation as shown below.

One of the boson representations, the Dyson-Maleev representation, is defined by

$$S_i^z = -S + a_i^+ a_i,$$
$$S_i^+ = S_i^x + iS_i^y = (2S)^{1/2} a_i^+ \left(1 - \frac{a_i^+ a_i}{2S}\right), \qquad (2.1.1)$$
$$S_i^- = S_i^x - iS_i^y = (2S)^{1/2} a_i,$$

and

$$[a_i, a_j^+] = \delta_{ij}, [a_i, a_j] = [a_i^+, a_j^+] = 0. \qquad (2.1.2)$$

where S = 1/2, 1, ..., **a** and $\mathbf{a}^+$ are boson destruction and creation operators respectively.

Using the Fourier transformation

$$a_l = \frac{1}{\sqrt{N}} \sum_k e^{-ikl} a_k \ , \qquad (2.1.3)$$

the Hamiltonian (2.1) in the boson representation is

$$H = E_0 + \sum_k \varepsilon_k a_k^+ a_k + \frac{1}{N} \sum_{k_1 k_2 q} v(k_1, k_2, q) a_{q/2+k_1}^+ a_{q/2-k_1}^+ a_{q/2+k_2} a_{q/2-k_2} \ . \qquad (2.1.4)$$

The first term E_0 is the ground state energy. The second term represents non-interacting magnons where ε_k is the simple spin wave (magnon) energy, and $a_k^+ a_k$ is the number operator for the magnons. The third term describes the interaction between magnons and contains two creation and two destruction magnons. The k_1 and k_2 represent, respectively, the incoming and outgoing wave vectors of an interacting spin wave pair, and q is the total wave vector of the pair. $v(k_1 , k_2, q)$ is the magnon interaction. It is this magnon interaction that results in the formation of BMs.

The ground state energy is

$$E_0 = -\gamma JNS^2 - hNS. \qquad (2.1.5)$$

The one-magnon energy is given by

$$\varepsilon_k = h + 2JS\,(1 - \gamma \cos k). \tag{2.1.6}$$

The magnon interactions is

$$v(k_1, k_2, q) = -J \cos k_2 (\cos k_1 - \gamma \cos q/2). \tag{2.1.7}$$

It can be seen that $v(k_1, k_2, q) \neq 0$ for the entire range of J. Thus, there is no threshold of J for the magnon interactions.

B. BM Excitations and Their Energies

The physical picture of BM is easier to see in the coordinate representation, since in the coordinate representation the excitation states of the system are classified in terms of magnons and BMs resulting from the magnon interaction.

A characteristic of the Hamiltonian given by Eq.(2.1) is that it commutes with the z component of the total spin which is $S_{tot}^z = \sum_i^n S_i^z - S_0^z$. The eigenvalues of S_{tot}^z, n = 0, 1, 2, 3, ... denote the number of spin deviations and S_0^z corresponds to the ground state $S_0^z = -SN$. Stationary states can be classified according to the value n. The n = 0 state corresponds to the ground state, and the n = 1 state is diagonalized by simple magnons. The n = 2 state is the first to exhibit the effect of interaction between magnons and the existence of BMs. It is necessary to take into account the magnon interaction to determine the energy of the states with $n \geq 2$.

For $n \geq 2$, two or more units of spin deviations (flipped spins for spin 1/2 case) can be distributed either on non-adjacent sites of chain or on adjacent sites. If spin deviations are on non-adjacent sites, interactions between them are very weak because of the short range interaction of J. Thus, for non-neighboring flipped spins, such excitations are linear spin waves and they do not interact with each other. The total energy of these spin waves states is the superposition of single spin wave energies. However, if spin deviations are on adjacent sites, interaction between spin deviations can not be ignored. The excitation energy of adjacent spin deviations is lower than that of non-adjacent one, and the lowered energy results from the (attractive) interactions between spin waves. Thus, for a complex of neighboring spin deviations (or flipped spins), the excited states are bound states of spin wave, the so-called bound magnons, in which n-neighboring spin deviations (or flipped spins) bond together and propagate though the 1D chain. The BMs are results of non-linear interactions of spin waves.

Therefore, the $n \geq 2$ spectrum is consist of magnons and BMs. A simple picture of a magnon and a BM excitation is shown in Fig.1.

The energy of an $n = 2$ BM was first derived by Bethe[1], Wortis[2], and Hanus[3] for the isotropic Heisenberg ferromagnet and by Orbach[4] for the anisotropic Heisenberg ferromagnet (AHF), and later was examined by a numerical analytical technique by Reklis[5]. In the AHF, the n-th BM energy has been derived by different methods[6,7]. The results of BM energies for spin 1/2 anisotropic Heisenberg ferromagnets are summarized below.

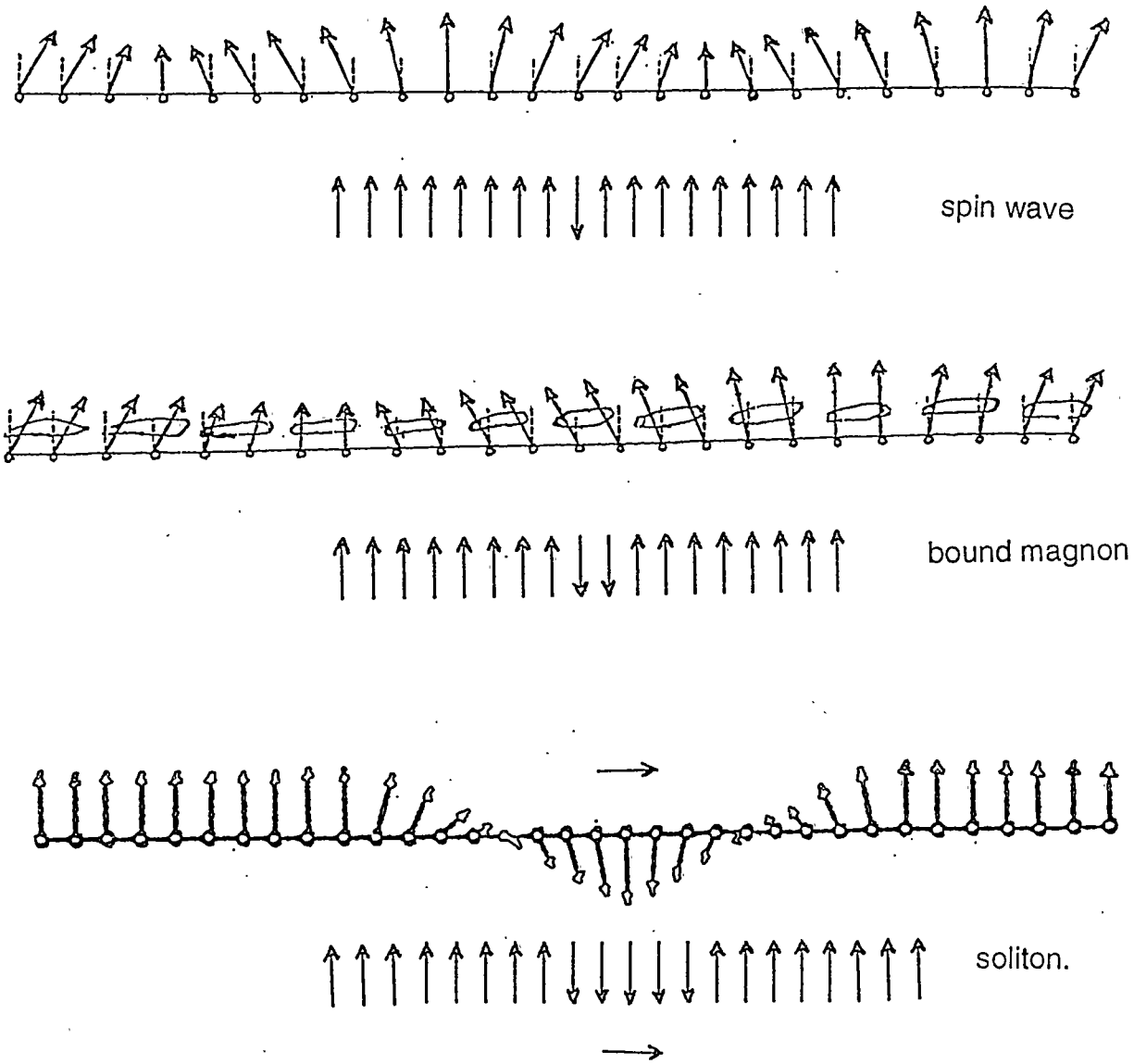


FIG. 1. Simple pictures of a bound magnon, a spin wave and a soliton.

The energies of BMs as function of J, γ and wave vector K of a BM are given by following expressions[6,7]

$$\gamma < 1: \; E_n = nh + \gamma J \frac{\sinh\Phi}{\sinh(n\Phi)}[\cosh(n\Phi) - \cos K] \qquad 1/\gamma = \cosh\Phi, \tag{2.1.8}$$

$$\gamma > 1: \; E_n = nh + \gamma J \frac{\sin\Phi}{\sin(n\Phi)}[\cos(n\Phi) - \cos K] \qquad 1/\gamma = \cos\Phi, \tag{2.1.9}$$

$$\gamma = 1: \; E_n = nh + \frac{J}{n}(1 - \cos K). \tag{2.1.10}$$

It is useful to compare BM energies to those of the non-interacting magnons. One examines the states of a system containing a *n-bound magnon* with total momentum K_1 and a complex of *p-magnons* with total momentum $K-K_1$. The system energy is then given by the sum (for $\gamma < 1$)

$$E_{tot} = E_n(K_1) + E_p(K-K_1)$$

$$= nh + \gamma J \frac{\sinh\Phi}{\sinh(n\Phi)}[\cosh(n\Phi) - \cos K] + \sum_{i=1}^{p}[h + \gamma J(\cosh\Phi - \cos k_i)] \tag{2.1.11}$$

with $k_1 + k_2 + \ldots + k_p = K - K_1$.

It can be shown that the minimum of E_{tot} is larger than the energy of a *(n+p)-bound magnon* with the same momentum K. Thus the energy of BM lies below the energies of the spin wave states, (the BM and SW energies become equal only at the point $\gamma = 1$, $K = 0$).

A result is well known for the n = 2 excitations. The bottom of the two-magnon continuum is given by

$$E_{2\text{-sw}}^{bot} = 2h + 2J[1 - \gamma \cos(K/2)]. \quad (2.1.12)$$

The n = 2 BM, 2-BM, lies lower than this by a binding energy

$$\Delta E = E_{2\text{-sw}}^{bot} - E_{2\text{-BM}} = 2J[1 - \gamma \cos(K/2)] - J[1 - \gamma^2 \cos^2(K/2)]. \quad (2.1.13)$$

This shows that there is a gap in the energy spectrum between the BM and SW continua. For $\gamma \neq 1$, the binding energy ΔE ranges from $J(1-\gamma)^2$ for K = 0 to J for $K = \pi$. For $\gamma = 1$, ΔE ranges from $J/4(K/2)^4$ for $K \ll 1$ to J for $K = \pi$. This means that 2-BM exist for arbitrary J, γ and K values. For higher-n excitations of BMs, it can be seen that BMs exist for arbitrary J and K and for most of the range of γ. Thus, there is no parameter space where the associated nonlinearities can be neglected.

2. Thermodynamics of Bound Magnon Effects

The low-temperature behavior is not determined just by the lowest-lying states but may be governed by all the energy levels, especially when the degeneracy of levels varies as high powers of n. This important point of statistical mechanics is ignored in spin-wave theory, which bases an account of the finite temperature properties of a system on the lowest-lying excitations (spin waves). Therefore, the two principal contributions to the low-T thermodynamics in the 1D Heisenberg ferromagnetic system are from the spin waves excitations and the bound magnons excitations.

To obtain the magnetization per spin M, the susceptibility χ and the specific heat C_h at a magnetic field, one uses the thermodynamic relations:

$$M = -\frac{\partial F}{\partial h} \tag{2.2.1}$$

$$\chi = \frac{\partial M}{\partial h} = -\frac{\partial^2 F}{\partial h^2} \tag{2.2.2}$$

$$C_h = -\frac{\partial^2 F}{\partial t^2} \tag{2.2.3}$$

where the free energy per spin is:

$$F = -kt \lim_{N\to\infty}\left\{\frac{1}{N}\ln Tr\exp(-H/kt)\right\}$$

$$= \int_{-\pi}^{\pi} \ln \sum_{n} \exp(-E_n(K)/kt)dK \tag{2.2.4}$$

In the derivation of F, χ and C_h, the mathematical complexity involved makes evaluating the integral impractical. Not only the energy levels but also the degeneracy of those energy levels are important to determine F, χ and C_h. Gaudin[8] has obtained a solution for the free energy per site in terms of the solutions of an infinite set of coupled nonlinear integral equations. Johnson and Bonner[9] (JB) have extended Gaudin's formalism to develop an analytic method for the low temperature thermodynamics of the Hamiltonian (2.1) with J'= 0. They found that BMs dominate thermodynamic properties over linear spin waves in certain parameter ranges.

The results of low-T thermodynamic properties from the JB analytic approach method is[9]

$$F(T) - Mh = -[h_0^2/4 + T^2 \exp(-\sqrt{1/\gamma^2 - 1}/T)]^{1/2}$$
$$-(T^{3/2}/\sqrt{2\pi})\exp(-(1/\gamma + h_0 - 1)) + \cdots \tag{2.2.5}$$

$$M = h_0 / [h_0^2/4 + T^2 \exp(-\sqrt{1/\gamma^2 - 1}/T)]^{1/2}/4 - T\exp(-(1/\gamma - 1)/T)[\exp(-h_0/T) - 1]/\sqrt{2\pi T} \quad (2.2.6)$$

$$\chi = T^2 \exp(-\sqrt{1/\gamma^2 - 1}/T)/4[h_0^2/4 + T^2 \exp(-\sqrt{1/\gamma^2 - 1}/T)]^{3/2} + \exp(-(1/\gamma + h_0 - 1))/\sqrt{2\pi T} \quad (2.2.7)$$

$$C_h = (1/\gamma^2 - 1)\exp(-\sqrt{1/\gamma^2 - 1}/T)/4T[h_0^2/4 + T^2 \exp(-\sqrt{1/\gamma^2 - 1}/T)]^{3/2} \times [h_0^2/2 + T^2 \exp(-\sqrt{1/\gamma^2 - 1}/T)] + (1/\gamma + h_0 - 1)^2 \exp(-(1/\gamma + h_0 - 1))/\sqrt{2\pi T^3}$$

where $h_0 = h/2\gamma J$, $T = t/2\gamma J$. (2.2.8)

The first term of M, χ and C_h is the contribution from bound magnons, and the second term is from spin waves. Fig. 2. shows BM and SW contributions to susceptibility from Eq.(2.2.7) in a certain parameter range. It can be seen that the BM contribution dominates the susceptibility and the validity of the linear SW theory is in considerable doubt.

The following simplified approach illustrates some of the physics of these results.

The n = 1 excitations are spin waves and the energies are $E_1(k)/\gamma J = h_0 + 1/\gamma - \cos k$. There are N such states with $k = 2\pi m/N$. By summing up these N states, n = 1 excitations provide a contribution to free energy F(T) of [9]

$$F(T) = -\frac{T}{2\pi}\int_0^{2\pi} dk \exp[-(h_0 + 1/\gamma - \cos k)/T] \; . \quad (2.2.9)$$

The next step is to sum out the high-n excitations which are BM excitations. The energy $E_n(K)$ of BM excitations are given by Eq.(2.1.8). Note that $E_n(K)$ saturates to a constant for large n, i.e., $E_n(K)/\gamma J \sim \sinh\Phi$. For large anisotropies (e.g., $\gamma = 0.13$), the energy

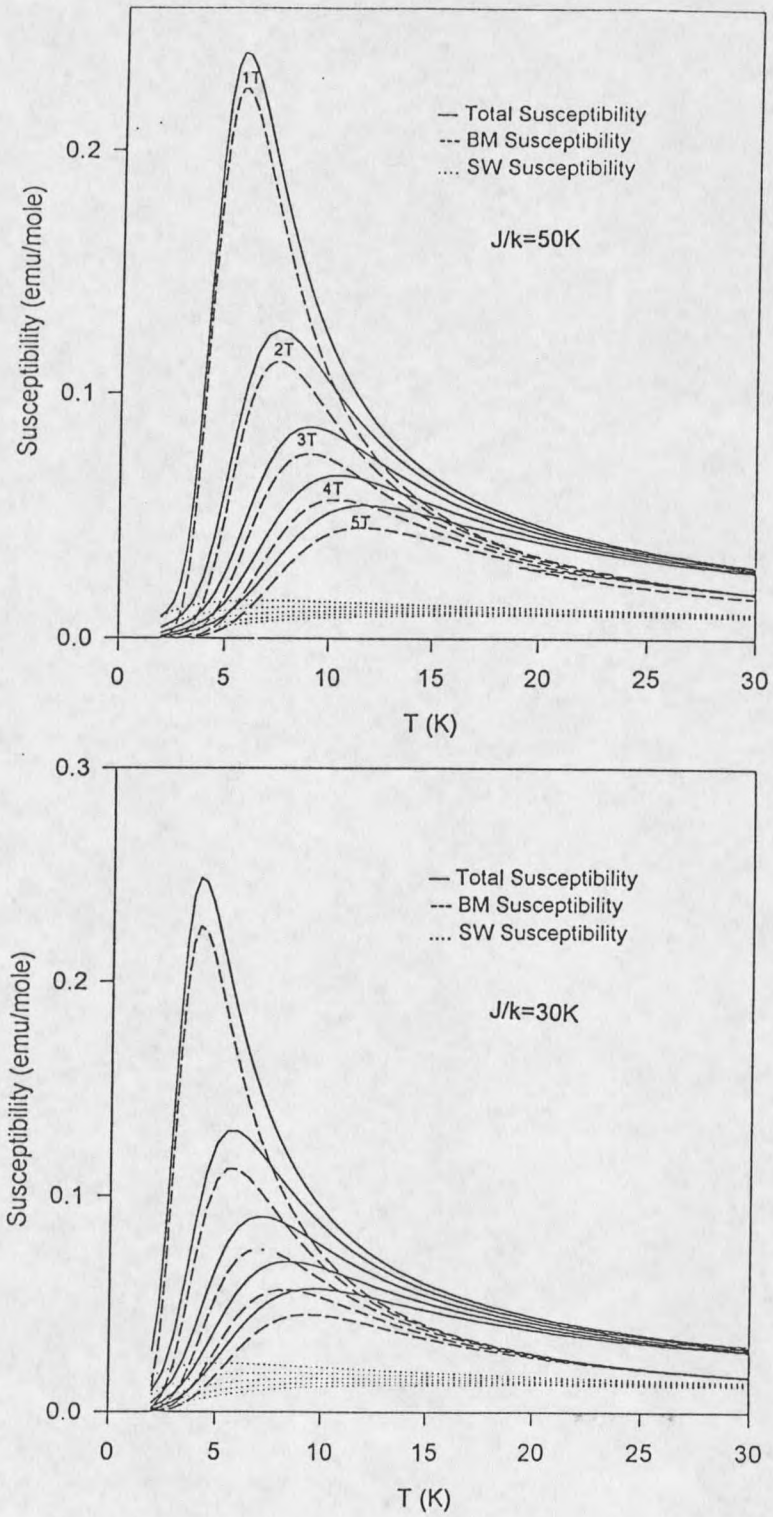


FIG. 2. Contributions to susceptibility from bound magnons and spin waves.

becomes almost constant for small n ($n \approx 3$). For small anisotropies (e.g., $\gamma = 0.8$), the constant value and K independence are reached for about $n \approx 7$.

Therefore, the high-n excitation energies are just those of a 1D Ising model whose exchange constant equals **sinhΦ** (normalized). The free energy for high-n excitations is[9]

$$F(T) = -T\ln\{\cosh(h_0/2T) + [\cosh^2(h_0/2T) - 2\exp[-\sinh\Phi/2T]\sinh(\sinh\Phi/2T)]^{1/2}\}. \quad (2.2.10)$$

The total free energy is

$$F(T) = -\frac{T}{2\pi}\int_0^{2\pi} dk \exp[-(h_0 + 1/\gamma - \cos k)/T] - T\ln\{\cosh(h_0/2T) + [\cosh^2(h_0/2T) - 2\exp[-\sinh\Phi/2T]\sinh(\sinh\Phi/2T)]^{1/2}\}. \quad (2.2.11)$$

Expanding Eq.(2.2.11) for low T, one obtains expressions for susceptibility and specific heat which are the same as Eq.(2.2.7) and Eq.(2.2.8). Thus, the low-T thermodynamic properties are from the n = 1 spin wave excitations and higher-n BM excitations.

The JB results shown above are good for $\gamma < 1$. The Heisenberg limit $\gamma = 1$ is an especially difficult problem. The finite-chain excitation spectrum shows clearly the low-lying BM states and also higher excitations which are not in the SW class. Thermodynamics of 1D isotropic Heisenberg ferromagnets have been derived [10,11].

3. Threshold of Intrachain Exchange for BM Effects

Although BM excitations exist over the entire range of J, whether there is a threshold of J for BM dominating thermodynamics remains unanswered. The next step is to determine at what level the exchange interaction becomes a determining factor for BMs to dominate the thermodynamics.

According to JB theory, the competition between BMs and SWs to contribute susceptibility in different ranges of J is calculated from Eq.(2.2.7) and shown in Fig.3. We found that the susceptibility is dominated by BMs in the range of J/k > 10K, and by SWs below 10K, i.e., the threshold of J/k for BM effects is about 10K. Also from Eq.(2.2.7), it can be seen that BMs dominate the susceptibility in the range[9]

$$\alpha < \alpha_0, \tag{2.3.1}$$

where $\alpha = (kT/2\gamma J)\ln(g\mu_b h/2\gamma J)$ and $\alpha_0 = [1/\gamma - 1 - (1/\gamma^2 - 1)^{1/2}]/3$.

When

$$(kT/2\gamma J)\ln(g\mu_b h/2\gamma J) < [1/\gamma - 1 - (1/\gamma^2 - 1)^{1/2}]/3\ , \tag{2.3.2}$$

or

$$h < (2\gamma J/g u_b)\exp(2\gamma J\alpha_0/kT)\ , \tag{2.3.3}$$

the first term (BM term) of expression(2.2.7) dominates the second term (SW term).

Eq. (2.3.3) shows that for fixed values of **h** and γ there exist ranges of J for the dominance of BMs on the susceptibility, except at zero field BMs dominate the susceptibility for the entire range of J values. As field **h** increases, the threshold of J arises. Thresholds of J can be solved by plotting two equations, $y_1 = J$, $y_2 = (gu_b h/2\gamma)/\exp(2\gamma J\alpha_0/kT)$, and when $y_1 > y_2$ BM

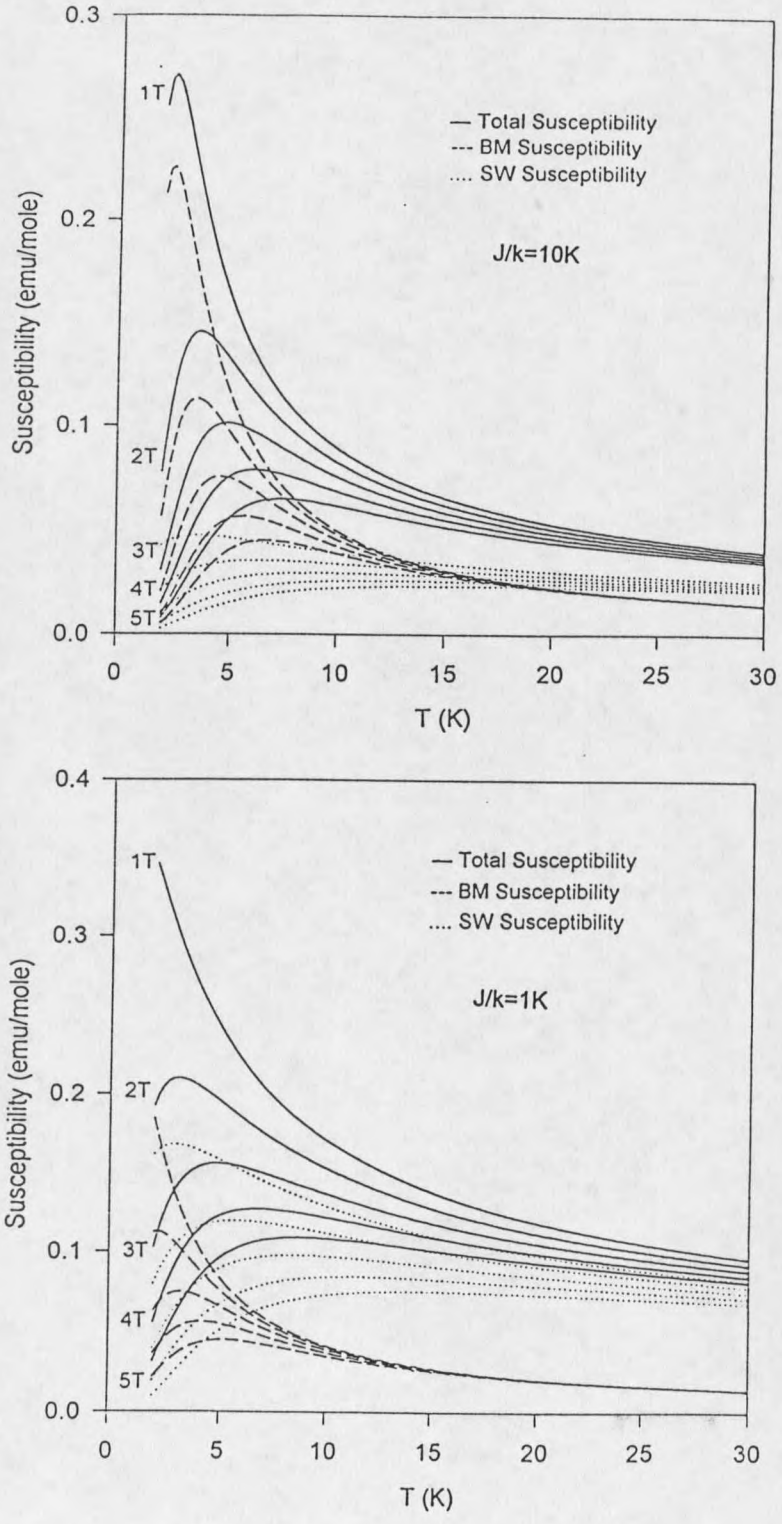


FIG. 3. Competition between bound magnons and spin waves.

dominate susceptibility. The results with parameter h =5T and T =10K is shown in Fig.4. and we found again that the threshold of J is below 10K. In Section 5 an experimental test for the threshold of J will be presented.

4. Threshold of Interchain Exchange for BM Existence

In general, the BM effect is a 1D effect, since in 1D ferromagnets BMs exist for any wave vector K. They exist only for small nonzero K in two-dimensional ferromagnets and for sufficient large K in three-dimensional ferromagnets. This is quite important because the absence of BMs over a considerable range of K allows some confidence in the validity of linear spin wave theory in higher dimensional ferromagnets. Therefore, any deviation from 1D will reduce BM effects, or eventually stop BM existence.

In the experimental 1D systems the only possible deviation from ideality that can have the effect of establishing a long range 3D ordering is the presence of a weak but finite interchain coupling J'. It is seen that at high temperature there is no appreciable difference from the isolated chain, but as the temperature is lowered the weak interchain coupling begins to take effect and finally causes a transition to long range three-dimensional order.

Although the ratio J'/J usually is very small in quasi-1D systems, the presence of a weak J' may nevertheless fundamentally alter the behavior of the system. The work of Goncharuk, et al.[17] has shown that a weak interaction can cause a considerable shift of the BM existence threshold.

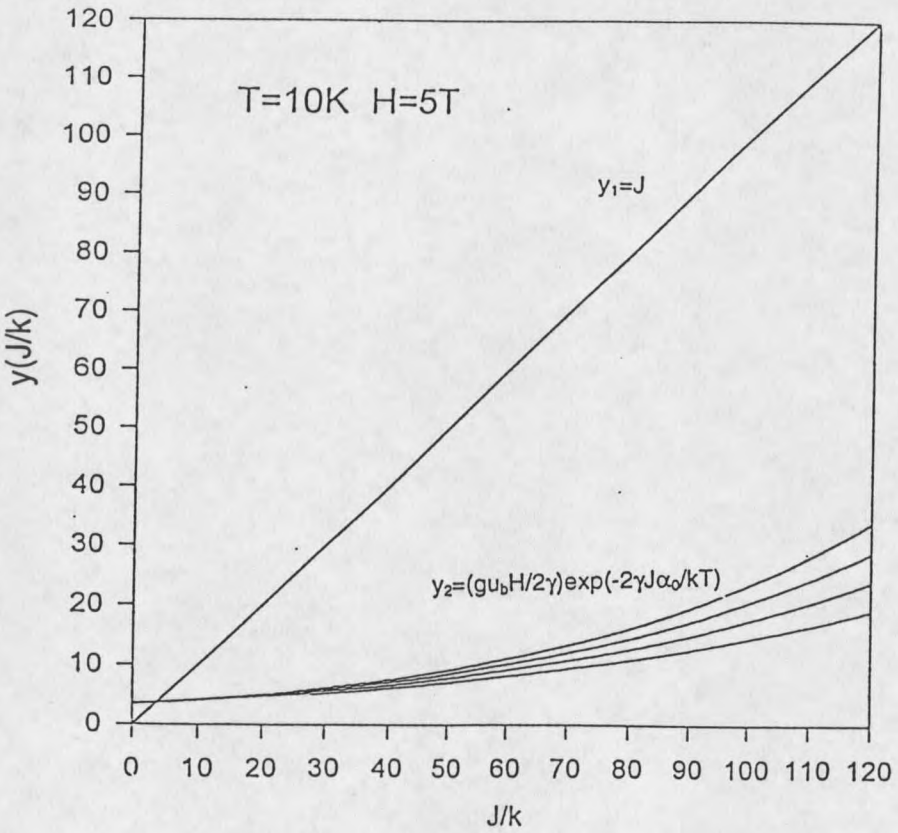


FIG. 4. Threshold of J for bound magnons dominance on susceptibility. When $y_1 > y_2$, bound magnons dominate susceptibility.

Goncharuk et al.[17] consider first an isotropic Heisenberg ferromagnet with a 3D rectangular lattice, $a_x = a_y \neq a_z$, and exchange interaction in one plane parallel to the xy plane. $J_x = J_y = J_{\parallel}$ and $J_z = J_{\perp}$. When $J_{\perp} >> J_{\parallel}$, one has a quasi -1D ferromagnet; $J_{\perp} << J_{\parallel}$ corresponds to a quasi-2D one; and $J_{\perp} = J_{\parallel}$ corresponds to a 3D one. To simplify, by considering only low-lying BM excitations, the BM existence condition is found from[2]

$$| \delta_{ij} - I_{ij}(E,k) | = 0, \quad i, j = x, y, z. \tag{2.4.1}$$

For quasi-1D ferromagnets ($J_{\perp} >> J_{\parallel}$), it is convenient to write the I_{ij} with the small parameter $J_{\parallel}/J_{\perp}$ [17]

$$I_{ij} = \frac{J_{\parallel}/J_{\perp}}{2S(2\pi)^3} \iiint dxdydz \frac{(\cos r_i - \alpha_i)\cos r_j}{\varepsilon + \alpha_x(2-\cos x-\cos y)(J_{\parallel}/J_{\perp}) + \alpha_z(1-\cos z)},$$

where

$$r_i = x, y, z, \quad \alpha = \cos(K/2), \quad \varepsilon = [E_{min}(K) - E]/(4SJ_{\perp}). \tag{2.4.2}$$

$E_{min}(k)$ is the bottom of the SW-continuum spectrum; E is the energy of a BM; and ε is the energy gap between SW and BM.

To find the quasi-momentum value α_{thresh} at which the BM disappears, one must consider Eq.(2.4.2) for $\varepsilon = 0$ and $\alpha = \alpha_{thresh}$. Fig.5 shows schematically the threshold of J' for BM existence in the BM spectrum.

By solving Eq.(2.4.1), α_{thresh} in the first nonvanishing order with respect to $J_{\parallel}/J_{\perp}$ is[17]

$$\alpha_{thresh} = 1 - (4S/c)(J_{\parallel}/2J_{\perp})^{1/2},$$

$$c = \frac{1}{(2\pi)^2} \iint_{(-\pi,\pi)} dxdy(2-\cos x-\cos y)^{-1/2} \approx 0.9 \tag{2.4.3}$$

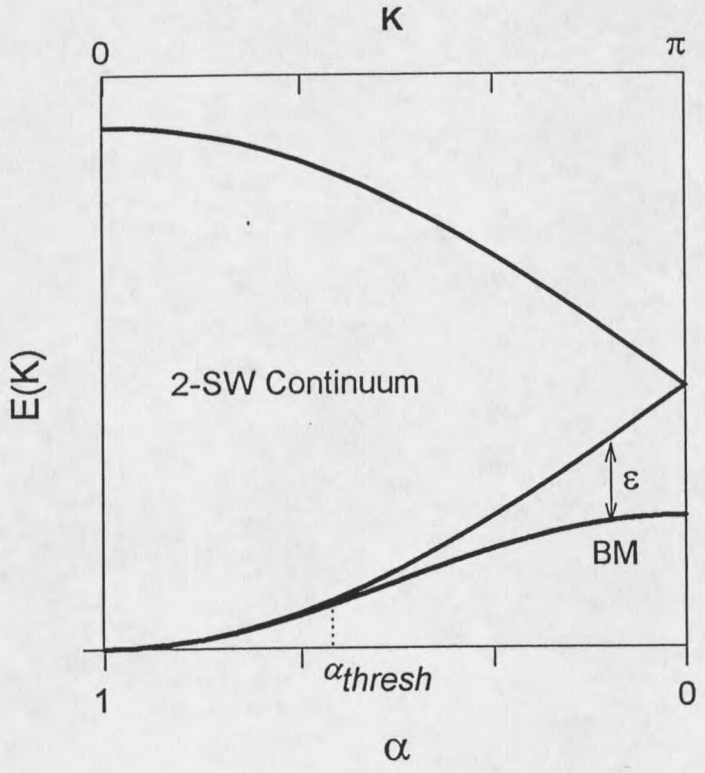


FIG. 5. A demonstration of threshold of J' for bound magnon existence. Here, $\alpha=\cos(K/2)$. When $\varepsilon=0$, $\alpha=\alpha_{thresh}$, and bound magnons cease to existence.

It shows that a small increment of the interchain interaction causes a considerable shift of the BM existence threshold in the quasi-1D Heisenberg ferrromagnet. In particular, when $J_{\parallel}/J_{\perp}$~0.1, α_{thresh}~0.5, BMs only exist 1/3 of the zone. When $J_{\parallel}/J_{\perp}$~0.4, α_{thresh}~0, no BMs exist for the entire range of K. Therefore, the threshold of J'/J for the BM existence is about 10^{-1}. An experimental test for the threshold of J' will be presented in Section 5.

5. Experiments

Experimental demonstrations of BM effects would be particularly challenging and interesting. Our motivation for the experiments is to study a series of 1D spin 1/2 Heisenberg ferromagnetic compounds with an emphasis on understanding the thresholds of intrachain and interchain exchange for the BM dominance on the thermodynamics.

A. Chains of Localized Spins

One of the simplest magnetic ions is Cu^{2+}, which has spin 1/2. The unpaired electron is often well represented by the Heisenberg Hamiltonian provided the electron does not become itinerant.

A truly 1D chain is clearly unattainable. A 3D ordering always exists in real materials. It is possible, however, to produce systems in which the magnetic ions have a strong coupling in one direction via an intrachain interaction J and a very weak coupling in the other directions via an interaction interaction J', if non-magnetic ions separate the chains. A small value for the ratio J'/J is required, in order to have a wide range of temperature over which 1D effects dominate.

The initial example of the quasi-1D spin 1/2, Heisenberg ferromagnet was $[(CH_3)_3NH]CuCl_3.2H_2O$ (CuTAC)[18]. In this compound the intrachain exchange is very weak (J≈1K). Lately, somewhat more strongly coupled, spin 1/2 ferromagnetic chains have been made, such as $(C_4H_8SO)CuCl_2$ (TMSO)[19] and $(C_2H_6SO)CuCl_2$ (DMSO)[19] which have middle range intrachain exchange (J≈40-50K), but significant interchain interactions, specially in DMSO, (J'/J~10^{-2}, TMSO has weaker J' than DMSO). The interchain coupling of TMSO and DMSO are probably large enough to preclude their study as ideal systems[19]. The compounds $(CH_3)_4NCuCl_3$ (TMCuC)[20] and $[(CH_3)_3NH]_3Cu_2Cl_7$ (TTMCuC)[20] also have middle range exchange (J≈40-50K) but have chains which are much more isolated, J'/J~10^{-4}. The best realizations of a 1D spin 1/2 system reported up until now, as so far we know, are $(C_6H_{11}NH_3)CuCl_3$ (CHAC)[21] and its bromine analog $(C_6H_{11}NH_3)CuBr_3$ (CHAB)[21], both of which have strong J of about 70K and weak J', J'/J~10^{-4}.

The available 1D spin 1/2 anisotropic Heisenberg ferromagnetic systems used in the experiments are listed in Table 1, with reported values of J/k, J'/k, and 3D ordering temperature T_c.

Table 1. 1D spin 1/2 anisotropic Heisenberg ferromagnetic systems and their properties.

Substance	Intrachain J/k (K)	Interchain J'/J	3D-ordering T_c (K)
CHAB[21]	50-70	10^{-3}-10^{-4}	1.50
TMCuC[20]	40-50	10^{-3}-10^{-4}	1.24
TTMCuC[20]	40-50	10^{-3}-10^{-4}	?
TMSO[19]	40-50	0.02	3.3
DMSO[19]	40-50	0.04	5.4
CuTAC[18]	0.85	0.01-0.05	0.165
TRIMER[22]	30	10^{-3}	1.7

All samples were provided by Dr. Roger Willett, Chemistry Department, Washington State University.

All of them show a phase transition to a 3D ordered magnetic states at sufficiently low temperatures. The preparation, structural analysis and characterization of these compounds were previously reported.[18-22] All compounds (except TRIMER) are built up from well-isolated, bibridged linear chains of the Cu-Cl-Cu (or Cu-Br-Cu) bridges. The common feature responsible for strong ferromagnetic coupling is the presence of a symmetrical Cu-Cl-Cu bridge (Cu-Br-Cu for CHAB) with the Cu-Cl-Cu bond angle less than 90^0. These halide bridged copper(II) systems exhibit a natural but small Ising anisotropy. The distance between Cu ions is large enough to ignore the next-nearest-neighbor interaction. The individual chains are effectively isolated by non-magnetic cations. Adjacent chains are hydrogen bonded with a weak interchain coupling J'.

B. Experimental Methods

The methods to observe and measure BM effects usually are: (1). Magnetic susceptibility; (2). Specific heat; (3). Neutron scattering. In this work, only measurement of *ac* susceptibility is used.

The magnetic *ac* susceptibilities of crystal samples of TMSO, DMSO, CHAB, and CuTAC, and powdered crystal samples of TMCuC, TTMCuC and TRIMER, were measured from 4.2K to 35K in an *ac* field $\boldsymbol{h}$ = 10 Oe, frequency f = 80Hz and *dc* magnetic fields $\mathbf{h}$ of 0, 1, 2, 3, 4, and 5 tesla. The total field $\mathbf{h} + \boldsymbol{h}\ \mathbf{sin}(2\pi f\mathbf{t})$ is along the easy-axis z direction for TMSO, DMSO and CuTAC, and along the chain direction for CHAB. All

measurements were performed on the LakeShore Model 7225 AC Susceptometer/DC magnetometer, which has been modified for measurements below 4.2K. Measurements were fully calibrated and performed automatically through data acquisition and control software packages. The system accuracies for both *ac* and *dc* measurements are ± 1 %, and the temperature accuracy is ± 0.2K. The high-field *ac* susceptibilities of crystal sample of TMSO were measured in a *ac* field $h = 10$Oe, frequency $f = 80$Hz, and in very high *dc* magnetic fields **h** of 7 and 9 tesla at the LakeShore Lab.

C. Data and Analysis

The temperature dependences of the *ac* susceptibilities of TMSO, TMCuC, TTMCuC, TRIMER, CHAB, CuTAC and DMSO are shown in Figs. 6-12, respectively. Most of the data curves (except in DMSO and CuTAC) of susceptibility vs. temperature show rounded peaks at different fields, which are typical for BM effects as predicted by the JB theory in Sec.2.2. All the data are first analyzed in term of BM and SW contributions, by using the JB model. The theoretical curves of total susceptibility are shown by solid lines, and the SW contributions are shown by dashed lines in Figs. 6-12. It can be seen that the susceptibility is mainly from BM contributions, and SW contribution cannot represent the experimental data in most of the samples. The linear SW theory fails in most of these 1D systems.

Despite the good agreement between data and JB theory, deviations appear in almost all data fits. The degree and the source of the deviation vary from sample to sample.

For TMSO shown in Fig.6: fitting parameters are J/k=50K, J'=-0.01K , J'/J~10^{-3}, and γ=0.975. The fitting is almost perfect except in the low-field and low-T ranges. Even in very high field up to 9 tesla, the data exhibit the broad maximum of BM effects. The deviations from the theoretical model only appear in low-T ranges (below 8K) and low fields (1 and 2 telsa). They are due to the reasonably stronger antiferromagnetic interchain exchange coupling J', which causes the variation from the ideal 1D behavior and generates 3D ordering at T~3K. The good fit to the BM model in this system confirms the BM dominance in the intermediate J range.

For TMCuC shown in Fig.7: fitting parameters are J/k = 45K, J'/k = - 0.6, γ = 0.92. Early experiments[14] at fields of 0, 1, 1.5, and 2 tesla showed a dominance of BMs, but with somewhat large deviation between the experiment data and the theoretical JB model. In this work ac susceptibility was remeasured at fields 1, 2, 3, 4, and 5 tesla in order to further confirm BM effects in the intermediate J range. The BM effect is clear from the rounded peaks of experimental data but these rounded peaks are lower than the theoretical values from BM model. The deviation can be explained by powder susceptibility. A powder sample was used because a big crystal was not available. The measured susceptibility is therefore the average values of easy and hard-axis single crystal susceptibility which is lower than the value along the easy axis (z direction). Therefore, deviations between the data and the JB model do not affect the conclusion which is that BMs dominate susceptibility, and the linear SW theory fails in this system.

For TRIMER, $(1,2\text{-DMP})_2Cu_3Br_8$, the crystal structure study[22] showed that the aggregation of $Cu_3Br_8^{2-}$ anions leads to a linear chain system. In the low temperature range[22], T < 100K, each trimer exists as a ground state doublet and acts as an effective spin 1/2 particle due to the strong antiferromagnetic coupling that exist within each trimer. The system therefore reduces to a chain of spin 1/2 species coupling by an inter-trimer exchange J. TRIMER has a small J value of about 30K. Its fitting parameters are J/k = 30K, J'/k = -0.1K and $\gamma = 0.9$. As shown in Fig.9, it is confirmed that BMs dominate susceptibility in the small J range.

For CHAB shown in Fig.10: The rounded peaks at different field indicate BM dominate the susceptibility. The best fit to the JB model gives parameters J/k = 65K, J'/k = -0.1K, and $1/\gamma = 0.95$. However, the JB model values are higher than the experimental data in the regions of the rounded peaks. Since a single crystal sample was used, the deviations can not be explained as in TMCuC and TTMCuC which are powdered samples. Some other type of contribution must reduce the susceptibility values. In Chapter 5, the soliton effect on this system will be discussed. The susceptibility of CHAB is a sum from contributions of magnons, bound magnons, and solitons, with bound magnons providing the main contribution.

CuTAC was chosen because of its extremely weak J value, which is below the theoretically predicted threshold of J for BM effects on the susceptibility. Fitting parameters are J/k=1K, J'/k=-0.024 and γ=0.90. Experimental data and JB model curves are shown in Fig.11. Data in all temperature and field ranges do not clearly show a BM

effect. Compared with susceptibilities of all the other compounds measured, the magnitudes of the rounded maximum in CuTAC are very small and fit the SW contribution levels. As predicted by JB theory, in this weak J range, SWs dominate the susceptibility. It confirms the theoretical prediction of the threshold of $J < 10K$.

Finally, all of the above experiments, except CuTAC, show existence of BMs. However, DMSO was chosen in order to test the threshold of interchain exchange J'. This sample has similar intrachain J but stronger interchain J' than TMSO. The ratio $J'/J < 10^{-2}$ in DMSO is close to the theoretically predicted threshold of J' for BM existence. Therefore, the interchain J' is an important factor in this system.

As shown in Fig.12, from the experimental data, typical BM rounded peaks did not appear in this system. BM effects can not be clearly identified due to large deviations between the data and the JB model.

First, the deviations at low-T (below 10K) data for all fields is clearly due to the stronger interchain interaction, which prevent BM formation. This agrees with the theoretical prediction for the threshold of J'.

Second, not only the stronger J', but also impurities play a role in the low-T behavior. The low-T behavior can be explained by the presence of a paramagnetic impurity, which can be seen especially from the 2 and 3 tesla data, which show divergences below 5K. The paramagnetic impurity exhibits its own characteristic divergence at low temperature even when it is quite dilute. It is likely intrinsic to these compounds due to crystal imperfection. Fragments with an odd number of copper ions between packing faults, which possess a

doublet ground state or have randomly oriented magnetic moments, will obey the Curie law and contribute to the susceptibility with a 1/T divergence at low temperatures. Therefore, the actual susceptibilities of the system can be described by contributions from the paramagnetic impurity and 1D ferromagnetic chains.

A summary of our experimental results is listed in the following.

Table 2. A summary of experimental results for thresholds of J and J'.

Substance	Intrachain J/k (K)	Interchain J'/k (K)	Anisotropy γ	BM dominance
CHAB	65	- 0.1	1.05	Yes
TMSO	50	- 0.01	0.975	Yes
TMCuC	45	- 0.6	0.92	Yes
TTMCuC	45	- 0.25	0.985	Yes
TRIMER	30	- 0.1	0.92	Yes
CuTAC	1	- 0.024	0.9	No
DMSO	45	-1.8	0.92	No

In conclusion, although there are small deviations between experimental data and the theoretical model for most of the compounds, the general agreement of the JB theory with the data is obvious. The experiments confirm the BM dominance in a large range of exchange J and field h (up to 9 telsa). The theoretically predicted intrachain exchange J thresholds below 10K and interchain J' threshold about $J\times10^{-1}$ are confirmed by the experiments.

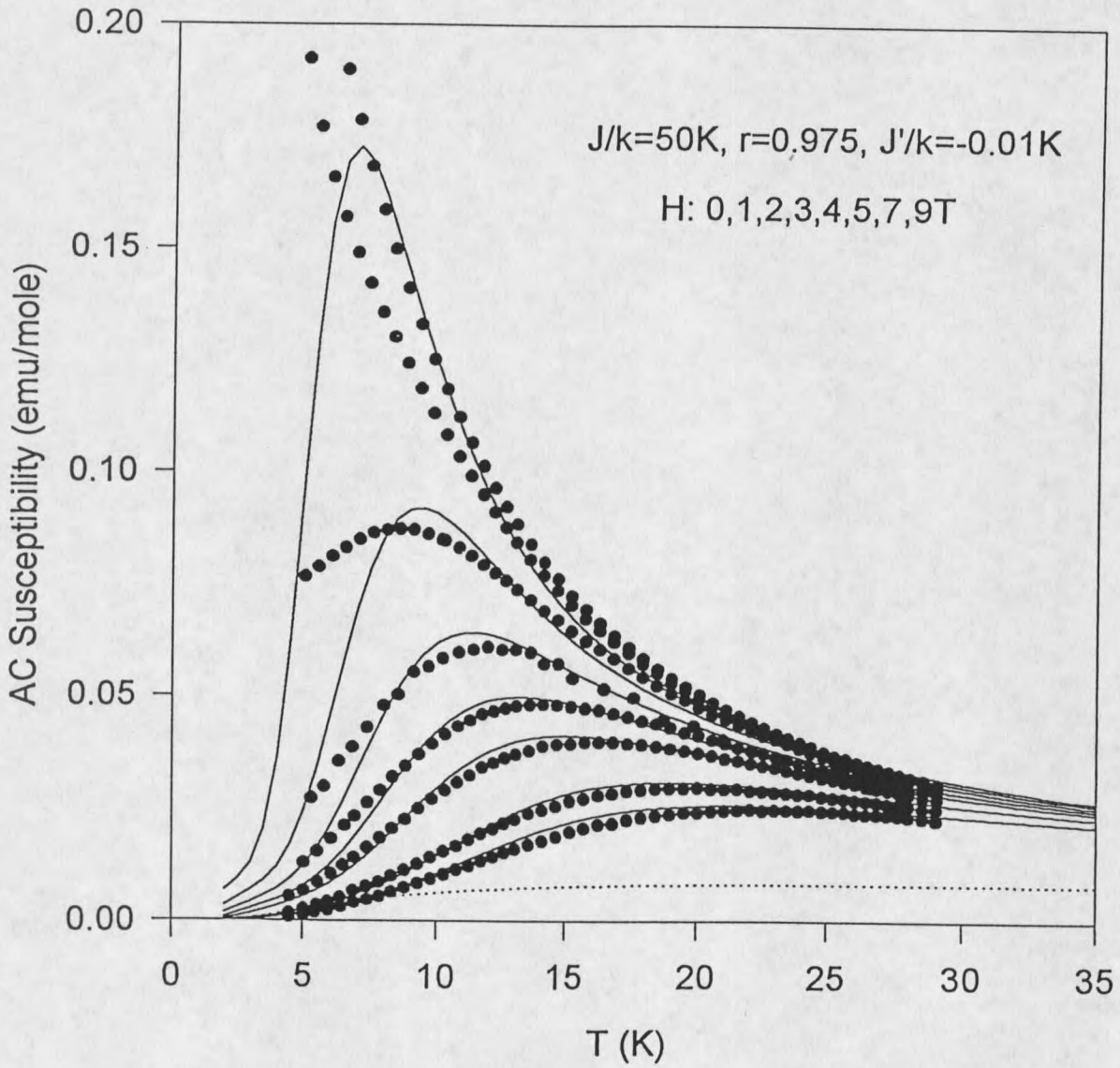


FIG. 6. Susceptibility of TMSO.
Solid lines: total susceptibility contributed from bound magnons and spin waves; dotted lines: spin wave susceptibility.

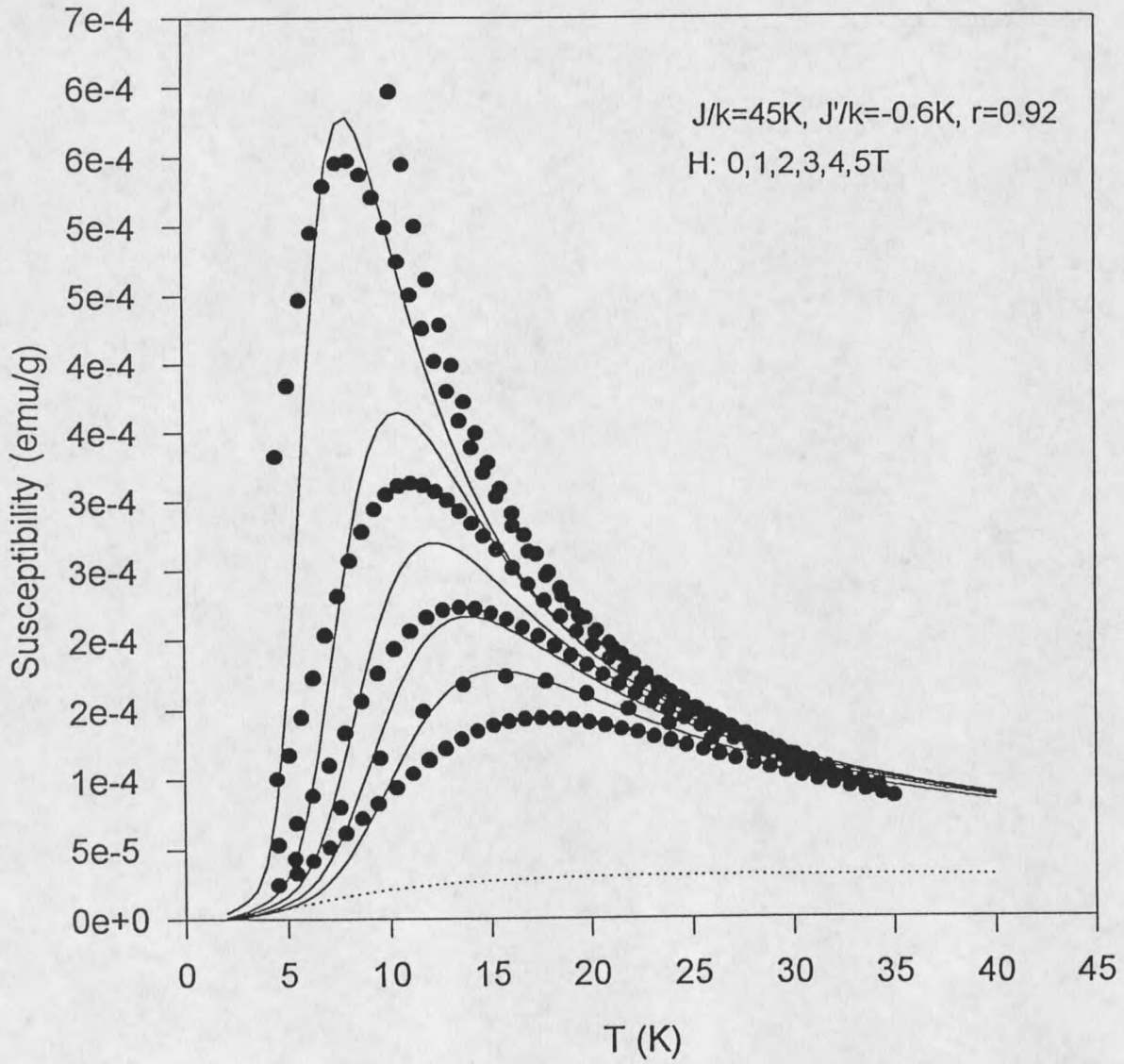


FIG. 7. Susceptibility of TMCuC.
Solid lines: total susceptibility contributed from bound magnons and spin waves; dotted lines: spin wave susceptibility.

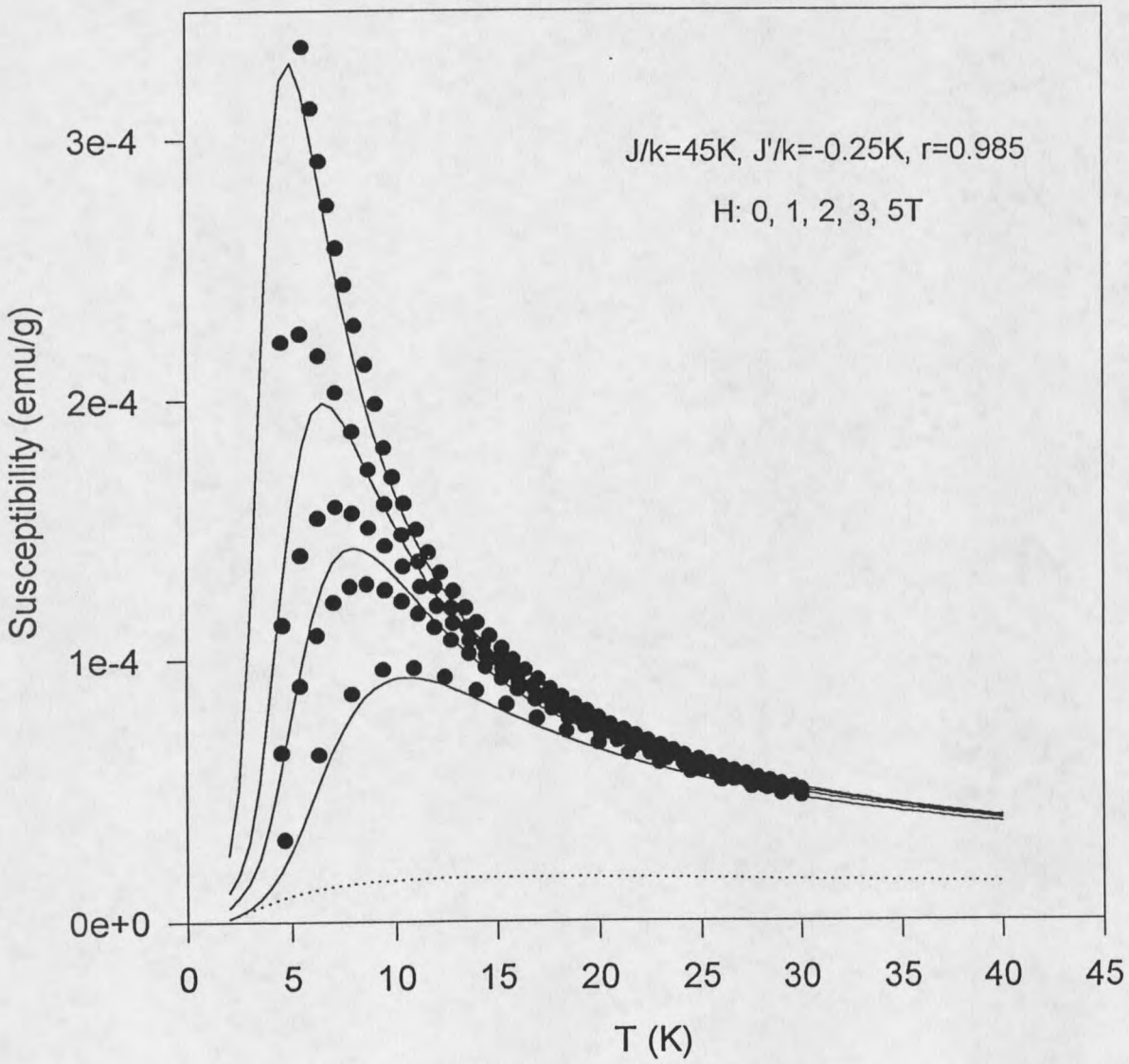


FIG. 8. Susceptibility of TTMCuC.
Solid lines: total susceptibility contributed from bound magnons and spin waves; dotted lines: spin wave susceptibility.

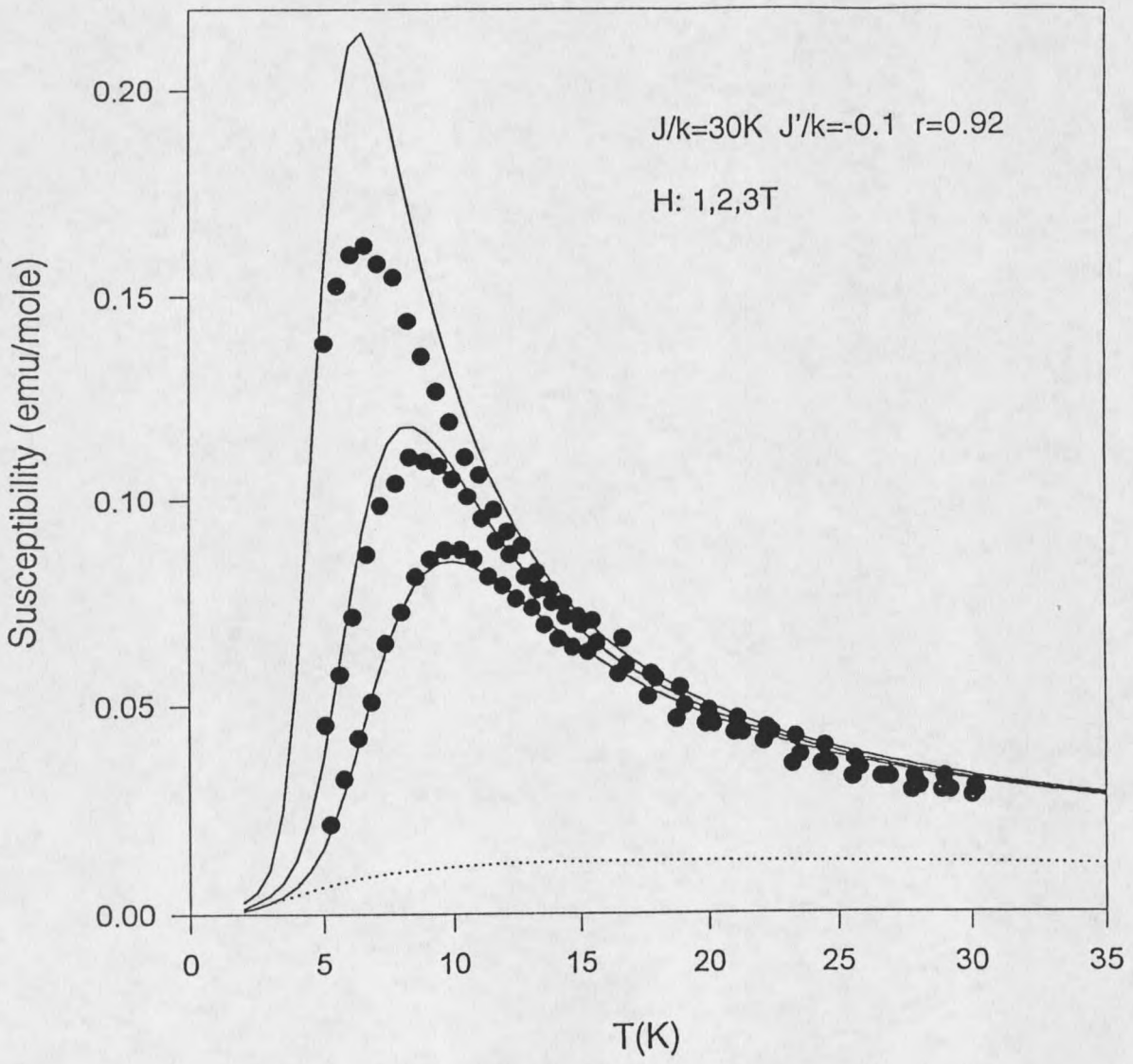


FIG. 9. Susceptibility of TRIMER.
Solid lines: total susceptibility contributed from bound magnons and spin waves; dotted lines: spin wave susceptibility.

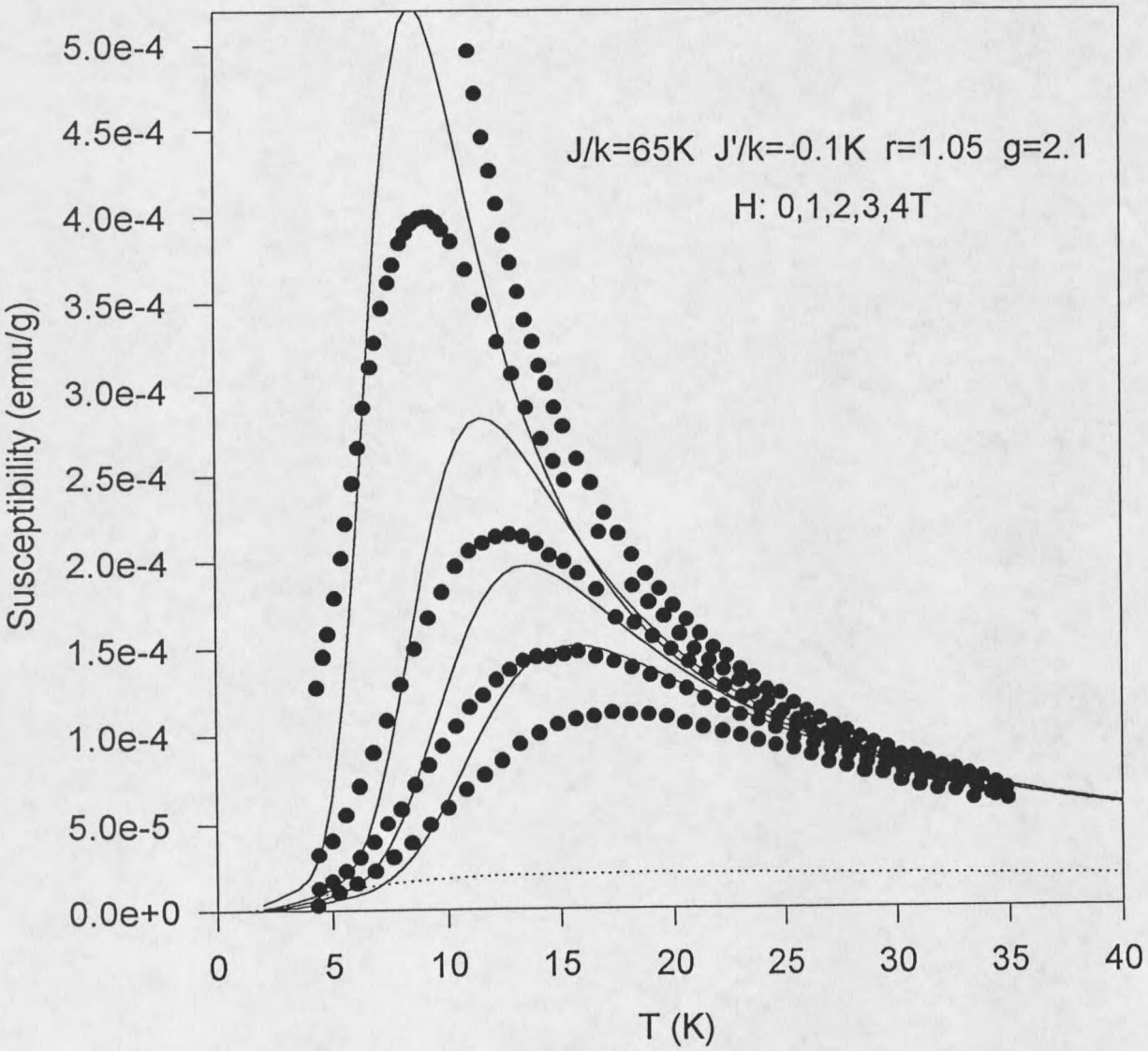


FIG. 10. Susceptibility of CHAB.
Solid lines: total susceptibility contributed from bound magnons and spin waves; dotted lines: spin wave susceptibility.

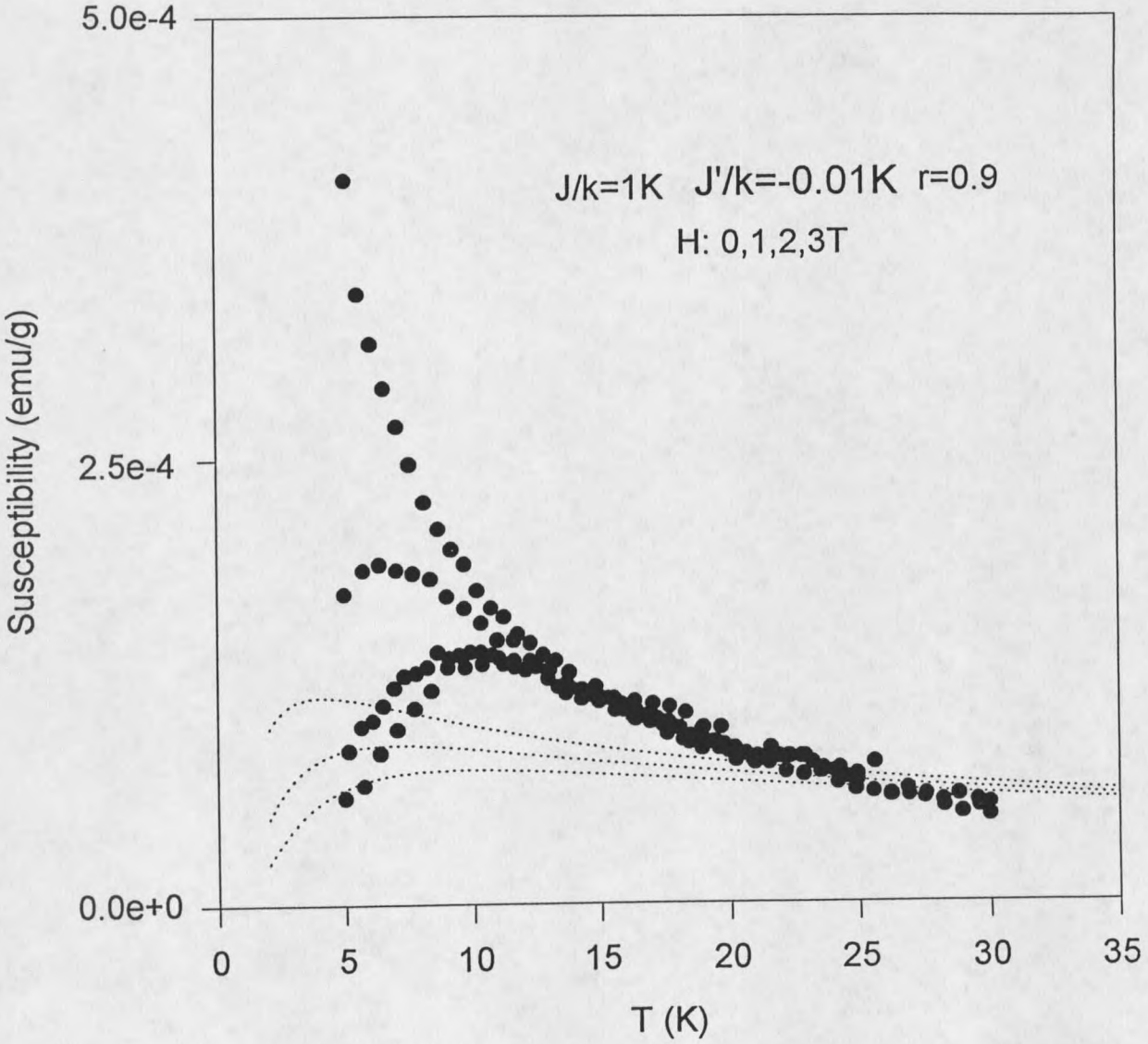


FIG. 11. Susceptibility of CuTAC.
Dotted lines: Dotted lines: susceptibility contributed from spin waves.

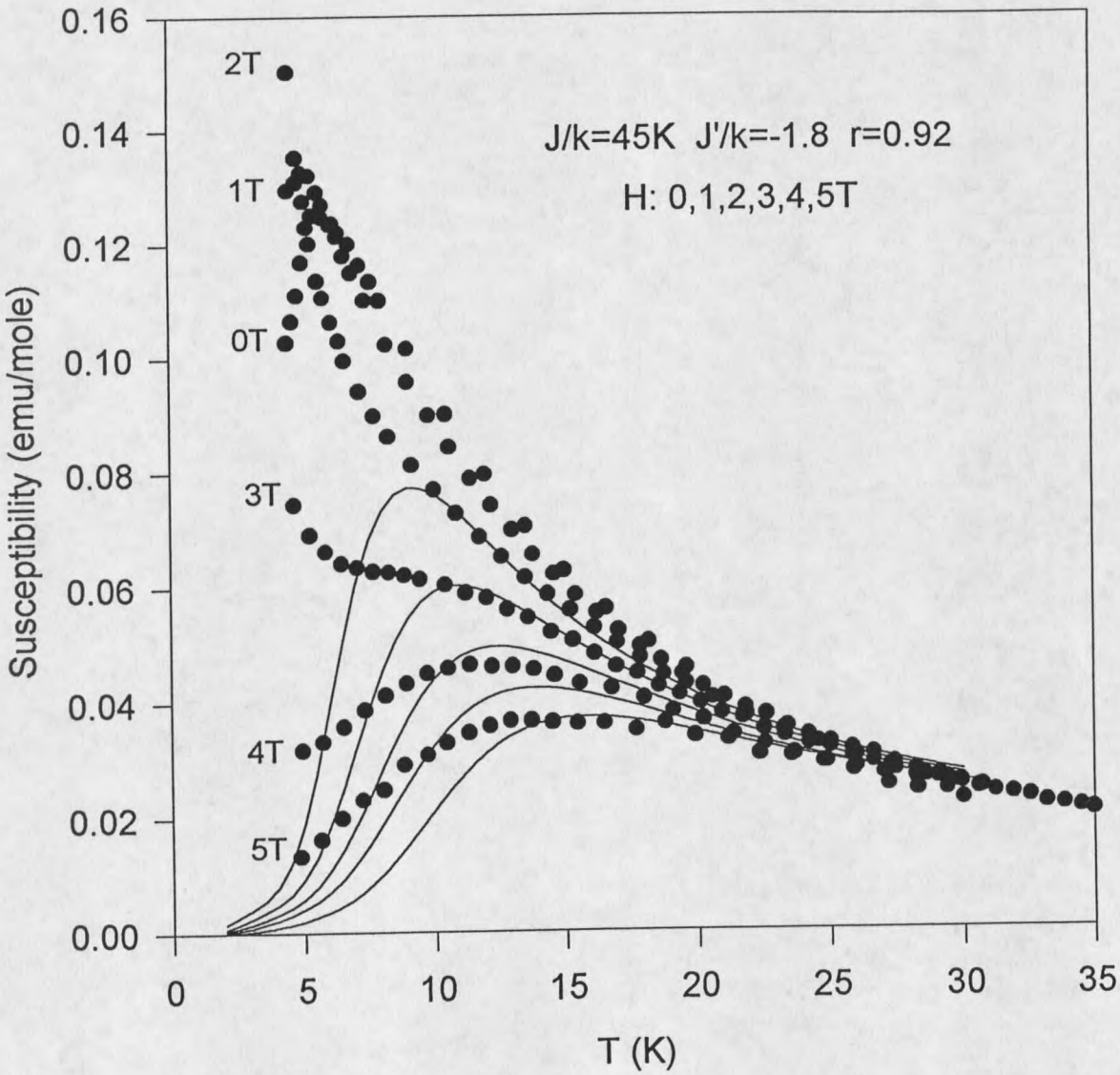


FIG. 12. Susceptibility of DMSO.
Solid lines: Theoretical susceptibility of bound magnons and spin waves.

CHAPTER 3

EFFECTS OF ANISOTROPIES ON BOUND MAGNONS

1. Introduction

An important portion of the investigation of BM is the effect on them of anisotropies, since in 1D systems even a small amount of anisotropy may drastically affect the excitations and therefore the thermodynamic properties at low temperatures. In general, the anisotropy can arise in at least two ways: (1) through anisotropic exchange interactions (two-site anisotropy) and (2) through single-ion (on-site) anisotropy. The exchange anisotropy is related to different sites (usually adjacent sites) but single-ion anisotropy occurs only at one site.

The Hamiltonian of 1D Heisenberg ferromagnets with anisotropic exchange and single-ion anisotropy is given by Eq.(1.1) without the terms for A and J':

$$H = -J\sum_{i}^{N}[S_i^z S_{i+1}^z + \gamma(S_i^x S_{i+1}^x + S_i^y S_{i+1}^y)] - D\sum_{i}^{N}(S_i^z)^2 - g u_B h\sum_{i}^{N} S_i^z \ . \qquad (3.1.1)$$

Here, as in Eq.(2.1), γ is an exchange anisotropy parameter which varies between the Ising limit (γ=0) and the isotropic Heisenberg model (γ=1), and D represents the single-ion anisotropy strength. Considering the usual exchange interaction, $-J\sum S_i^z S_{i+1}^z$, (written here in the Ising limit for simplicity), one finds that the excitation energy of two *adjacent* spin deviations is lower by J than that of two *non-adjacent* ones, giving rise to an effective

attractive interaction between spin waves and resulting in the formation of BM. Considering the single-ion anisotropy $-D\sum(S_i^z)^2$, this term causes the excitation energy of two units of spin deviations at a *single site* to be lower by 2D than that of two units of spin deviations distributed on *two sites*. Thus, single-ion anisotropy also gives rise to an effective attractive interaction between spin waves.

Since the degree and the type of anisotropy plays an important role on the thermodynamic behavior, the effect of the single-ion anisotropy as well as the exchange anisotropy should be considered in the BM-bearing systems. In this chapter, these two types of anisotropy effects on BM excitations will be discussed in order to make a complete study of BM.

Note that the single-ion anisotropy is also related to the soliton excitations in that the classical limit of Hamiltonian (3.1.1) corresponds to a soliton model. The connection between BMs and solitons will be discussed in Chapter 5.

2. Effect of Single-ion Anisotropy on Bound Magnons

A. The Origin of the Single-ion Anisotropy

Single-ion anisotropy appears in both spin 1/2 and spin greater than 1/2 systems. In the spin=1/2 case, the single-ion anisotropy is caused primarily by the crystal field entering via the spin-orbit coupling, i.e., the crystalline field action on a single ion gives rise to anisotropy. Coupling between electron orbital and spin angular momenta under a crystal field gives rise to a Hamiltonian term of the form $\mathbf{S}\cdot\mathbf{D}\cdot\mathbf{S}$, where $\mathbf{D} \propto (g_e - \mathbf{g})$. ($\mathbf{g}$ is the g tensor and g_e is

the value for the free electron). Single-ion anisotropy strength **D** is represented by the anisotropic **g** tensor. For a crystalline field with axial symmetry, e.g., preferred spin orientation is along the z axis, the term $\mathbf{S}\cdot\mathbf{D}\cdot\mathbf{S}$ reduces to $\mathbf{D}S_z^2$.

In systems with spin greater than 1/2, at small distances, two unpaired electrons will experience a strong dipole-dipole interaction. The dipole-dipole interaction between the electrons leads to a term of the same form $\mathbf{S}\cdot\mathbf{D}\cdot\mathbf{S}$. Experimentally, it is not possible to separate the spin-spin interaction contribution to **D** from the anisotropic part of the spin-orbit coupling contribution.

The single-ion anisotropy provides the easy-plane or easy-axis character of the system only at sufficiently low temperatures, while at higher temperatures the system becomes less and less affected by the single-ion anisotropy.

B. Effect of Single-ion Anisotropy on BM Excitations

Since the interaction between magnons results in the formation of BMs, it is easier to see the effect of D on BM formation from the boson representation where the magnon interaction can be seen more clearly (see Chapter 2). The Hamiltonian (3.1.1) in the boson representation is

$$H = E_0 + \sum_k \varepsilon_k a_k^+ a_k + \frac{1}{N}\sum_{k_1 k_2 q} v(k_1, k_2, q) a^+_{q/2+k_1} a^+_{q/2-k_1} a_{q/2+k_2} a_{q/2-k_2} , \qquad (3.2.1)$$

which has the same form as Eq. (2.1.4) in Chapter 2. Solving this Hamiltonian gives the ground state energy E_0, a single magnon energy ε_k and the magnon interaction $v(k_1, k_2, q)$ for two-magnon problem, which are[23]

$$E_0 = -\gamma JNS^2 - hNS - DNS^2, \quad (3.2.2)$$

$$\varepsilon_k = h + 2JS(1 - \gamma \cos k) + 2D(S-1/2), \quad (3.2.3)$$

$$v(k_1, k_2, q) = -J \cos k_2(\cos k_1 - \gamma \cos q/2) - D. \quad (3.2.4)$$

Comparing this to the results of the D = 0 case given in Chapter 2,

$$\varepsilon_k = h + 2JS(1 - \gamma \cos k), \quad (3.2.5)$$

$$v(k_1, k_2, q) = -J \cos k_2(\cos k_1 - \gamma \cos q/2), \quad (3.2.6)$$

it is interesting to find that single magnon energy ε_k is not affected by single-ion anisotropy D for S=1/2, but the magnon interaction which results in formation of BMs is always changed by D for all S values.

The associated BM energies were obtained by Green's function techniques[24] or other methods[25]. The results show that there are two BM solutions for $q \neq 0$. It is easiest to find the two solutions at the zone boundary $q = \pi$ for the isotropic Heisenberg case:

$$E^{I}_{2\text{-BM}}(q=\pi) = 2h + 4SJ + 4D(S - 1/2) - J, \quad (3.2.7)$$

$$E^{II}_{2\text{-BM}}(q=\pi) = 2h + 4SJ + 4D(S - 1/2) - 2D. \quad (3.2.8)$$

As can be seen, in addition to the usual exchange BM ($E^{I}_{2\text{-BM}}$), a new BM ($E^{II}_{2\text{-BM}}$) appears, the so called "single-ion BM".[24]

Comparing $E^{I}_{2\text{-BM}}$ and $E^{II}_{2\text{-BM}}$ with the spin wave (SW) energy, the top and bottom of the 2-SW continuum merge to a single energy at the zone boundary $q = \pi$,

$$E_{2\text{-sw}}(q = \pi) = 2h + 4JS + 4D(S-1/2). \quad (3.2.9)$$

Therefore, the energy of the exchange BM is lower by J, and the energy of the single-ion BM is lower by 2D, than the 2-SW continuum at the zone corner. When D = 0, $E^{II}_{2\text{-BM}}$ is degenerate with the energy of the 2-SW continuum. *It is the presence of the single-ion anisotropy D that leads to a new BM.*

A simple picture of the single-ion anisotropy effect on 2-SW & 2-BM energy dispersion of the Heisenberg ferromagnet is shown in Fig.13(a).

To understand the physical picture of the single-ion BM, it is easier to look from the Ising limit, since the Ising picture is straightforward and Ising energies are the exact solutions of the Hamiltonian (3.1.1) at the zone boundary q = π. The Hamiltonian (3.1.1) in the Ising limit, which is the case of fully anisotropic exchange, is

$$H = -J\sum_{i}^{N} S_i^z S_{i+1}^z - D\sum_{i}^{N} S_i^z S_i^z. \qquad (3.2.10)$$

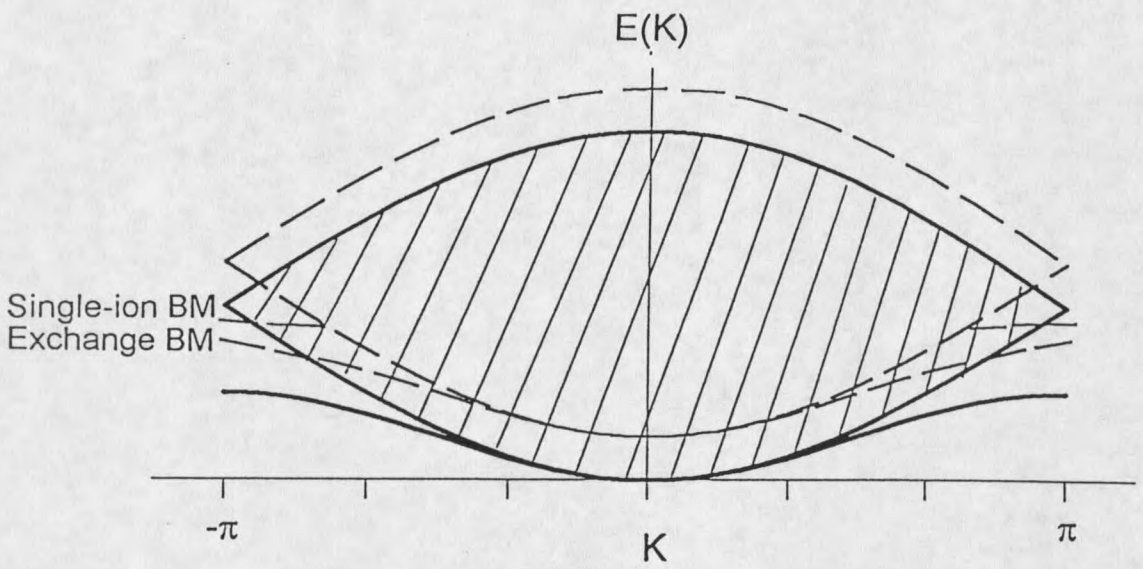
The one magnon state is one unit of the z-component of total spin above the ground state, i.e., the value of S^z at site i changes from S to (S-1). The excitation energy is

$$E_1 = -J[S(S-1) + (S-1)S - (S^2 + S^2)] - D[(S-1)^2 - S^2] = 2SJ + (2S-1)D. \qquad (3.2.11)$$

Two units of spin deviations can be constructed in three different way, as shown in Fig.13(b). The first case is *spin deviations on two non-adjacent sites,* which corresponds to two non-interacting magnons (2-SW) . The energy in this case is

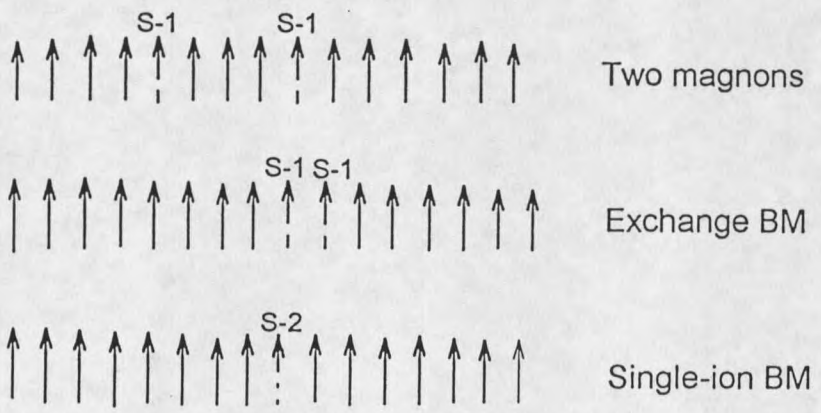
$$E_{2\text{-sw}} = 2E_1 = 2[2SJ + (2S-1)D] = 4SJ + 4(S-1/2)D. \qquad (3.2.12)$$

The second case is two units of *spin deviation on two adjacent sites,* which is the usual exchange BM. The S^z values at site i and site i+1 change from S to (S-1), and the excitation



Solid line: D=0; Dashed line: D=0.25

(a) Heisenberg Limit



(b) Ising Limit

FIG. 13. Single-ion anisotropy effect on bound magnon energy.

energy of this BM is

$$E_{2\text{-BM}} = -J[S(S-1)+(S-1)(S-1)+(S-1)S-(S^2+S^2+S^2)]-2D[(S-1)^2-S^2]$$

$$= 4SJ + 4(S-1/2)D - J. \qquad (3.2.13)$$

In the third case, two units of *spin deviation can be set on a single site.* (In the Ising limit, this case only occurs for S>1/2 since the physical state with two units of spin deviation at a single site does not exist for spin 1/2). In this case, the value S^z at site i changes from S to (S-2) and the excitation energy is

$$E_2^* = -J[S(S-2)+(S-2)S-(S^2+S^2)]-D[(S-2)^2-S^2]$$

$$= 4SJ + 4(S-1/2)D - 2D. \qquad (3.2.14)$$

This excitation state has a different energy than that of either 2-SW or the usual exchange 2-BM when $D \neq 0$. It is called a single-ion BM since two spin deviations occur on a single site and it is caused by single-ion anisotropy. The results from Eqs.(3.2.13) and (3.2.14) are just the same as the BM solutions $E^{I}_{2\text{-BM}}(q=\pi)$ and $E^{II}_{2\text{-BM}}(q=\pi)$ in Eqs. (3.2.7) and (3.2.8).

A simple picture of the single-ion BM in the Ising case is shown in Fig.13(b). In the Ising limit, the single-ion BM corresponds to two units of spin deviation on the same site, while two unit of spin deviations of the exchange BM are on adjacent sites and two unit of spin deviations of spin waves are on non-adjacent sites. The difference between the single-ion BM and the spin wave with two units of spin deviation is caused by D. Clearly, the distinction between exchange BM and single-ion BM persists for all systems, except in the limit of vanishing anisotropy D.

The general assumption is that the single-ion anisotropy energy is significantly smaller than the exchange energy. Generally speaking, the dominant interaction of magnons seems to be

from the exchange interaction. However, as the magnitude of D is increased, single-ion BM arise and compete with exchange BM to dominate the BM spectrum. BM energies and their dependence on the single-ion anisotropy D/J are discussed in the following cases.

(1). Easy-axis single-ion anisotropy with isotropic exchange:

In the easy-axis single-ion anisotropy ($D > 0$) with isotropic exchange ($\gamma = 1$), the energy spectrum of 2-BM can be determined by[25]

$$x^3 + [\,2(S-1)\cos(K/2) - d/\cos(K/2)]\,x^2 + (1 + 2dS)\,x - 2S\cos(K/2) = 0, \quad (3.2.15)$$

$$\Omega_{2\text{-BM}} = 2(2S-1)D + 4SJ\,[1 - (1/2)\,(x + 1/x)\cos(K/2)], \quad (3.2.16)$$

where $\mathbf{d = D/SJ}$, and $\mathbf{x}$ are real roots required[25] in the interval [0,1] of $\mathbf{x}$ in the algebraic equation (3.2.15). $\Omega_{2\text{-BM}}$ is the energy of 2-BM, and K is the BM momentum ($-\pi < K < \pi$). Eqs.(3.2.15) and (3.2.16) summarize all the information needed for calculating the spectrum of 2-BM.

First note that the cubic equation $y^3 + py^2 + qy + r = 0$ has three real roots when

$$b^2/4 + a^3/27 \le 0, \quad (3.2.17)$$

where $a = (3q - p^2)/3$ and $b = (2p^3 - 9pq + 27r)/27$. When $b^2/4 + a^3/27 > 0$ the cubic equation only has one real root. By replacing $p = [\,2(S-1)\cos(K/2) - d/\cos(K/2)]$, $q = (1 + 2dS)$, and $r = -2S\cos(K/2)$ into Eq.(3.2.17) three (or one) real roots for Eq.(3.2.15) can be solved. It is found[25] that (3.2.15) possesses two real roots in the interval [0,1] for $|K| < \pi$, which means two BM branches appear in the BM spectrum.

For example, at the zone boundary $K \approx \pi$, or $\cos K/2 \approx 0$, two real roots are found in the interval [0,1] for $d \neq 0$, (the third real root lies outside of the interval [0,1]),

$$x_1 \approx (SJ/D)\cos K/2\,, \quad x_2 \approx 2S\cos K/2\,. \tag{3.2.18}$$

The corresponding BM energies calculated from Eq.(3.2.16) are

$$\Omega_I = 4SJ + 4(S-1/2)D - J, \tag{3.2.19}$$

$$\Omega_{II} = 4SJ + 4(S-1/2)D - 2D. \tag{3.2.20}$$

These solutions are significant by comparing them with Eqs.(3.2.13) and (3.2.14) in the Ising limit. They are exactly the values found earlier in the Ising limit, as well as in Eqs. (3.2.7) and (3.2.8). They are the energies of the exchange BM and the single-ion BM respectively.

Furthermore, the threshold of D/J for the single-ion BM appearance depends on the number of real roots in Eq.(3.2.15) as determined by Eq.(3.2.17).

The solutions[25] calculated from Eqs.(3.2.15) and (3.2.16) for a 2-BM spectrum is shown in Fig.14 for various values of the anisotropy D/J in S = 1. The noticeable characteristic of this figure is that two separate branches of BM energies develop for $D/J \neq 0$. For small values of D/J, e.g., D/J = 0.25, the dominant feature of the spectrum is the exchange BM. This can also be seen from Eq.(3.2.7) and (3.2.8) by forming the difference $E^{I}_{2\text{-BM}} - E^{II}_{2\text{-BM}} = J - 2D$, which is positive for $D < J/2$. In this range of couplings the exchange BM extends throughout the zone whereas the single-ion BM occupies only a small portion of the zone near the boundary. For $D > J/2$, the role of the two modes is exchanged. The single-ion BM occupies the entire zone and becomes the lowest BM, and dominants over the exchange BM.

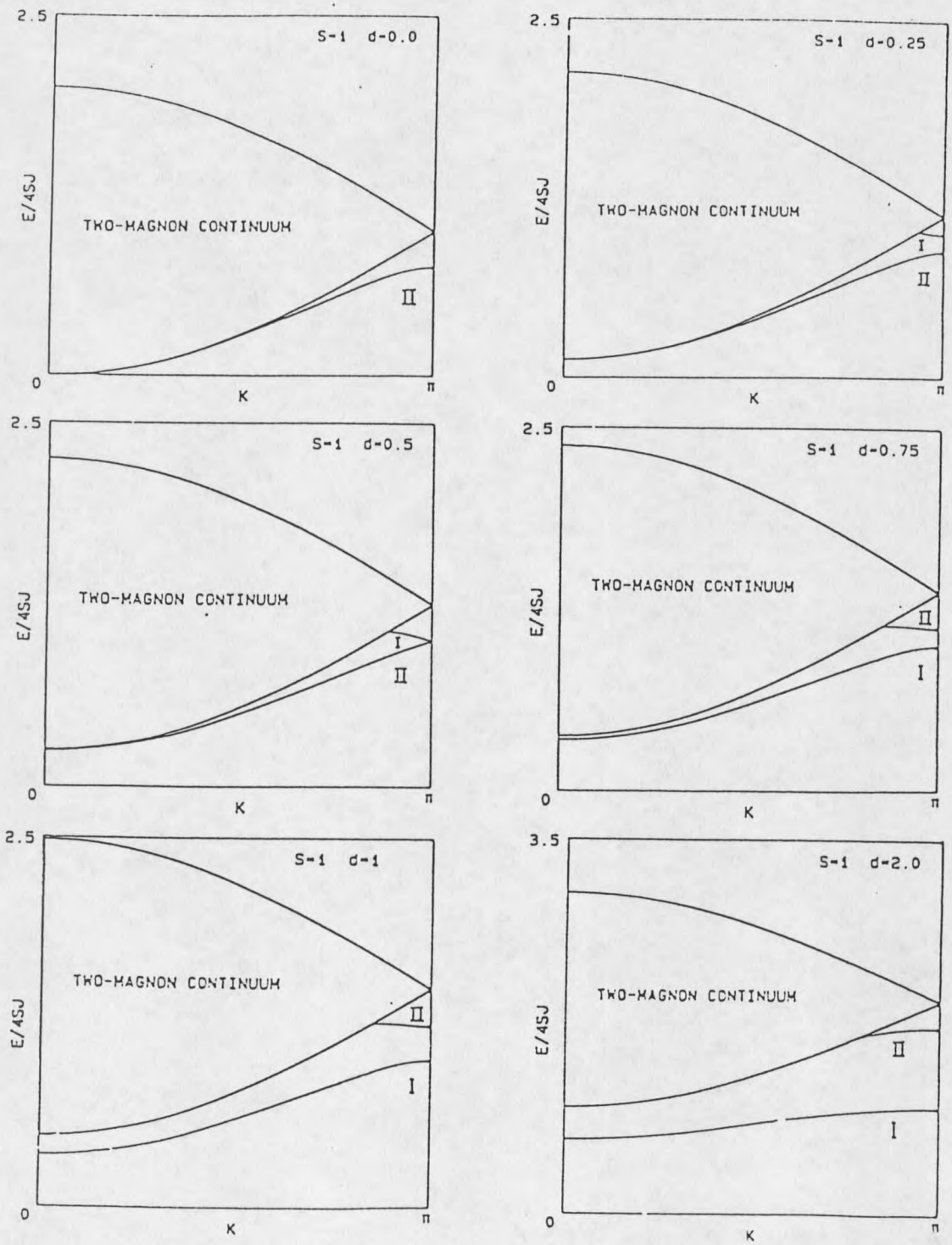


FIG. 14. Two-magnon spectra with an easy-axis single-ion anisotropy.[25] I and II stand for the single-ion BM and exchange BM, respectively.

At the zone center K = 0, only the lower BM survives. This lower BM would be either the exchange BM or the single-ion BM, depending on the value D/J. As shown in Fig.14 (d=D/J=1), the single-ion BM is presented at K = 0, while the exchange BM does not appear until $K \geq 5/6\ \pi$.

As the ratio of D to J is increased further, the single-ion BM is split considerably below the 2-SW continuum, and becomes dispersionless with energy $\Omega \cong 4(S-1)D$. The large D/J case is shown in Fig.15, where D/J = 10 and S = 1. The single spin wave state for zero field is shown in the same figure, and there is a crossing of the single spin wave and single-ion BM energies. The use of an external magnetic field would make experimental observation of this crossover considerably simpler, since the single-ion BM state shifts in proportion to 2h, while the single spin wave state shifts only in proportion to h. When D/J is somewhat larger, the single-ion BM can become the lowest excitation, even lower than single SW.

(2). Easy-plane single-ion anisotropy with isotropic exchange:

In the easy-plane $D < 0$ and $\gamma = 1$ case, for weak magnetic fields, the system develops a nontrivial ground state with planar behavior. The derivation of the excitation spectrum by the method developed in the $D > 0$ case fails. However, the ground state is ordered in the z direction if the magnetic field **h** exceeds a critical value h_c,[25] where $\mathbf{h_c = (2S-1)D}$. Under this condition the 2-BM excitation energies can be derived by the same method as in the easy-axis case and obtained by the simple replacement $\mathbf{a \rightarrow -d = -D/SJ}$ in Eqs.(3.2.15) and (3.2.16), as shown in Fig.16. In this case, the BM energy shifts upward instead of downward as was seen with the easy-axis case. The picture changes drastically; the single-ion BM appears above the

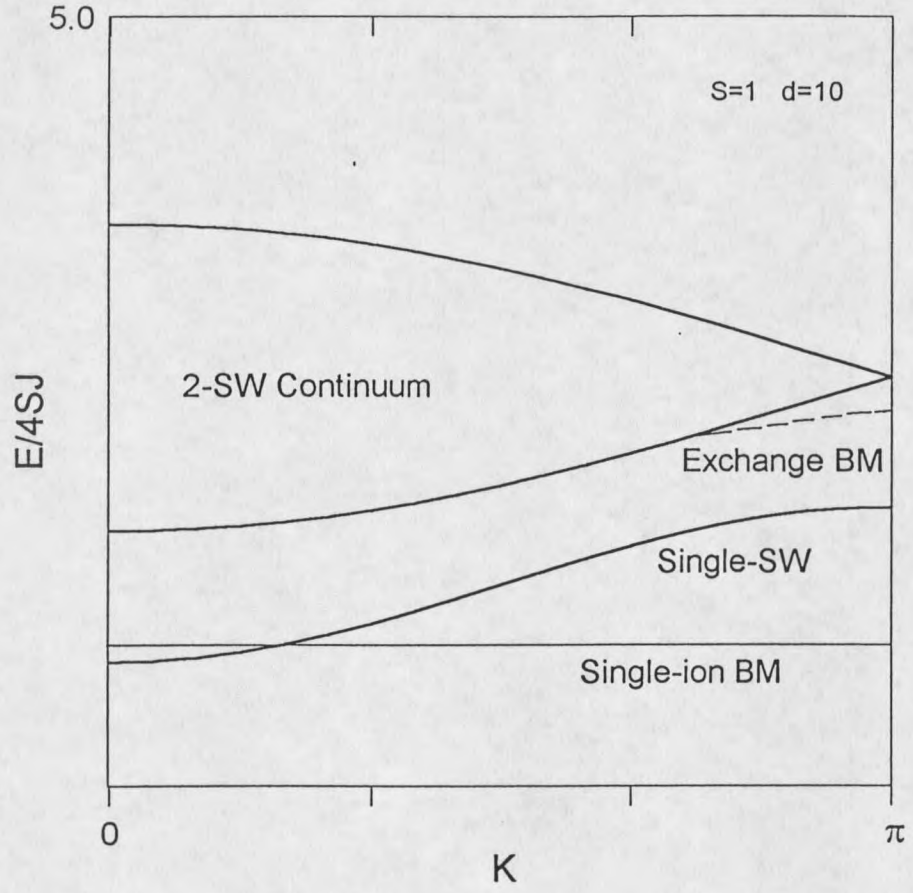


FIG. 15. Two-magnon spectra with large single-ion anisotropy.

2-magnon continuum and extends throughout the zone for sufficiently strong anisotropy (a >1.4), while it is below the 2-magnon continuum in the easy-axis case.

(3). Single-ion anisotropy and exchange anisotropy:

A further example is the case of the single-ion anisotropy together with anisotropic exchange, i.e., exchange anisotropy $\gamma \neq 1$ in the Hamiltonian (3.1.1).

The spectrum of the 2-BM is determined by [25]

$$\Omega = 2(2S - 1)D + 4SJ\,[\,\gamma - (1/2)\,(x + 1/x)\cos(K/2)], \tag{3.2.21}$$

$$\gamma x^3 + [2(S - 1)\cos(K/2) + \gamma d/\cos(K/2)]x^2 + (\gamma + 2dS)x - 2S\cos(K/2) = 0, \tag{3.2.22}$$

where d = D/SJ.

Compared to the case $\gamma = 1$ (see Eqs.(3.2.15) and (3.2.16)), nonvanishing values of γ yield significant quantitative changes in the energy spectrum but the qualitative picture remains more or less the same.

(4). Effect of quartic exchange interaction on BMs:

The last example considered is the effect of quartic exchange interaction on BMs, since it is related to the single-ion anisotropy and the exchange anisotropy. The Hamiltonian with quartic exchange interaction is[25]

$$H = -\sum_{i}^{N} [(J + G)S_i S_{i+1} + 2G(S_i S_{i+1})^2] \tag{3.2.23}$$

The state with all spins ordered in the z direction is an eigenstate of (3.2.23) with energy $E_0 = -N(J + 3G)$, for all values of the exchange constants. However, the ordered state ceases to be the ground state for coupling such that $G > J$.[25]

When S = 1, Eq.(3.2.23) is the most general isotopic Hamiltonian involving two-site exchange interactions. The derivation of the energy spectrum is identical to that described in Sec.3.2.A.

The one-magnon excitation energy is

$$E_1 = 2(J + G)(1 - \cos k). \tag{3.2.24}$$

The 2-SW excitation energy is

$$\Omega_{sw} = 4(J + G)\,[1 - (\cos k_1 + \cos k_2)/2]\,. \tag{3.2.25}$$

The 2-BM energies are determined by[25]

$$\Omega_{BM} = 4(J + G)\,[1 - (1/2)\,(x + 1/x)\cos(K/2)], \tag{3.2.26}$$

where x is a real root in the interval [0,1] of the algebraic equation[25]

$$(J + 3G)\,x^3 - 12G\cos(K/2)\,x^2 + (J + 3G + 8G\cos^2(K/2))\,x - 2(J + G)\cos(K/2) = 0. \tag{3.2.27}$$

Solving the full equations (4.2.26) and (4.2.27) for arbitrary momenta K, it was found[25]

(i) G < J: x = 1 is the only real root in Eq.(4.2.27). There is only one BM in this coupling region, which is the usual exchange BM extending throughout the zone.

(ii) G > J: the excitation energy becomes negative, and ferromagnetic order is impossible in this coupling region[25].

(iii) G = J: This is a special coupling. Only one stable BM exists[25], with $\Omega_{BM} = 4G(1-\cos K)$. The energy spectrum for S=1 involving quartic exchange interactions is shown in Fig.17. As shown in Fig.17, only one BM branch arises. Since only one BM exists in the two-magnon

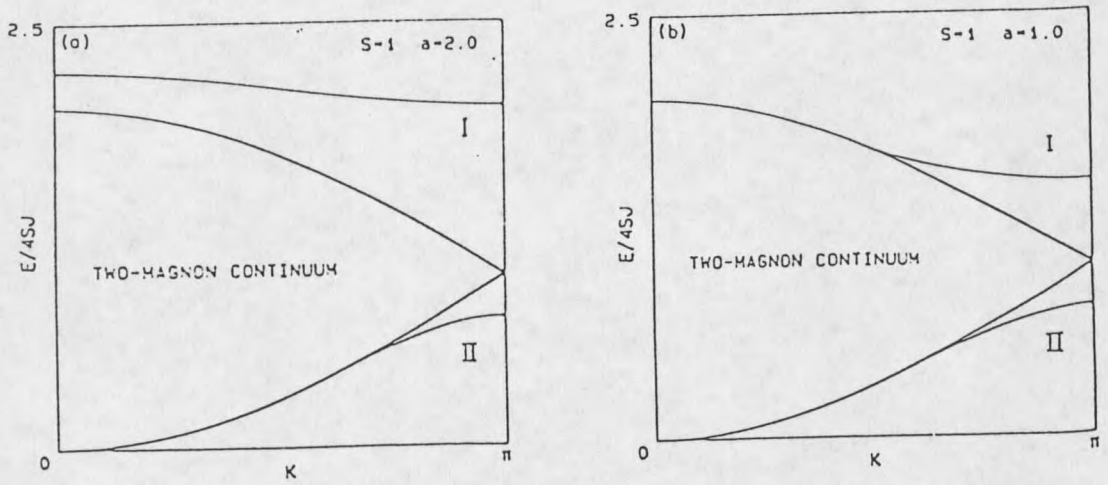


FIG. 16. Two-magnon spectra with an easy-plane single-ion anisotropy.[25] I and II stand for the single-ion BM and exchange BM, respectively.

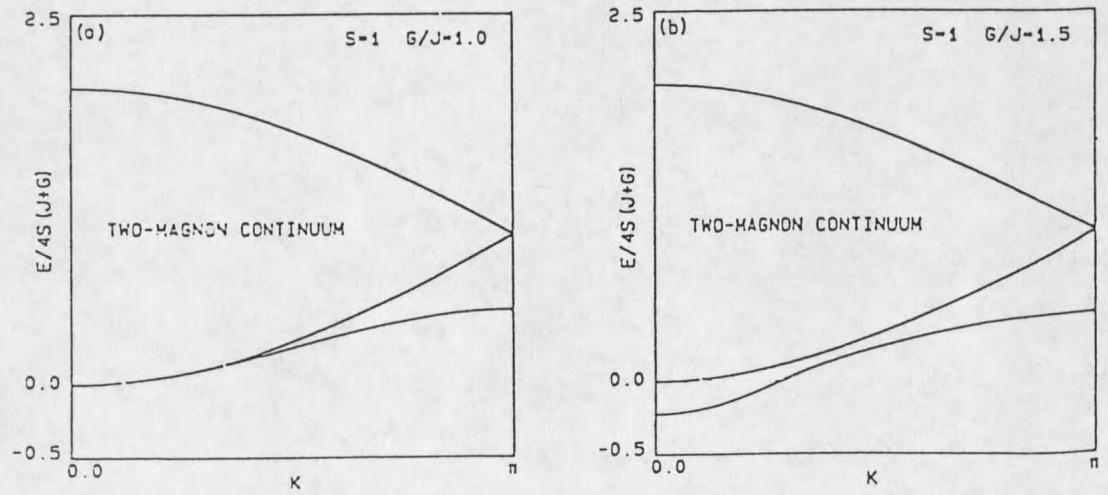


FIG. 17. Two-magnon spectra involving quartic exchange interaction.[25]

spectrum, one may think that the single-ion mode does not play any role in the present model. However, this is not true. It can be found that the single-ion BM lies within the (bottom) boundary of the two-magnon continuum. On the other hand, the single-ion BM energy is degenerate with the magnon energy given by Eq.(3.2.24) restricted to the critical coupling G = J. Eq.(3.2.24) may be the limiting form of a single-ion BM which is a resonance for all couplings in the region G < J.[25] At this point it is tempting to assume that the single-ion BM and the 2-SW join at the G = J to form a doublet which remains degenerate for all couplings in the region G < J.[25]

To summarize of this section, the single-ion anisotropy gives rise to a new type of BM, in addition to the usual exchange BM. In the easy-axis case, two BM energies are below the spin-wave continuum. For smaller D/J, the exchange BM dominates. As the ratio of D to J is increased , the single-ion BM exists over an extent of K space. For sufficiently large D/J, there is a critical anisotropy strength D/J above which the single-ion BM exists throughout the Brillouin zone. When the magnitude of D is comparable to the exchange interaction, i.e., $D \approx J$, the single-ion BM is the dominant feature of the BM spectrum. In the easy-plane case, the single-ion BM appears above the spin wave continuum and the exchange BM is below the spin wave continuum.

It is clear that the presence of single-ion BM will enhance the possibility of experimental observation of BM, especially in systems with strong single-ion anisotropy. However, because of the complexities caused by the single-ion anisotropy term in the Hamiltonian, complete single-ion BM excitation spectra and their effects upon low-temperature thermodynamic

properties has not yet been solved, as far as the author knows. Further study on these aspects will be suggested in Chapter 6.

3. Effect of Exchange Anisotropy on Bound Magnons

A. Effect on BM Energy Spectrum

Anisotropic exchange occurs when, in addition to the direct (or indirect) exchange interaction, spin-orbit coupling is considered. The Hamiltonian of the system is given by Eq. (3.1.1) without the term for D:

$$H = -J\sum_{i}^{N}[S_i^z S_{i+1}^z + \gamma(S_i^x S_{i+1}^x + S_i^y S_{i+1}^y)] - g u_B h \sum_{i}^{N} S_i^z \quad . \tag{3.3.1}$$

Here $\gamma < 1$ represents the easy-axis anisotropy and $\gamma > 1$ represents the easy-plane anisotropy.

As discussed in Chapter 2, the expression for BM energies for $\gamma < 1$ is:

$$E_n = \gamma J \frac{\sinh\Phi}{\sinh(n\Phi)}[\cosh(n\Phi) - \cos K] + nh \qquad (1/\gamma = \cosh\Phi) \tag{3.3.2}$$

Fig.18 shows that the 2-SW and BM spectrum E(K) vary as function of anisotropic exchange γ at zero field. As anisotropy increases, i.e., the value of γ decreases, the BM energy curve becomes flat and less dependent on K. In the Ising limit ($\gamma = 0$) , the BM energy is a constant and completely independent of K and n.

In the case of the easy-plane $\gamma > 1$, the BM energy is:

Exchange anisotropy effect on bound magnon energy

Solid lines: r =1; Dashed lines: r =*0.8, 0.5, 0.0*

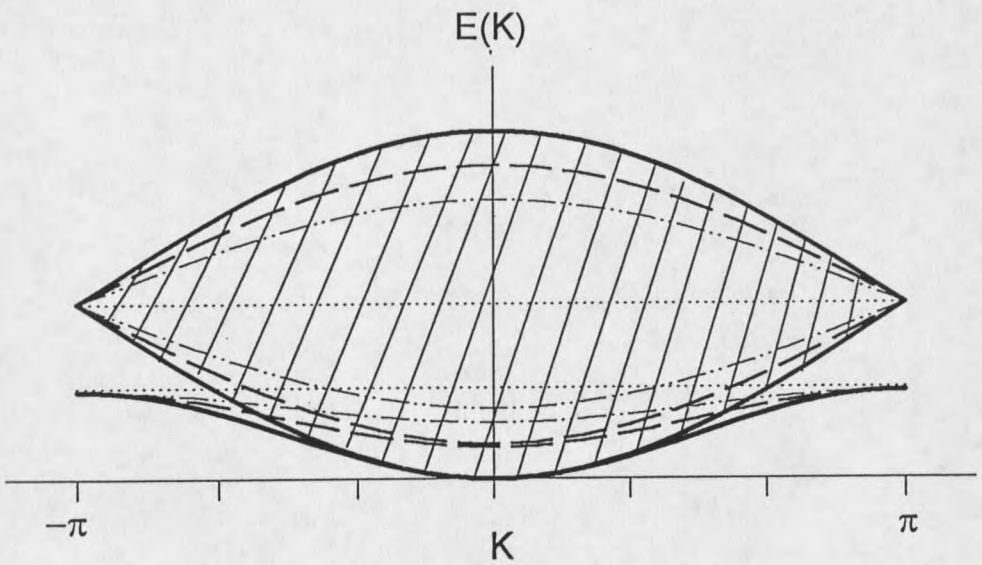


FIG. 18. Exchange anisotropy effect on bound magnon energy.

$$E_n = nh + \gamma J \frac{\sin\Phi}{\sin(n\Phi)}[\cos(n\Phi) - \cos K] \qquad (1/\gamma = \cos\Phi)\,. \qquad (3.3.3)$$

Generally speaking, BM excitations do not exist for all values of $\gamma > 1$. For a given number of flipped spins n, the regions of BM existence are a set of intervals of values of γ and the lengths and numbers of those intervals are determined by n.[7]

First, the energy expression Eq.(3.3.3) requires

$$\sin(n\Phi) \neq 0$$

$$\Phi \neq l\pi/n, \qquad l = 1, 2, \ldots n/2. \qquad (3.3.4)$$

The number l can be regarded as the label of the allowed interval for Φ.

Secondly, the requirement that the wavefunction of the BM be bounded, corresponds to the following inequalities[7]

$$\sin(v\Phi)\sin(n-v)\Phi\,[\cos(n\Phi) - \cos K] > 0 \quad v=1, 2, 3, \ldots, n-1. \qquad (3.3.5)$$

The inequalities (3.3.4) and (3.3.5), which are regarded as conditions for the parameters Φ and K, must be fulfilled simultaneously.

Thus for a fixed number n, under the above conditions which determine a set of overlapping intervals of values of Φ, $(1/\gamma = \cos\Phi)$, BMs can exist. As Φ approaches the boundary of the intervals the BM " loosens up" and it ceases to exist. In particular, when $\Phi = \pi/2$, $1/\gamma = \cos\Phi = 0$, which is the XY-model case, there are no BMs.

B. Effect on Thermodynamic Properties

Important analytic results about the effect of exchange anisotropy on BM and therefore on thermodynamics have been obtained by Johnson and Bonner[9]. In particular, an expression has been obtained for the zero-field thermal excitation energy gap.

A thermal excitation gap exists at zero field for all $\gamma < 1$, vanishing linearly as $1-\gamma$ as the isotropic limit is approached. For $0 \leq \gamma \leq 0.6$: [9]

$$\Delta E(\gamma) = (E_i - E_0)/2 = J(1 - \gamma^2)^{1/2}, \tag{3.3.6}$$

where the E_i are the dominant excited states and E_0 is the ferromagnetic ground state. The dominant excitations E_i are BMs in this range, easily seen in the Ising limit (γ=0).

For $0.6 \leq \gamma < 1$: [9]

$$\Delta E(\gamma) = 2J(1 - \gamma). \tag{3.3.7}$$

In this range, spin-wave excitations dominate the thermal gap.

The thermal excitation gap of Eqs.(3.3.6) and (3.3.7) governs the low-T behavior of the specific heat[9]. Therefore, for anisotropy greater than $\gamma = 0.6$, the dominant excitations to specific heat correspond to BMs. For anisotropy less than $\gamma = 0.6$, the dominant excitations are spin waves.

First, the expression Eq(3.3.6) and (3.3.7) is unusual in that it changes its form at an intermediate value of exchange anisotropy γ. This special value ($\gamma = 0.6$) does not correspond to any symmetry change in the Hamiltonian, but is associated with an important change in the physical significance of the results. Secondly, the existence of this gap for all $\gamma < 1$ implies exponential behavior of the thermodynamic function as $T \rightarrow 0$. Further, the predicted behavior

of this anisotropic thermal excitation gap indicates clearly that the different classes of low-lying excitations are competing for dominance.

The susceptibility is determined by the effective magnetic excitation gap[9]

$$\Delta E(\gamma) = (E_i - E_0)/2 = J(1.-\gamma^2)^{1/2}. \qquad (3.3.8)$$

This magnetic gap is dominated by the BMs for all anisotropy $0 \leq \gamma < 1$[9]. Therefore, the low-T behavior of the susceptibility is governed over the whole range of γ by the BM excitation at zero field.

The low-T thermodynamic behavior in external fields depends strongly on the anisotropy of the systems. There are several regions in H-1/γ parameter space in which BMs or SWs dominate thermodynamic properties. The types of excitation that give rise to the low-T thermodynamic behavior change from region to region.

From the expressions for χ and C_h shown in Eqs.(2.2.7) and (2.2.8) in Chapter 2, the temperature dependences of the susceptibility $\chi(T)$ and specific heat $C_h(T)$ as functions of anisotropy γ can be calculated and are shown in Fig.19 and Fig.20. When exchange anisotropy increases (γ value becomes smaller), both susceptibility $\chi(T)$ and specific heat $C_h(T)$ have a temperature dependent shift and the curves move toward higher temperature.

From the calculated χ and C_h, the susceptibility and specific heat are governed by the BM excitations in a complex crossover range of field-anisotropy (H-γ) parameter space. The dominant behavior of χ and C_h varies in different regions of H-γ parameter space[9], as shown in Fig.21 and Fig.22. For the susceptibility, BMs dominate over spin waves throughout

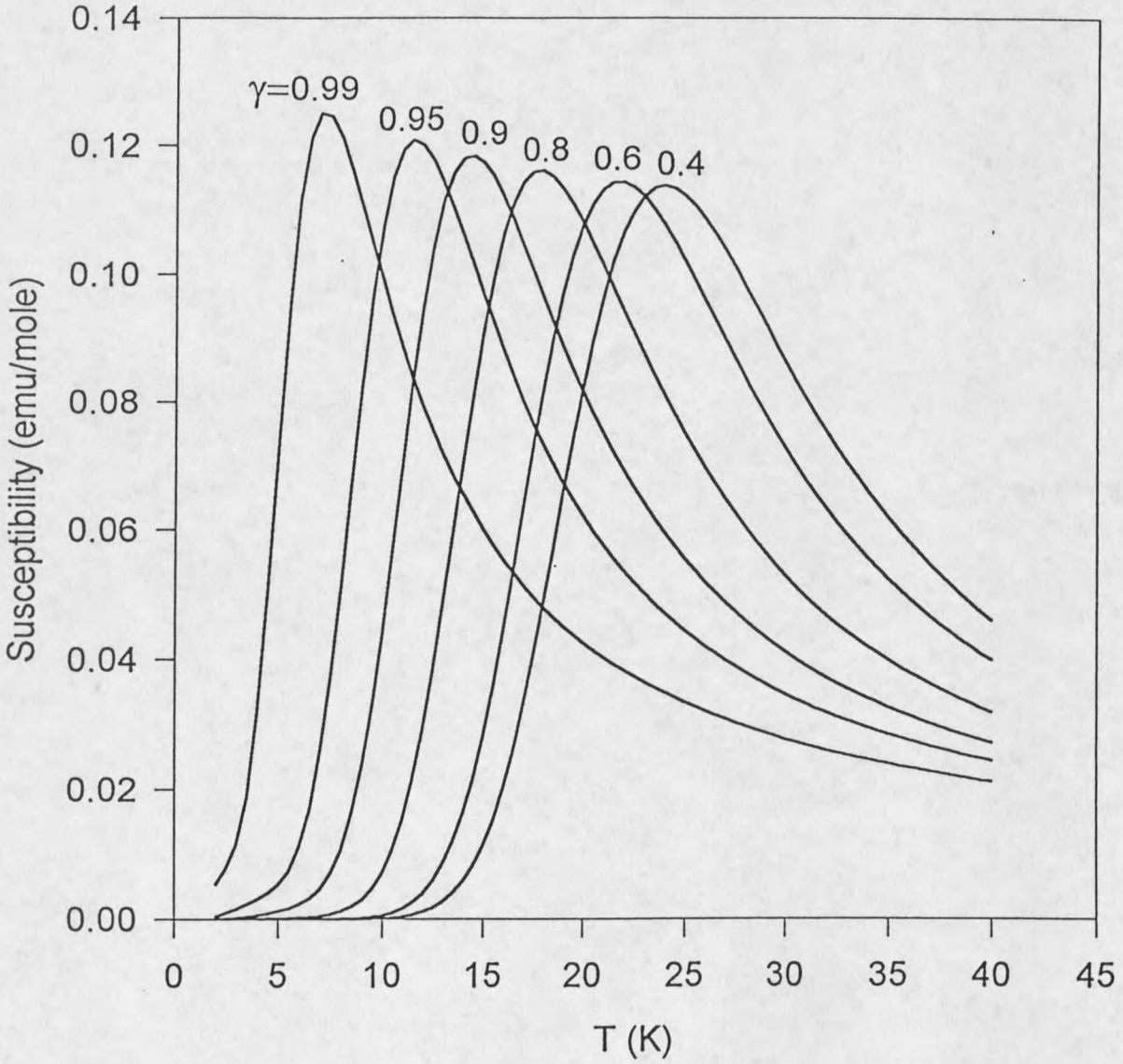


FIG. 19. $\chi(T)$ for various values of exchange anisotropy γ.

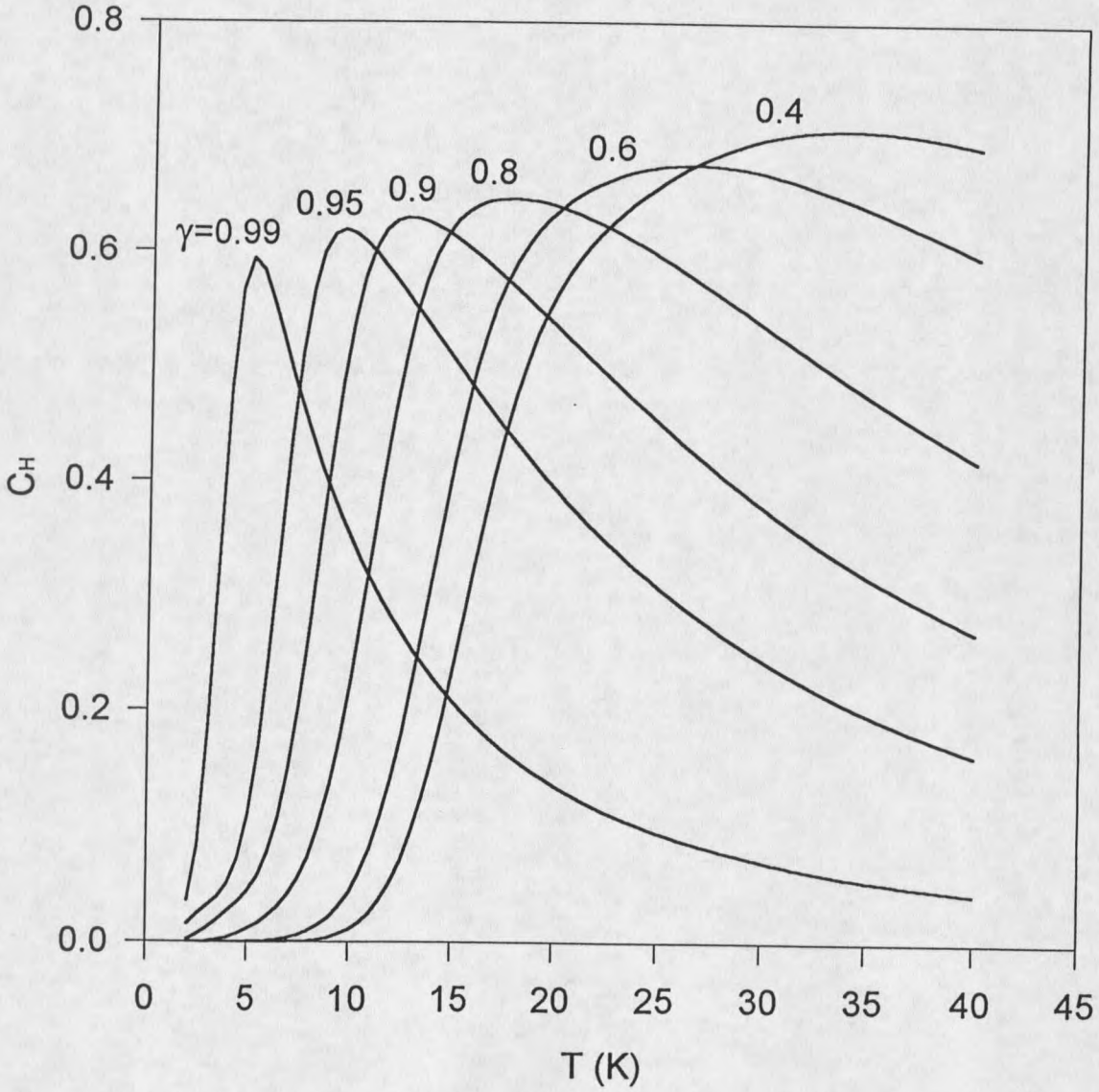


FIG. 20. $C_h(T)$ for various values of exchange anisotropy γ.

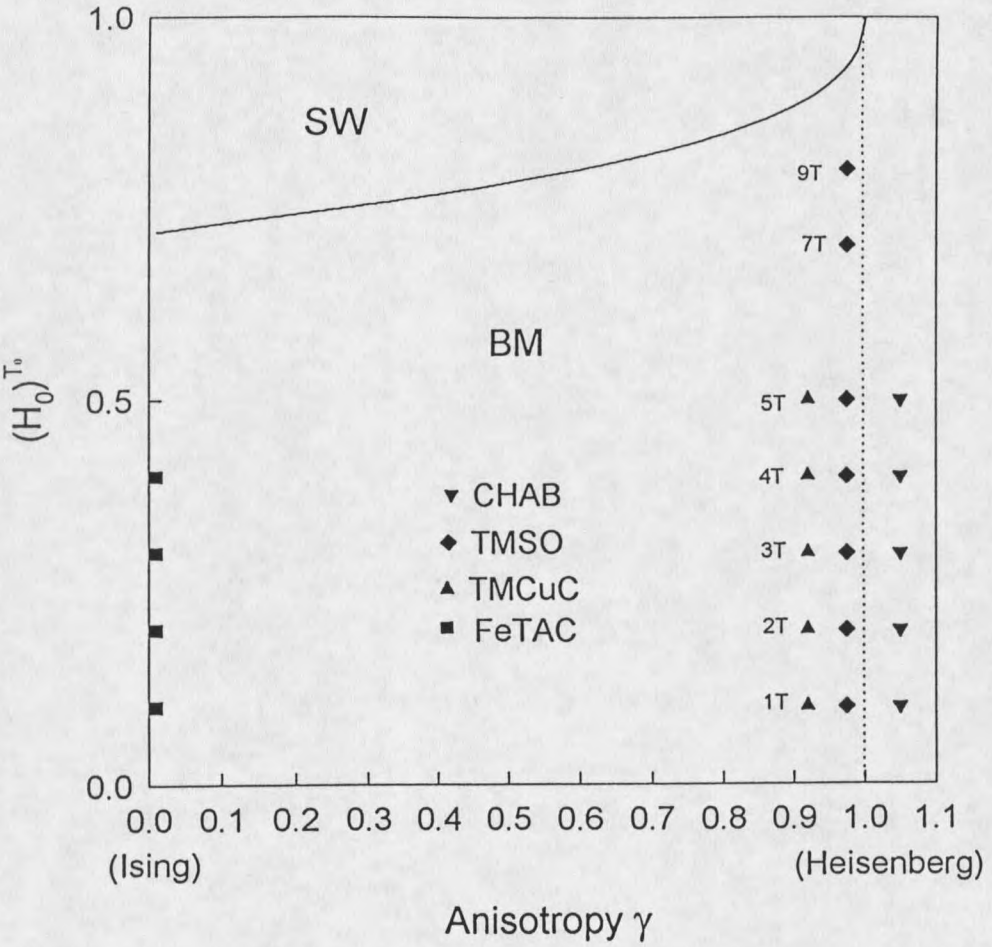


FIG. 21. Regions and corresponding crossover boundary which determine BM and SW dominance on susceptibility as a function of field H and anisotropy γ.[8] Points represent experimental results.

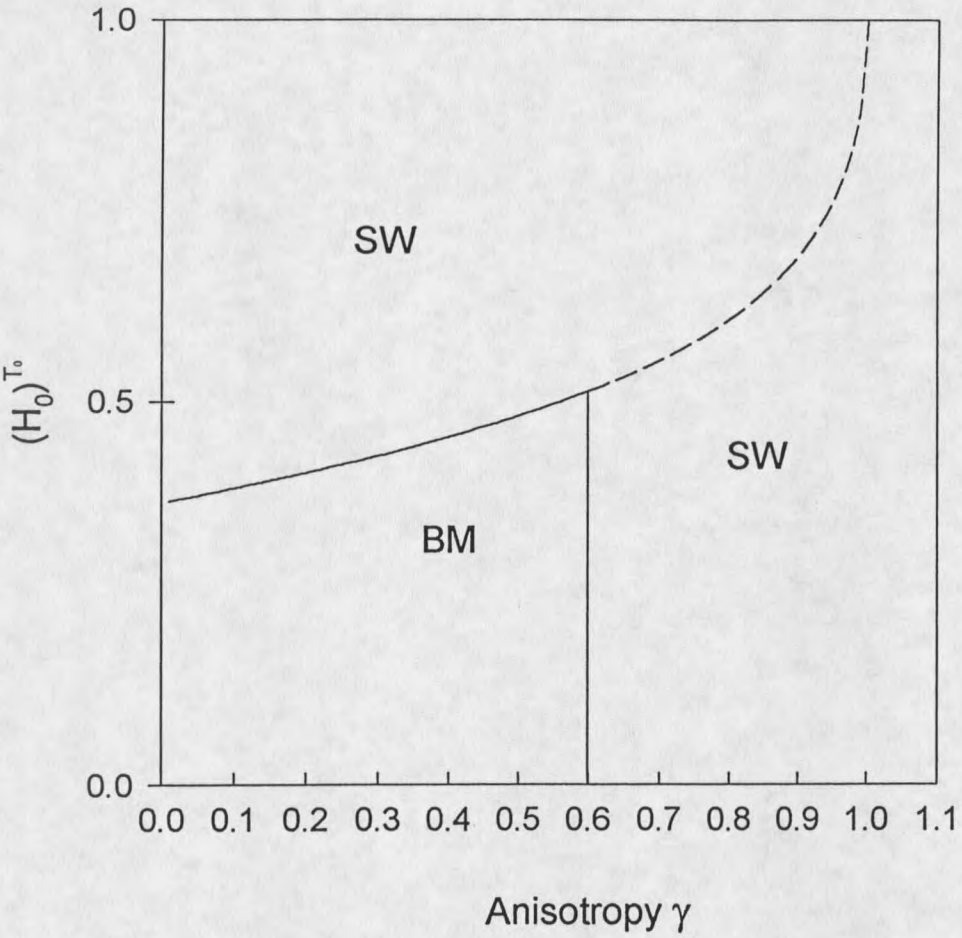


FIG. 22. Regions and corresponding crossover boundary which determine BM and SW dominance on specific heat as a function of field H and anisotropy γ.[8] Points represent experimental results.

the range $0 < \gamma < 1$ and in most of the range of H (except very high field). For specific heat, the situation is very different: spin waves give the main contribution in most of the range of H-γ and BMs dominance only occurs in the range $0 < \gamma < 0.6$ with smaller field H.

4. Experiments

Experimental confirmation for effects of anisotropies on BMs is quite important. Several good 1D spin 1/2 Heisenberg-like ferromagnets CHAB, TMSO, TMCuC, and Ising-like FeTAC permit experimental tests in which range of the γ-H parameter space that BMs dominate susceptibility.

The details of the experimental determination of the susceptibilities of the above compounds were described in Chapter 2. CHAB, TMSO, TMCuC, and FeTAC have γ values of 1.05 (easy-plane), 0.975, 0.92, and 0.05 (Ising), respectively, and were measured in dc fields 0~5 telsa. (TMSO was measured in fields up to 9 telsa at the Lakeshore lab). The experimental data of the BM dominance on susceptibilities at H = 1, 2, 3, 4, 5, 7, and 9T and γ = 1.05, 0.975, 0.92, and 0.05 are shown in Fig.21 by points. We see clearly that the experiments confirm that the BMs exist and dominate susceptibility in the entire range of γ (γ <1.05) with fields up to 9 tesla. The linear spin wave theory can not be applied in these ranges.

In all the above compounds, there exist weak single-ion anisotropies. For example, EPR measurements[19,20,21] on **g** values show (3~10)% values of $\Delta g/g$, which indicate single-ion anisotropies are about $D/J < 0.1$. Unfortunately, this is too weak to observe single-ion BMs, as

the prediction presented in Section 3.2. Single-ion BM effects were not clearly identified in the experimental measurements. Further experiments on stronger D/J systems or spin greater than 1/2 compounds are suggested since in systems with strong single-ion anisotropy the presence of single-ion BMs should increase the possibility of experimental observation of the BM effects.

CHAPTER 4

EFFECT OF SPIN CANTING ON BOUND MAGNONS

1. Introduction to Spin Canting

The thermodynamics of 1D spin 1/2 Heisenberg ferromagnets with the spin canting effect, as far as the author knows, has not been considered yet. In this chapter a succeed attempt to fill this gap by generalizing the formalism[8] of Gaudin and the calculation of Johnson and Bonner[9] from the 1D spin 1/2 Heisenberg model to the modified model with a spin canting term has been made.

The motivation for solving this problem is to explain the experimental data measured in the 1D, spin 1/2, Heisenberg ferromagnetic compounds CHAB, CHAC, TMCuC and TTMCuC in which the existence of spin canting[20,21] is reported . Fitting the susceptibility data to the Johnson and Bonner (JB) model, it is shown that theoretical curve has a generally larger value of susceptibility than the experimental data, as seen in Chapter 2. This suggests that there must be some mechanisms that cause the reduction of the susceptibility. The spin canting effect is considered as one of the mechanisms.

Canted spin structure seems to occur more commonly with 1D chain systems than with 2D or 3D systems. Weak spin canting originates from a coupling between the spins such as the antisymmetric part of the anisotropic exchange interaction, the so-called

Dzyaloshinskii-Moriya (DM) interaction[26]. The Dzyaloshinskii-Moriya interaction was first introduced phenomenologically by Dzyaloshinskii and then derived by Moriya[26] by extending the theory of superexchange interaction to include spin-orbital coupling. The term $\vec{A}\cdot(\vec{S}_1\times\vec{S}_2)$ is the general expression for the DM interaction, where $\vec{A}$ is a constant vector representing the strength of the spin canting. This coupling acts to cant the spins because the coupling energy is minimized when two spins are perpendicular to each other. The crystal symmetry is of particular importance for the **A** vector since some components of it vanish for certain crystal symmetries.

The 1D spin models include the Ising, XY, and Heisenberg models. In the case of the Ising model $\vec{A}\cdot(\vec{S}_1\times\vec{S}_2)$ always is zero because spins are either parallel or antiparallel, therefore there is no DM interaction. In the case of the XY model, A_x and A_y vanish and only the A_z component exists, because all spins lie in the XY plane. In the case of Heisenberg models, if z direction is chosen as the easy axis, usually only the A_z component exists, so $A = A_z$.

The Hamiltonian for the 1D spin 1/2 anisotropic Heisenberg ferromagnet with a spin canting term is

$$H = -J\sum_i^N [S_i^z S_{i+1}^z + \gamma(S_i^x S_{i+1}^x + S_i^y S_{i+1}^y)] + A\sum_i^N (S_i^x S_{i+1}^y - S_i^y S_{i+1}^x) - g\mu_B h\sum_i^N S_i^z . \quad (4.1)$$

In Section 1 the excitation energies of the system, which includes spin wave and bound magnon excitations with the effect of spin canting, is calculated. In Section 2 the thermodynamic properties of the model are solved. In Section 3 the thresholds of spin

canting **A** for BM existence is discussed. In Section 4, comparison with earlier reported results of the 1D spin 1/2 XY-model with spin canting term is made. Finally, a example of consideration of the spin canting effect in fitting experimental susceptibility data is presented.

2. Spin Canting Effect on BM Excitation Energies

Adding a spin canting term does not affect the fact that the Hamiltonian (4.1) commutes with the z component of the total spin $S_{tot}^{z} = \sum_{i}^{n} \mathbf{S}_i^z = 1/2N - n$, and excitation states can still be classified according to the value S^z, or n, the number of spin deviations from the ground state.

A. No Spin Canting: A = 0

First , consider the case without spin canting effects, i.e., A = 0 in Hamiltonian (4.1).

Through the use of Bethe's hypothesis[1], the energy levels of the Hamiltonian (4.1) are given by the coupled equations[27]

$$\mathbf{E} = -\mathbf{J}\sum_{a=1}^{n}(\cos\kappa_a - \gamma) - \mathbf{h}\mathbf{S}^z \qquad (4.2.1)$$

with

$$\mathbf{e}^{\mathbf{i}\mathbf{N}\mathbf{k}_a} = \prod_{\substack{b=1 \\ b\neq a}}^{n} \mathbf{e}^{\mathbf{i}\psi_{ab}} \qquad a=1, 2, ..., n. \qquad (4.2.2)$$

It is easier to manipulate the above equations if one parametrizes the κ_a and ψ_{ab} by applying the following transformations $\kappa_a \leftrightarrow \phi_a$, in the range $\gamma < 1$ and $\gamma > 1$ respectively.

For $\gamma < 1$, the easy-axis anisotropy case:[27]

$$e^{ik_a} = \frac{1 - e^{\Phi - i\phi_a}}{e^{\Phi} - e^{-i\phi_a}} \tag{4.2.3}$$

$$e^{i\psi_{ab}} = \frac{1 - e^{2\Phi - i(\phi_a - \phi_b)}}{e^{2\Phi} - e^{-i(\phi_a - \phi_b)}} \tag{4.2.4}$$

with

$0 \le \kappa_a \le 2\pi$, and $-\pi \le \phi_a \le \pi$, and $-\pi \le \psi_{ab} \le \pi$,.

Φ is defined by

$\cosh\Phi = 1/\gamma$, $0 \le \Phi \le \pi/2$.

For $\gamma > 1$, the easy-plane anisotropy case,

$$e^{ik_a} = \frac{1 - e^{i\Phi + \phi_a}}{e^{i\Phi} - e^{\phi_a}} \tag{4.2.5}$$

$$e^{i\psi_{ab}} = \frac{1 - e^{2i\Phi + (\phi_a - \phi_b)}}{e^{2i\Phi} - e^{(\phi_a - \phi_b)}} \tag{4.2.6}$$

where $\cos\Phi = 1/\gamma$, $0 \le \Phi \le \pi/2$.

For large N, for any particular solution of the coupled equations (4.2.1) and (4.2.2), the ϕ_a are grouped in strings characterized by an order p and common real value ϕ, i.e., $\phi_u = \phi + i\mu\Phi$, where $\mu = -(p-1), -(p-3), \ldots, (p-1)$. Bound magnons are characterized by taking p equal to n.[27]

The total momentum K of a BM is related to the κ_a by

$$K = \sum_{a=1}^{n} \kappa_a = 2\pi m / N \tag{4.2.7}$$

where m is an integer and K is restricted to the first Brillouin zone, $0 \le K \le 2\pi$.

To obtain the relation between the total momentum K of the BM and the real value ϕ of the ϕ_a, one forms (for $\gamma < 1$)

$$e^{i\Sigma_a k_a} = \prod_{u=-(p-1)}^{p-1} (1 - e^{\Phi + u\Phi - i\phi}) / (e^{\Phi} - e^{u\Phi - i\phi}) \quad \text{with } p = n \tag{4.2.8}$$

and, in performing the product, one gets

$$e^{iK} = \frac{1 - e^{n\Phi - i\phi}}{e^{n\Phi} - e^{-i\phi}} . \tag{4.2.9}$$

To extract the energies of the bound magnons as function of total momentum K, one expresses the $\cos\kappa_a$ in Eq.(4.2.1) by its exponential form, substitutes Eq.(4.2.3) for the $e^{\pm ika}$, sums the resulting expression over the string, and using Eq.(4.2.9), writes the resulting expression in terms of K: (which has same form as Eqs.(2.1.8)-(2.1.10))

$$\gamma < 1: \; E_n = nh + \gamma J \frac{\sinh\Phi}{\sinh(n\Phi)} [\cosh(n\Phi) - \cos K] \quad (1/\gamma = \cosh\Phi); \tag{4.2.10}$$

$$\gamma > 1: \; E_n = nh + \gamma J \frac{\sin\Phi}{\sin(n\Phi)} [\cos(n\Phi) - \cos K] \quad (1/\gamma = \cos\Phi); \tag{4.2.11}$$

$$\gamma = 1: \; E_n = nh + \frac{J}{n}(1 - \cos K). \tag{4.2.12}$$

B. Spin Canting $A \neq 0$

It has been shown[28] that the spin canting primarily affects the dependence of the magnon energy on the momentum. In the one spin-flipped state, the energy dispersion curve shifts by k_0, and an n-spin-flipped state causes a shift of nk_0. The energy levels of the Hamiltonian have the form

$$E = -J\sum_{a=1}^{n}[\cos(\kappa_a - \kappa_0) - \beta] - hS^z \tag{4.2.13}$$

with momentum

$$K - n\kappa_0 = \sum_{a=1}^{n}(\kappa_a - \kappa_0). \tag{4.2.14}$$

The following definitions are introduced:

$$\kappa_0 = -\operatorname{arctg}(A/J), \tag{4.2.15}$$

$$\beta = (1/\gamma)\cos\kappa_0 = J/(A^2 + \gamma^2 J^2)^{1/2}, \tag{4.2.16}$$

which plays the role of an effective anisotropy. $\beta > 1$ is the effective anisotropy of the easy-axis type. $\beta < 1$ is the effective anisotropy of the easy-plane type.

To obtain the energies of BM with spin canting effects, we use a process similar to Eqs.(4.2.3) - (4.2.12). In this case, Eq. (4.2.3) becomes

$$e^{i(k_a - k_0)} = \frac{1 - e^{\Phi - i(\phi_a - \phi_0)}}{e^{\Phi} - e^{-i(\phi_a - \phi_0)}}, \tag{4.2.17}$$

comparing with Eq.(4.2.3), a shift of k_0 corresponds a shift of ϕ_0.

$$e^{i\Sigma_a(k_a - k_0)} = \prod_{u=-(n-1)}^{n-1}(1 - e^{\Phi + u\Phi - i(\phi - \phi_0)})/(e^{\Phi} - e^{u\Phi - i(\phi - \phi_0)}) \tag{4.2.18}$$

$$e^{i(K-nk_0)} = \frac{1-e^{n\Phi-i(\phi-\phi_0)}}{e^{n\Phi}-e^{-i(\phi-\phi_0)}} \qquad (4.2.19)$$

with $\beta = \cosh\Phi > 1$ or $\beta = \cos\Phi < 1$ in $0 \le \Phi \le \pi/2$. Comparing with the A=0 case, it can be see that β replaces $1/\gamma$.

Finally, we get the results of BM energies with the spin canting effect, which are

$$\beta > 1: E_n = nh + \frac{J}{\beta}\frac{\sinh\Phi}{\sinh(n\Phi)}[\cosh(n\Phi) - \cos(K + n\kappa_0)] \quad (\beta=\cosh\Phi) \qquad (4.2.20)$$

$$\beta < 1: E_n = nh + \frac{J}{\beta}\frac{\sin\Phi}{\sin(n\Phi)}[\cos(n\Phi) - \cos(K + n\kappa_0)] \quad (\beta=\cos\Phi) \qquad (4.2.21)$$

$$\beta = 1: E_n = nh + \frac{J}{n}[1 - \cos(K + n\kappa_0)] \; . \qquad (4.2.22)$$

It is noted that the same result for E_n was obtained[28] earlier by the diagonalization of Hamiltonian of Eq.(4.1) in the wavefunction space (which is wavefunction of BM) and the solution of Schrodinger's equation.

It can be seen then that the spin canting affects the dependence of the BM excitation energy on the momentum K. The dispersion curve is no longer even in K, the center of Brillouin zone is shifted by nk_0 from the point K=0. The shape of dispersion curves remain unchanged except for a factor change from γ to $1/\beta$. The spin canting effect on excitation energy of 2-BM is shown in Fig.23. The solid line is for A = 0 case, and the dashed line is for $A \neq 0$.

3. Spin Canting Effect on Thermodynamics

As discussed before, the two principal contributions to the low-T thermodynamics of

Spin canting effect on bound magnon energy

Solid line: A=0 Dashed line: A/J=0.5 k_0=arctg(A/J)

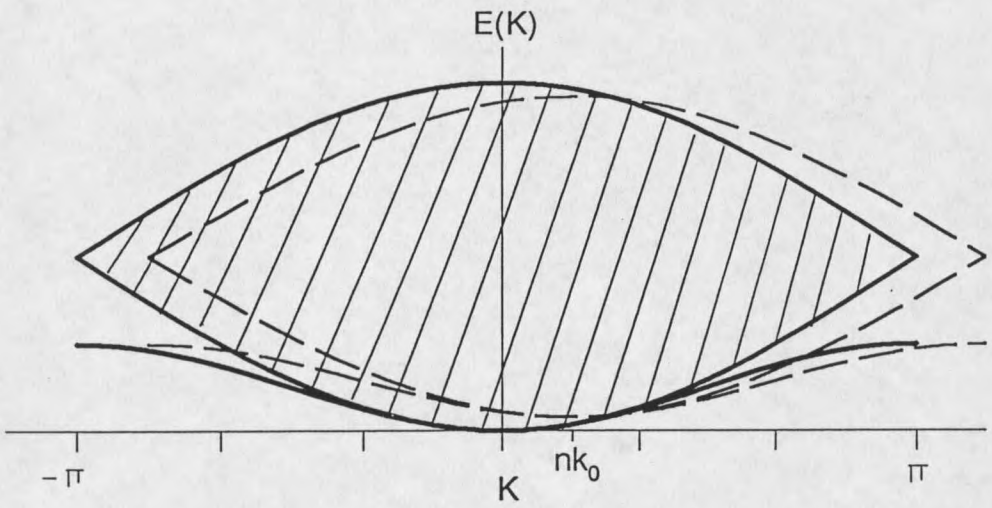


FIG. 23. Spin canting effect on bound magnon energy.

1D Heisenberg system are from the spin wave excitations and the bound magnons excitations. The results of thermodynamics of BM without spin canting effects have been obtained by Gaudin's formalism and JB's method, and presented in Eqs.(2.2.5)-(2.2.8) in Chapter 2. In order to derive the thermodynamics with spin canting effect, several steps of Gaudin's formalism and JB's method need to be illustrated here.

A. No Spin Canting: **A** = 0

Gaudin[8] derived the equations for the free energy per spin (for $\gamma < 1$):

$$\mathbf{F(T) = nh - \frac{T}{2\pi}\int_{-\pi}^{\pi} dn(\phi) \ln[1+\exp(\varepsilon_1(\phi)/T)]d\phi}\ , \qquad (4.3.1)$$

where ϕ is defined by Eq.(4.2.3) in Sec. 2, and $\mathbf{dn}(\phi)$ is defined by

$$\mathbf{dn(\phi) = \frac{1}{2}\sum_{l} \frac{e^{il\phi}}{\cosh(l\phi)}}\ . \qquad (4.3.2)$$

The $\mathbf{dn}(\phi)$ is given by $\mathbf{dn}(\phi) = (K_k/\pi)\ \mathbf{dn}(\phi \mathbf{K_k}/\pi, \mathbf{k})$, where K_k is the complete elliptic integral of the first kind and $\mathbf{dn}(\phi, \mathbf{k})$ is one of the Jacobian elliptic functions with the period 2π.

For n = 1[8]

$$\mathbf{\varepsilon_1(\phi) = \frac{T}{2\pi}\int_{-\pi}^{\pi} dn(\phi-\phi') \ln[1+\exp(\varepsilon_2(\phi')/T)]d\phi' - J \sinh\Phi\, dn(\phi)}\ , \qquad (4.3.3)$$

where $\cosh \Phi = 1/\gamma$.

For n≥2[8]

$$\varepsilon_n(\phi) = \frac{T}{2\pi}\int_{-\pi}^{\pi} dn(\phi-\phi')\ln[(1+\exp(\varepsilon_{n+1}(\phi')/T)(1+\exp(\varepsilon_{n-1}(\phi')/T)]d\phi' \qquad (4.3.4)$$

A point to note is that the $\varepsilon_n(\phi)$ are not energy dispersion curves, although they are related to them. The boundary condition on the set of equations for the $\varepsilon_n(\phi)$ are

$$\lim_{n\to\infty}\varepsilon_n(\phi)/n = h\,. \qquad (4.3.5)$$

As **n** increases, the $\varepsilon_n(\phi)$ goes to a constant independent of both **n** and ϕ.

Equations (4.3.1) through (4.3.4) completely determine the free energy F(T). Clearly, to determine the F(T), an expression for the function $\varepsilon_1(\phi)$ must be found. Johnson and Bonner[9] have solved the above set of coupled, nonlinear, integral equations. Using a low temperature expansion, the result is

$$\varepsilon_1(\phi) = \varepsilon_1(\phi)^{(1)} + \varepsilon_1(\phi)^{(2)} + \varepsilon_1(\phi)^{(3)} + \ldots\,, \qquad (4.3.6)$$

where $\varepsilon_1(\phi)^{(1)}$, $\varepsilon_1(\phi)^{(2)}$ and $\varepsilon_1(\phi)^{(3)}$ are first, second and third order of the expansion respectively. From Eq.(4.3.4) it is observed that $\varepsilon_n(\phi) > 0$ for all n and ϕ. Therefore, in Eq(4.3.4) for small temperatures, the exponentials are large. $\varepsilon_n(\phi)^{(2)}$ are observed to be exponentially small in T and $\varepsilon_n(\phi)^{(3)}$ is exponentially smaller in T than $\varepsilon_n(\phi)^{(2)}$. $\varepsilon_1(\phi)$ has the form[9]:

$$\varepsilon_1(\phi) = nh + \sinh\Phi\, g_1(\phi)$$

$$+ \frac{T}{2\pi}\int_{-\pi}^{\pi} g_2(\phi-\phi')\ln[1+\exp(-\varepsilon_1(\phi')^{(1)}/T)]d\phi' + 2T\, e^{-\sinh\phi/2T} + \ldots \qquad (4.3.7)$$

where

$$g_n(\phi) = \sinh(n\Phi) / [\cosh(n\Phi) - \cos\phi] \quad . \tag{4.3.8}$$

The $\varepsilon_1(\phi)$ is periodic function with the period 2π. As will see later this periodic property gives a free energy independent of the shift of ϕ.

The results for F(T), M(T), χ(T) and C_h(T) are presented in Eqs.(2.2.5) - (2.2.8) in Chapter 2.

B. Spin Canting $A \neq 0$

The question then is whether or not Gaudin's formalism and JB's method may be used on more complex systems such as a system including spin canting effect, and whether it can be used to predict the behavior of such systems. Here we will prove that Gaudin's formalism and JB's method can be generalized to calculate the thermodynamics for the modified Hamiltonian with a spin canting term.

When $A \neq 0$: the energy dispersion curve (as a function k) shifts k_0 with a corresponding shift ϕ_0 in ϕ, as discussed in Sec. 2. It can be seen from

$$e^{ik_a} = \frac{1 - e^{\Phi - i\phi_a}}{e^{\Phi} - e^{-i\phi_a}} , \tag{4.3.9}$$

to

$$e^{i(k_a - k_0)} = \frac{1 - e^{\Phi - i(\phi_a - \phi_0)}}{e^{\Phi} - e^{-i(\phi_a - \phi_0)}} . \tag{4.3.10}$$

Therefore $\phi \rightarrow \phi - \phi_0$ and $\varepsilon_n(\phi) \rightarrow \varepsilon_n(\phi - \phi_0)$, so that Eq.(4.3.1) becomes

$$F(T) = nh - \frac{T}{2\pi}\int_{-\pi}^{\pi} dn(\phi-\phi_0)\ln[1+\exp(\varepsilon_1(\phi-\phi_0)/T)]d\phi$$
$$= nh - \frac{T}{2\pi}\int_{-\pi}^{\pi} dn(\phi)\ln[1+\exp(\varepsilon_1(\phi)/T)]d\phi. \quad (4.3.11)$$

Here

$$\varepsilon_1(\phi-\phi_0) = nh + \sinh\Phi\, g_1(\phi-\phi_0)$$
$$+\frac{T}{2\pi}\int_{-\pi}^{\pi} g_2(\phi-\phi_0-\phi')\ln[1+\exp(-\varepsilon_1(\phi')^{(1)}/T)]d\phi' + 2T\, e^{-\sinh\Phi/2T} + \ldots . \quad (4.3.12)$$

Note that here $\cosh\Phi = \beta$ replaces $\cosh\Phi = 1/\gamma$ in A =0 case.

Because all functions of ϕ involved in the free energy are periodic with period 2π, ϕ can be restricted to be one period without loss of generality, i.e., a shift in ϕ_0 does not effect the values of F(T). It can be seen that the free energy is only effected by the factor change $\gamma \to 1/\beta$.

By replacing $1/\gamma$ with $\beta = J/(A^2+\gamma^2J^2)^{1/2}$, the thermodynamic properties with spin canting effects become:

$$M = h/[h^2/4 + T^2\exp(-\sqrt{J^2/(A^2+\gamma^2J^2)} - 1/T)]^{1/2}/4$$
$$-T\exp(-(\sqrt{J^2/(A^2+\gamma^2J^2)} - 1)/T)[\exp(-h/T) - 1]/\sqrt{2\pi T} \quad (4.3.13)$$

$$\chi = T^2\exp(-\sqrt{J^2/(A^2+\gamma^2J^2)} - 1/T)$$
$$/4[h^2/4 + T^2\exp(-\sqrt{J^2/(A^2+\gamma^2J^2)} - 1/T)]^{3/2} \quad (4.3.14)$$
$$+\exp(-(\sqrt{J^2/(A^2+\gamma^2J^2)} + h - 1))/\sqrt{2\pi T}$$

$$C_h = (J^2/(A^2+\gamma^2J^2)-1)\exp(-\sqrt{J^2/(A^2+\gamma^2J^2)-1}/T)$$
$$\times[h^2/2+T^2\exp(-\sqrt{J^2/(A^2+\gamma^2J^2)-1}/T)]$$
$$/4T[h^2/4+T^2\exp(-\sqrt{J^2/(A^2+\gamma^2J^2)-1}/T)]^{3/2} \qquad (4.3.15)$$
$$+[\sqrt{J^2/(A^2+\gamma^2J^2)}+h-1]^2\exp(-(\sqrt{J^2/(A^2+\gamma^2J^2)}+h-1))/\sqrt{2\pi T^3}$$

The spin canting effect on the susceptibility and specific heat are plotted in Fig.24 and Fig.25. The solid lines represent $A \neq 0$, and the dashed line is for $A = 0$. These results show that the spin canting shifts the temperature dependence of χ and C_h to higher temperatures and slightly reduce χ_{max}.

A simple approach to understand spin canting effects on thermodynamics can be obtained from the free energy expression F(T) given by Eq.(2.2.4) in Chapter 2 and the BM energy expression $E_n(K)$ as function of K given by Eq.(4.2.10). From $E_n(K)$, although the center of the Brillouin zone is effectively shifted by $n\kappa_0$ from the point $K = 0$ by the spin canting, the energy dependence of K inside the Brillouin zero is not changed. So the thermodynamic of both bound magnons and spin waves, which is calculated inside one Brillouin zone, is not influenced by the shift $n\kappa_0$ of K. What does affect the thermodynamics function F(T) is a change of the factor $\gamma \rightarrow 1/\beta$ or $\cosh\Phi=1/\gamma \rightarrow \cosh\Phi=\beta$ in $E_n(K)$ due to spin canting. Therefore, we conclude that spin canting effect on thermodynamics is equivalent to changing exchange anisotropy γ of the system, and it shifts the temperature dependence of thermodynamic properties to higher temperatures.

4. Threshold of Spin Canting Effect on Bound Magnons

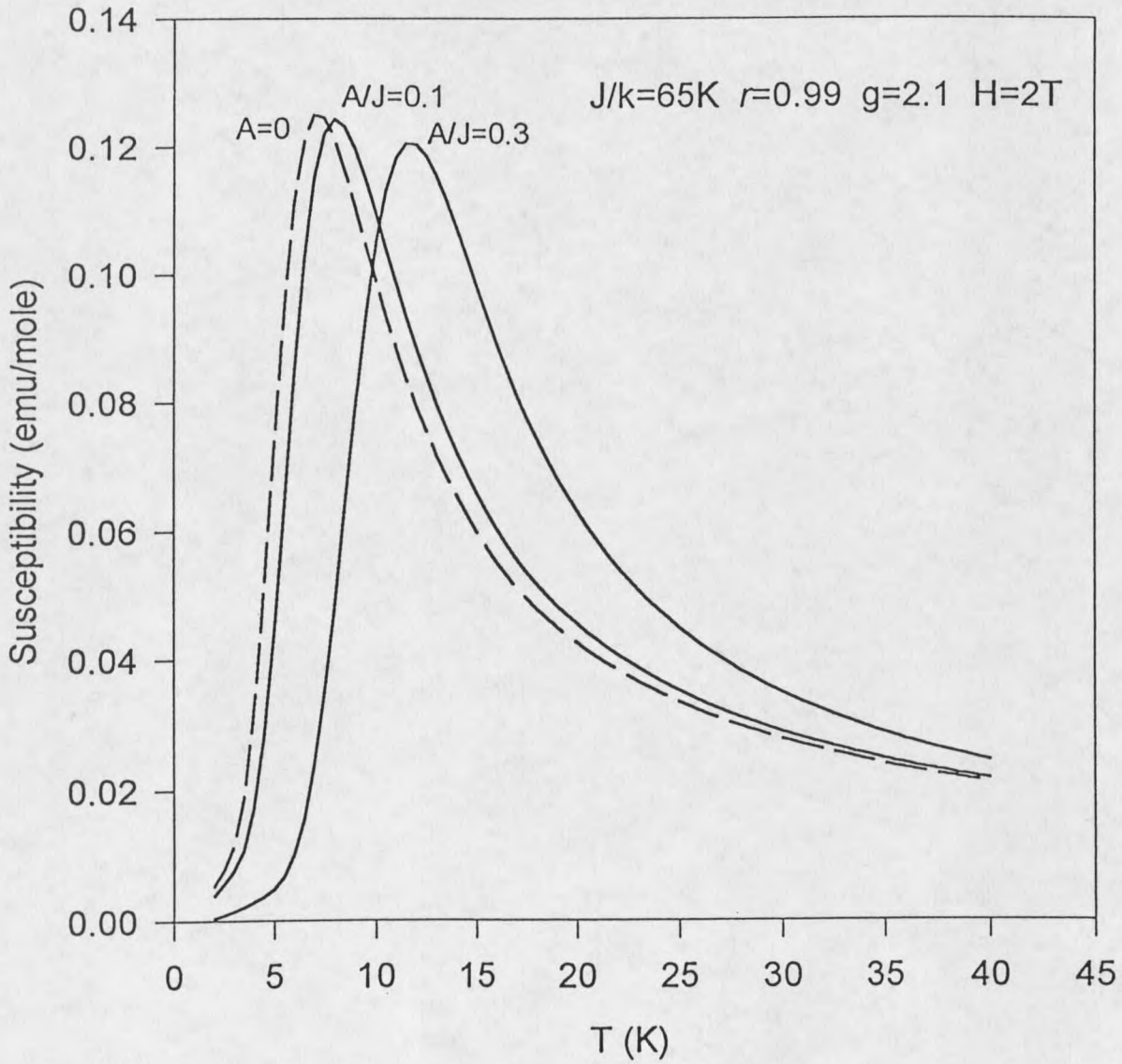


FIG. 24. Spin canting effect on susceptibility.

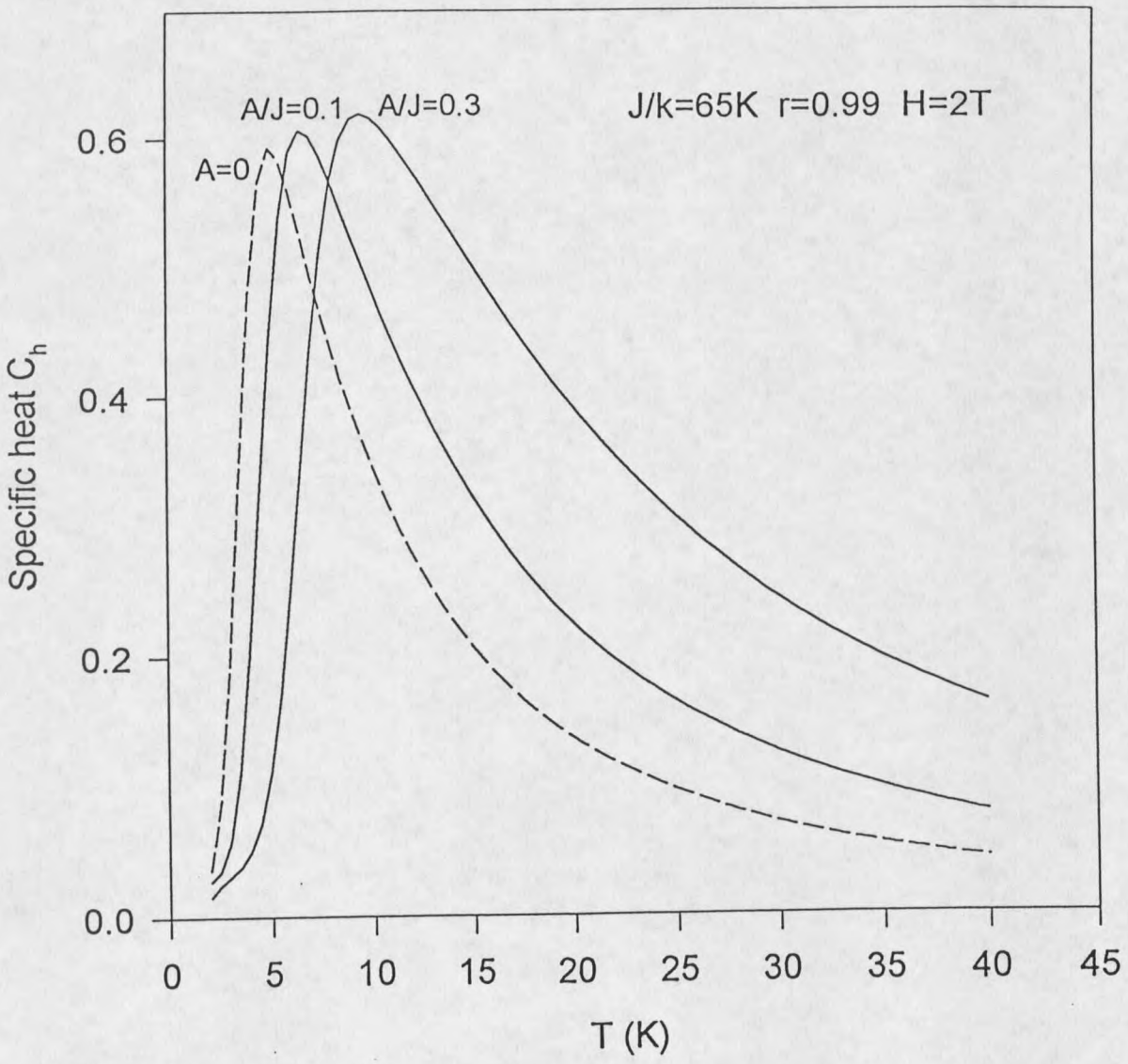


FIG. 25. Spin canting effect on specific heat.

To get thresholds of spin canting effect on BM, we use an analysis analogous to that carried out in Section 3 of Chapter 3 for A = 0 case.

In the case of effective easy-axis $\beta > 1$, BM exists for all β values, similar to the case of $\gamma > 1$[7] in Chapter 3. From

$$\beta = 1/\gamma \cos\kappa_0 = J/(A^2+\gamma^2 J^2)^{1/2} > 1 \qquad (4.4.1)$$

the values of A for BM existence in the $\beta > 1$ is:

$$A < J(1 - \gamma^2)^{1/2} \qquad (4.4.2)$$

In the case of an effective easy-plane $0 \leq \beta \leq 1$, generally speaking, BM do not exist for all values $0 \leq \beta \leq 1$. For a given number of flipped spins n, the region of BM existence are a set of intervals of values β, the lengths and numbers of those intervals are determined by n.

The requirement that the wavefunction of BM be bounded gives the following inequalities, which has the similar form as the Eq. (3.3.4) in Chapter 3:

$$\sin(v\Phi)\sin(n-v)\Phi\,[\cos(n\Phi)-\cos(K+nk_0)] > 0 \quad v=1, 2, 3, ..., n-1. \qquad (4.4.3)$$

where Φ must be such that

$$\sin(n\Phi) \neq 0,$$

$$\Phi \neq l\pi/n, \qquad l=1, 2, ...n/2. \qquad (4.4.4)$$

The number l can be regarded as the label of the allowed interval for Φ. The l-th allowed interval of values of Φ is determined by the inequalities[7]

$$\max\,[m\pi/(mn/l+1)] < \Phi < \min\,[m\pi/(mn/l)] \qquad (4.4.5a)$$

$$\max [m\pi/(mn/l+1)] < \arccos[J/(A^2+\gamma^2J^2)^{1/2}] < \min [m\pi/(mn/l)] \qquad (4.4.5b)$$

where m = 1, 2, ..., l-1.

Thus for a fixed number of n, in the above sets of overlapping intervals of values of Φ, or values of γ and **A**, it is possible for BM to exist.

In the region of allowed values of K, for intervals with even l, $\cos n\Phi < \cos(K+nk_0)$, and K from the neighborhood of $K = -nk_0$ are admissible, while for intervals with odd l, $\cos n\Phi > \cos(K+nk_0)$, and K from the neighborhood of $K = \pm\pi - nk_0$ are admissible. Thus BM with K = 0 can not exist in a system with the spin canting.

5. Comparison with Spin Canting Effect on XY Model

For comparison, the thermodynamics of an XY model with spin canting term is presented here. Generally, one expects an XY model system to behave as intermediate between Ising and Heisenberg systems. The influence of the spin canting on the thermodynamics of the 1D, spin 1/2, XY model has been calculated recently by Derzhko[29].

The Hamiltonian of the 1D, spin 1/2, XY model with spin canting term is

$$H = -J\sum_i^n (S_i^x S_{i+1}^x + S_i^y S_{i+1}^y) + A\sum_i^n (S_i^x S_{i+1}^y - S_i^y S_{i+1}^x) - g\mu H\sum_i^n S_i^z . \qquad (4.5.1)$$

The additional term of spin canting still keeps the model in the class of 1D, spin 1/2, XY models because including the spin canting term does not change the symmetry of the Hamiltonian and only leads to changes in the values of constants. However, after the

diagonalization, the spectrum of energies E(K) no longer is an even function of K, which only leads some technical complications in the calculation of thermodynamics.

The Hamiltonian (4.5.1) after a Jordan-Wigner transformation will have quadratic forms in Fermi operators[29]. The diagonalization of quadratic forms is completed by a Bogolyubov transformation[29]. The result has the form[29]

$$H = \sum_k E_k (\beta_k^+ \beta_k - 1/2) \tag{4.5.2}$$

where β_k is Fermi type operators, which obey $\{\beta_k, \beta_{k'}^+\}=\delta_{kk'}$, $\{\beta_k, \beta_{k'}\}=\{\beta_k^+, \beta_{k'}^+\}=0$.

The excitation energies E_k have the form[29]

$$E_k = A \sin K \pm [(h + J\cos K)^2 + A^2 \sin^2 K]^{1/2} \tag{4.5.3}$$

The spectrum E_k no longer is an even function of K because of the spin canting term in the Hamiltonian. This is connected with the absence of symmetry with respect to spatial inversion.

The free energy per spin in the limit $N\to\infty$ is[29]

$$\begin{aligned}
F &= -\frac{1}{\beta}\lim_{N\to\infty}\left\{\frac{1}{N}\ln \mathrm{Tr}\exp(-\beta H)\right\} \\
&= -\frac{1}{\beta}\lim_{N\to\infty}\left\{\frac{1}{N}\ln \mathrm{Tr}\prod_k \exp[-\beta E_k(\beta_k^+\beta_k - 1/2)]\right\} \\
&= -\frac{1}{\beta}\lim_{N\to\infty}\left\{\frac{1}{N}\ln \prod_k 2\cosh(\beta E_k/2)\right\} \\
&= -\frac{1}{\beta}\lim_{N\to\infty}\left\{\frac{1}{N}\sum_k \ln[2\cosh(\beta E_k/2)]\right\} \\
&= -\frac{1}{\beta}\frac{1}{2\pi}\int_{-\pi}^{\pi} dk \ln[2\cosh(\beta E_k/2)]
\end{aligned} \tag{4.5.4}$$

The specific heat, the transverse magnetization and susceptibility become[29]

$$C = \frac{1}{2\pi}\int_{-\pi}^{\pi} dk(\beta E_k/2)^2 \cosh^{-2}(\beta E_k/2),$$

$$M = -\frac{1}{4\pi}\int_{-\pi}^{\pi} dk \frac{\partial E_k}{\partial h}\tanh(\beta E_k/2), \qquad (4.5.5)$$

$$\chi = -\frac{1}{4\pi}\int_{-\pi}^{\pi} dk \frac{\partial^2 E_k}{\partial^2 h}\tanh(\beta E_k/2) - \frac{\beta}{8\pi}\int_{-\pi}^{\pi} dk\left(\frac{\partial E_k}{\partial h}\right)^2 \cosh^{-2}(\beta E_k/2).$$

The results of numerical calculations[29] of C and M are shown in Fig.26, where dashed lines are for A = 0 and the solid lines are for A ≠ 0. They clearly show that the presence of the spin canting influences the thermodynamics of the system. The spin canting decreases magnetization at certain fields and shifts the temperature dependence of C, similar to the situation in the Heisenberg model, except here the magnitude of the shift is smaller than in the Heisenberg case.

6. Experiment

Comparison to the experimental data may clarify whether the spin canting model is appropriate to characterize the measurements.

The existence of spin canting has been reported[20,21] in several 1D spin 1/2 Heisenberg ferromagnetic compounds such as CHAC, CHAB, TMCuC and TTMCuC. Among these compounds, CHAC has strongest spin canting and is chosen to test above theoretical calculation.

The crystal structure[21] of $[C_6H_{11}NH_3]CuCl_3$, cyclohexylammonium trichlorocuprate(II) (CHAC), is orthorhmobic, space group $P2_12_12_1$ with a = 19.441(5), b = 8.549(2) and c =

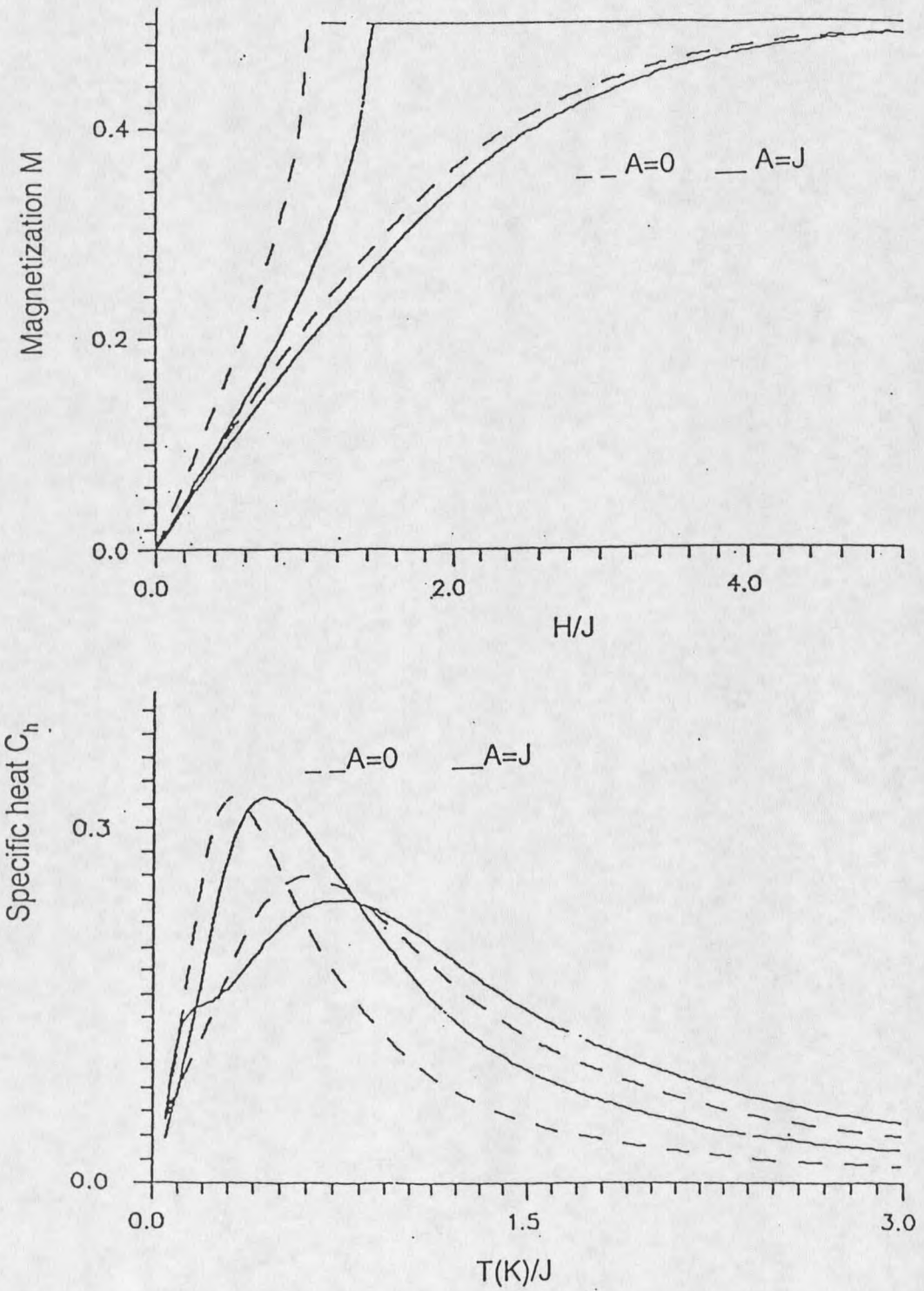


FIG. 26. Spin canting effect on thermodynamics of 1D spin 1/2 XY-model.[29]

6.190(1)A. The salt contains chains of $CuCl_3$- ions along the *c* axis. It was reported earlier[21] that this compound behaves as a 1D spin 1/2 Heisenberg ferromagnet with J/k = 70K and is one of the best known approximations to the 1D Heisenberg ferromagnet. The interchain interactions are $J'/J \sim 10^{-4}$ and the 3D ordering states is below 1.5K. A small exchange anisotropy $\gamma \approx 0.995$ is found[21] in the intrachain interaction.

From the earlier reported measurements[21], the spins lie nearly in the *ab* plane and the intrachain interaction has an antisymmetric component **A**. This interaction causes the ferromagnetically coupled spins in a chain to be somewhat tilted with respect to each other. The magnitude of the antisymmetric intrachain interaction or spin canting can be estimated from the **g** value anisotropy, i.e., $A/J \sim 2\nabla \mathbf{g}/g_e$. The **g** values of CHAC were determined from EPR measurements using a single crystal at T = 80K[21]. A **g** tensor was found with orthorhombic symmetry, with values g_a=2.090(2), g_b=2.234(2) and g_c=2.122(2). These values indicate that the symmetry is nearly axial with $g_b = g_{//} > g_{\perp}$. The magnitude of spin canting therefore is $A/J \sim 2(g_b-2)/2 = 0.23$. The spins are thus titled at an angle of $(A/J)/2 \sim 7^0$ (degree) out of the *ab* plane.

The *ac* susceptibility of a powder crystal sample of CHAC was earlier[13] measured from temperatures of 4.2K to 40K in *dc* fields of 0, 1, 2, 3 tesla. The experimental data[13] is shown in Fig.27 by dots. This data was fit[13] by the JB model with parameters J/k = 78K, γ^* = 0.975, shown by dashed and solid lines in Fig.27. The magnitude of experimental data is smaller than JB model because the measured susceptibility of a powder sample consists of an average of easy-axis and hard-axis single crystal susceptibility. However, the value of

exchange anisotropy $\gamma^* = 0.975$ is smaller than the value $\gamma \approx 0.995$ reported in other experiments[21]. Whereas all theoretical studies of spin 1/2 anisotropic Heisenberg chains indicate that a small change in anisotropy dramatically affects thermodynamic properties, the effect caused by the difference between $\gamma = 0.995$ and $\gamma^* = 0.975$ should not be ignored.

To compare with the susceptibility difference between $\gamma^* = 0.975$ and $\gamma = 0.995$, susceptibility curves of JB model with J/k = 78K, $\gamma = 0.995$ are shown in Fig. 27 by solid lines. From Fig.27, it can be seen that susceptibilities has a temperature dependent shift when $\gamma = 0.995$ changes to 0.975. According to the analysis of spin canting effects on susceptibility, which predicts that spin canting effect is equivalent to changing exchange anisotropy γ of the system and cause susceptibility to has a temperature dependent shift to higher temperature, the disagreement between the data fit $\gamma^* = 0.975$ and $\gamma = 0.995$ can be explained by the spin canting effect. The difference of anisotropy values between γ and γ^* is equivalent to the difference between $A = 0$ and $A \neq 0$. The change from γ to γ^* corresponds the change from $A = 0$ to $A \neq 0$ (A/J~0.23) due to the spin canting effect. Therefore, spin canting effect should cause $\gamma^* = J/(A^2+\gamma^2J^2)^{1/2} = 1/[0.23^2+0.995^2)^{1/2} = 0.977$. (It is close to the value 0.975).

As shown in Fig.27, the data fit with $\gamma^* = 0.975$ ($A \neq 0$) is reasonably good, and it is generally better in higher temperature data range. The data fit with $\gamma = 0.995$ ($A = 0$) is only good at very low temperatures. Therefore, spin canting model gives a better explanation of data in this system.

In conclusion to this chapter, the presence of the spin canting in the 1D spin 1/2 Heisenberg ferromagnet leads the energy spectrum of BM shift of nk_0 on the momentum K, and a factor change of exchange anisotropy from γ to $1/\beta$ for the BM energies. The thermodynamics of the system is not affected by the shift of momentum K, but rather by the factor change γ to $1/\beta$ due to spin canting. In other words, the spin canting effect is equivalent to changing exchange anisotropy γ of the system. It has been shown that spin canting effect shifts the temperature dependence of $\mathbf{C_h}$ and χ to higher temperatures, and slightly reduces χ_{max}. From the experiment on CHAC, considering spin canting effects in the system gives a better description of susceptibility data.

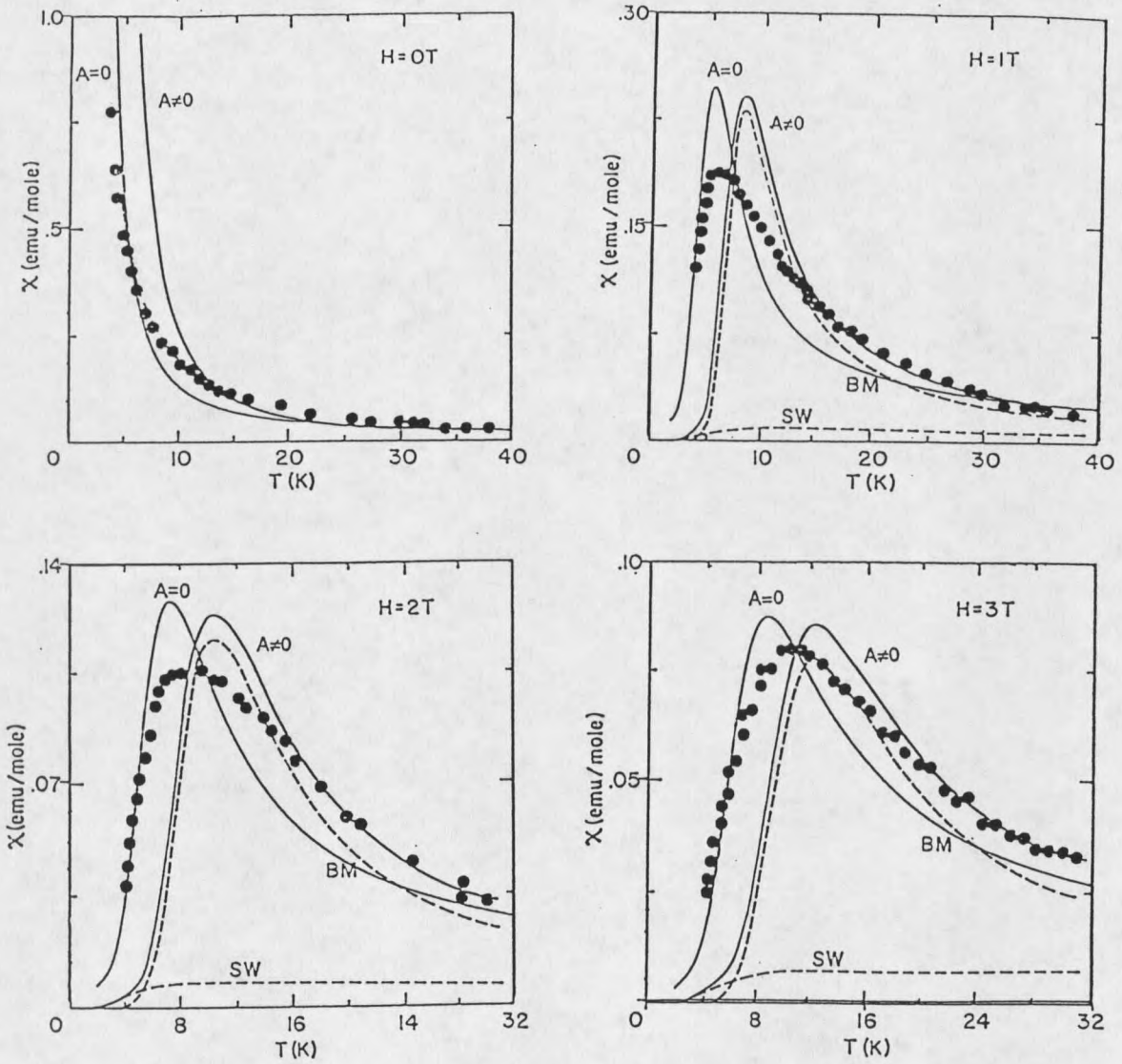


FIG. 27. Susceptibility[13] of CHAC with consideration of spin canting effect. A=0 curves represent the susceptibility without spin canting effect (γ=0.995); A≠0 curves represent the susceptibility with spin canting effect (γ^*=0.975).

CHAPTER 5

COMPARISON OF BOUND MAGNONS AND SOLITONS

The importance of bound magnons is further underscored when considering magnetic solitons since they are closely related. Solitons are characteristic non-linear excitations in 1D ferromagnets and are basically a property of the classical solution of the system, whereas BMs are a quantum feature of the system. Both BMs and solitons are a consequence of inherent nonlinearities. Originally, our investigation of solitons in the BM-bearing spin chain was motivated mainly by interpreting experimental susceptibility of BM-bearing systems, in which the experimental data always have lower values than that of the theoretical BM model in some temperature range. Important questions arise whether other types of excitations such as soliton excitations should be considered in the quantum BM-bearing spin chain and have contributions in experimentally observed susceptibility. How the classical soliton is related to the quantum BM has not been fully elucidated. A comparison of experimental data to the BM model and an appropriate soliton model not only enhances physical understanding of BMs and solitons, but also provides insights importance to the quantum soliton problem.

In this chapter, a comparative study of bound magnons and solitons, i.e. the quantum and the classical aspects of Heisenberg ferromagnetic chains, will be made. In section 1 the soliton models and BM models are presented. In section 2 the relations between BMs and

solitons are discussed by comparisons of quantum and classical results from the Hamiltonian of the system. In section 3 the thermodynamics of the system is considered. Finally, in section 4, experiments on 1D spin 1/2 Heisenberg ferromagnet CHAB show that both BM and soliton contribution to the susceptibility gives a good interpretation of experimental data, and further provide a method for separating the BM contribution from the soliton contribution.

1. Soliton and Bound Magnon Models

In order to understand the relation between quantum BM and classical solitons, several soliton models and BM model are presented in following.

A. The Sine-Gordon (SG) Chain

The simplest soliton model is the SG chain model. It is the most popular model system for more complicated spin chains, and has applicability to real spin chains and Heisenberg spin chains with various types of anisotropy.

A special way[42] to show the SG chain system is by considering M+1 physical pendula in Earth's gravitational field and coupled to one another by a torsion spring. The Hamiltonian of this system is[42]:

$$H = T + V(1,\ldots,M+1) = \sum_i [\tfrac{1}{2} I\omega_i^2 - E_1 \cos\theta_i + \tfrac{1}{2} E_2 (\theta_{i+1} - \theta_i)^2], \qquad (5.1.1)$$

where θ_i is the displacement of the ith pendulum from equilibrium, E_1 = mgR, and E_2 measures the strength of the torsion spring that couples the i and i+1 pendula. The

possible motions of the pendula are motions of the phase, e.g., the relative phase of a near-neighbor pair, $\theta_{i+1}-\theta_i$, the phase change along a segment of the chain.

The magnetic analog of this system is to replace pendula by spins, the torsion spring by the exchange coupling, the gravitational field by the magnetic field, and defining θ as the angle between spin and field.

In general, the classical SG model defined on a 1D lattice is given by the Hamiltonian[31]

$$H = Aa\sum_i [\tfrac{1}{2}\dot{\phi}_i^2 + m^2(1-\cos\phi_i) + \frac{1}{2c^2}(\phi_{i+1}-\phi_i)^2], \tag{5.1.2}$$

where ϕ_i is the dimensionless field on the i-th lattice site, **c** is characteristic velocity and **m** is the mass parameter of the system which determines the strength of the nonlinear potential, and **A** sets the energy scale. **a** is a lattice constant required for dimensional reasons.

In the continuum limit ($1/m >> a$, $\phi_i \rightarrow \phi(x,t)$), the SG model is converted to[31]

$$H = Aa\int dx\left[\frac{1}{2}\left(\frac{\partial\phi}{\partial x}\right)^2 + \frac{1}{2c^2}\left(\frac{\partial\phi}{\partial t}\right)^2 + m^2(1-\cos\phi)\right]. \tag{5.1.3}$$

The corresponding equation of motion for ϕ is the SG equation

$$\frac{1}{c^2}\frac{\partial^2\phi}{\partial t^2} - \frac{\partial^2\phi}{\partial x^2} + m^2\sin\phi = 0\ , \tag{5.1.4}$$

where **t** is the time and **x** is the coordinate along the 1D lattice. From this equation of motion, the time evolution of the field variable $\phi(x,t)$ can be decomposed into the contributions from three different types of independent models:

(1) Small amplitude oscillations (called phonons or magnons in the various applications to solid state systems) which are plane-wave solutions.

(2) Solitons which are finite amplitude spin deviations traveling with permanent shape at arbitrary velocities.

(3) Solitons with an internal process, or an additional degree of freedom related to an internal vibration, called breather solitons.

Solitons are non-linear elementary excitations. A soliton reflects the absence of complete ordering by describing turns in the angle ϕ, and corresponds to a 1D moving domain wall which separates the spin-up or spin-down regions of a ferromagnetic spin chain. A visualization of a basic soliton is illustrated in Fig.1.

B. The Landau-Lifshitz Model

Another soliton-bearing model is the Landau-Lifshitz model. The equation of motion for the classical spin vector field $\vec{S}(x)$ is described by the Landau-Lifshitz equation[30]

$$-\hbar\frac{d\vec{S}}{dt}=\vec{S}\times\frac{\delta H}{\delta\vec{S}} \quad \text{or} \quad \frac{\partial\vec{S}}{\partial t}=\vec{S}\times\frac{\partial^2 S}{\partial z^2}\,, \tag{5.1.5}$$

The solutions to this equation are classified in terms of linear modes and envelope solitons. The envelope solitons are similar to the breather solitons of the sine-Gordon system, which are traveling waves of permanent localized profile with an inner degree of freedom, whose form remains unchanged after collisions.

C. Heisenberg Ferromagnetic Chains with Various Anisotropies

The Heisenberg ferromagnetic chains with various anisotropies are BM-bearing models, as discussied in Chapter 4. The Hamiltonian for these systems is:

$$H = -J\sum_{i}^{N}[S_i^z S_{i+1}^z + \gamma(S_i^x S_{i+1}^x + S_i^y S_{i+1}^y)] - D\sum_{i}^{N}(S_i^z)^2 - gu_B\sum_{i}^{N}B\cdot S_i\,, \qquad (5.1.6)$$

The external field B can be in the z direction or the xy-plane. The quantum spectrum of this Hamiltonian is consist of magnons and BMs as discussied in Chapter 4.

As shown in this section, it is important to realize that:

(1) solitons are classical and BMs are quantum features of Heisenberg spin chains;

(2) a soliton is a dynamic excitation, and is not related to a static configuration, (except the immobile soliton), whereas BMs are stationary excitations;

(3) both BMs and solitons are large(er) amplitude fluctuations, whereas magnons are small(er) amplitude fluctuations.

A simple picture of a magnon, a bound magnon, and a soliton is shown in Fig.1.

2. Relations Between Bound Magnons and Solitons

In view of the fact that both the soliton solutions of classical equations of motion and the BM of the quantum description are a consequence of nonlinearity, solitons are considered to be closely related to the quantum BMs. A further question is whether the quantum BM-bearing model can be reduce to classical soliton-bearing model in the continuum limit, or whether the soliton effects have a certain stability when one goes from the classical (continuum) to the quantum (discrete) model. This can be expected, at least

under certain approximations for which the discrete model is well approximated by the continuum one. This leads to the consideration of the classical soliton effect in the quantum spin chain. The correspondence between quantum BM-bearing and classical soliton-bearing models is discussed below.

A. Correspondence Between BM Models and Soliton Models

(1). Easy-axis symmetry:

The BM model given by Hamiltonian (5.1.6) with easy-axis symmetry is

$$H = -J\sum_{i}^{N}[S_i^z S_{i+1}^z + \gamma(S_i^x S_{i+1}^x + S_i^y S_{i+1}^y)] - D\sum_{i}^{N}(S_i^z)^2 - gu_B B\sum_{i}^{N}S_i^z, \qquad (5.2.1)$$

where $\gamma \leq 1$, $D \geq 0$, and a applied field B is in the easy-axis z direction.

The classical or continuum limit of the Hamiltonian is obtained by replacing the spin operators S_i by vectors with slowly varying orientations from site to site, which implies a long wave-length limit, so that

$$\vec{S}_{i+1} - \vec{S}_i = \frac{\partial \vec{S}(x)}{\partial x}a. \qquad (5.2.2)$$

As $a \to 0$, $\sum a \to \int dx$, which implies a weak anisotropy limit,

$$H = \int H(x)dx \ ,$$

where the Hamiltonian densities are given by[30]

$$H(x) = \frac{J}{2}\left(\frac{\partial \vec{S}}{\partial x}\right)^2 + (\gamma - 1)\left[\left(\frac{\partial S^x}{\partial x}\right)^2 + \left(\frac{\partial S^y}{\partial x}\right)^2\right] - J(1-\gamma)(S^z)^2 - D(S^z)^2 + BS^z. \qquad (5.2.3)$$

This is a special case of the Landau-Lifshitz model given by Eq.(5.1.5), which gives soliton solutions in the system.

The simplest case of above equation is $\gamma = 1$, the isotropic Heisenberg. The equation of motion in the continuum approximation is the Landau-Lifshitz equation:

$$\frac{\partial \vec{S}}{\partial t} = \vec{S} \times \frac{\partial^2 S}{\partial z^2}. \tag{5.2.4}$$

Thus, in the classical limit the BM-bearing Hamiltonian (5.2.1) leads to the soliton-bearing Landau-Lifshitz model. The continuum model should be a good approximation of the discrete model for long wave-lengths and small anisotropies. Therefore, systems described by the Hamiltonian (5.2.1) could have both quantum and classical properties for a certain range of parameters.

(2). Easy-plane symmetry:

The BM model given by Hamiltonian (5.2.1) with easy-plane symmetry is

$$H = -2J\sum_{i}^{n}[S_i^z S_{i+1}^z + \gamma(S_i^x S_{i+1}^x + S_i^y S_{i+1}^y)] - gu_B B\sum_{i}^{n} S_i^x \tag{5.2.5a}$$

or

$$H = -2J\sum_{i}^{N} S_i S_{i+1} - D\sum_{i}^{N}(S_i^z)^2 - gu_B B\sum_{i}^{N} S_i^x \ , \tag{5.2.5b}$$

where $\gamma > 1$, $D < 0$, and a applied field **B** is in the xy-plane.

In the classical limit, or in a certain region of field and temperature, this Hamiltonian can be mapped onto the classical SG Hamiltonian defined by Eq.(5.1.3), with the following identification of parameters[31]:

$$m = (g\mu_B B/2JS)^{1/2}/a; \quad (5.2.6a)$$

$$Aa = 2JS^2 ; \quad (5.2.6b)$$

$$c = aS[4J(1-1/\gamma)]^{1/2} \quad \text{for Eq.(5.2.5a);} \quad (5.2.6c)$$

or

$$c = aS[4JD]^{1/2} \quad \text{for Eq.(5.2.5b).} \quad (5.2.6d)$$

Thus, both easy-axis and easy-plane Heisenberg ferromagnets have not only quantum feature of magnons and bound magnons, but also classical feature of solitons, in a certain range of parameters.

B. Coincidence Between Bound Magnons and Solitons

The short review in section 5.2.A is enough to indicate that the 1D anisotropic Heisenberg chains represent suitable models to investigate the connection between the quantum excitation spectrum BMs and the soliton solutions of the associated classical continuum models. Since in the classical continuum limit the quantum Heisenberg easy-axis model belongs to the class of Landau-Lifshitz soliton models and the Heisenberg easy-plane model can be mapped to SG soliton model, the quantum and classical results of the Heisenberg chain models are now used to establish the relation between BM and solitons.

(1). BM in the *weak* anisotropic Heisenberg chain:

The fact that the classical continuum version of the easy-axis Heisenberg model leads to the Landau-Lifshitz equation supposes the long-wave approximation. Since the long-

wave approximation leads to the weak anisotropy condition $[(1/\gamma - 1)/2]^{1/2} << 1$[33] in the model, the quasiclassical energies of the soliton solutions of the Landau-Lifshitz equation now are compared with the BM energies in the weak anisotropy condition.

The energy of BM has been found in Chapter 2 to be

$$E_n = \gamma J \frac{\sinh\Phi}{\sinh(n\Phi)}[\cosh(n\Phi) - \cos K] , \tag{5.2.7}$$

where $\gamma = \cosh\Phi$. In the weak anisotropy condition $\eta = [(1/\gamma - 1)/2]^{1/2} << 1$,

$$E_n \approx 2\eta\gamma J[\cosh(2n\eta) - \cos K] / \sinh(2n\eta) . \tag{5.2.8}$$

The quasiclassical consideration of the system is described by the Landau-Lifshitz equation (LLE)

$$-\frac{\hbar}{2\mu}\hbar\frac{dM}{dt} = M \times \frac{\delta W}{\delta M} , \tag{5.2.9}$$

where μ is the Bohr magneton, M is the magnetic momentum density and W(M) is the energy function. The energy W(M) includes the exchange energy, the anisotropy energy and the magnetic-dipole interaction. The energy function takes the form[32,33]:

$$W(M) = \tfrac{1}{2}\int dx[\alpha(\partial M/\partial x)^2 - \beta M_z^2] , \tag{5.2.10}$$

where $\alpha = Ja^2/4\mu M_0$, $\beta = J\eta^2/\mu M_0$ in the weak anisotropy. M_0 is the saturation magnetic density. The constant α and β are chosen such that the frequency of the classical magnon be equal to the energy of the quantum magnon for K<<1.

The following expression of energy for the soliton solutions of the LLE Eq.(5.2.9) is obtained[34]

$$E_n(P) = \hbar\omega_0 N_1[\tanh(n/n_1) + \frac{2\sin^2(\pi P/P_0)}{\sinh(2n/n_1)}]. \qquad (5.2.11)$$

In the weak anisotropy condition $\hbar\omega_0 = 2J\eta^2$, $n_1 = 1/\eta$, $\pi P/P_0 = K$.[34] Inserting these values in Eq.(5.2.11), the energy becomes

$$E_n = 2\eta\gamma J[\cosh(2n\eta) - \cos K]/\sinh(2n\eta), \qquad (5.2.12)$$

which coincides with the quantum result Eq.(5.2.8) for BM at $\eta << 1$, with arbitrary **n** and **K**. Thus, at weak anisotropy the quasiclassical energies of the Laudan-Lifhitz solitons coincide with the BM energies.

(2). High-n BM (heavy BM) in (not necessarily weak) anisotropic Heisenberg chains:

It was shown[35] that the bound state of a large number of phonons in an anharmonic chain is the quantum analog of the classical self-localized vibrations of a nonlinear string. A similar situation should be obtained in a magnetic chain to which the quantum Heisenberg ferromagnet chain is applicable. It is known that the presence of self-localized oscillations from the classical nonlinear Landau-Lifshitz model implies that in a bounded region of space, i.e., a finite section of the chain, the magnetization along the easy axis differs from the nominal value, which is a immobile soliton or 1D domain wall. Therefore, it is natural to ask if self-localized solutions of a nonlinear Landau-Lifshitz equation correspond to the heavy BMs, or in other words, if an immobile soliton corresponds a heavy BM in Heisenberg chains.

Now, the quantum and classical results of the anisotropic Heisenberg chain are compared in the case of immobile solitons and high-n BMs.

The quantum excitation spectrum of BMs is given by Eq.(2.1.8) in Chapter 2. In the limit of $n >> 1$,

$$E_n \approx \gamma J \sinh\Phi = J (1 - \gamma^2)^{1/2} \qquad (5..2.13)$$

Thus, the energy of large-n BM is constant and independent of n and K. This property of the quantum solution is simply related to the existence of an immobile domain wall in the classical model.

The energy of a self-localized oscillation, or an immobile soliton, from the classical LLE Eqs.(5.2.9) and (5.2.10) is[36]

$$E = 4a^2 M_0^2 (\alpha\beta)^{1/2}, \qquad (5.2.14)$$

which is a constant, and coincides with the quantum heavy BM energy. Therefore, a heavy BM corresponds an immobile envelope soliton in the anisotropic Heisenberg chains in the classical limit.

(3). Low-n BM in anisotropic Heisenberg chains:

The correspondence between BMs and solitons is not completely understood in this case.

(4). BM in the Ising limit: (the strongest anisotropy $\gamma = 0$)

In the Ising limit a BM is a cluster of adjacent flipped spins, i.e., an immobile domain wall. Each cluster breaks two bonds and has an excitation energy of 2J, independent of the number of spins (n) in the cluster, which should be considered analogous to the energy of a classical domain wall. While a soliton corresponds to a moving domain wall, a BM is an immobile (stationary) soliton for all n in the Ising case.

(5) Quantum solitons:

The picture of the soliton discussed above is basically classical. The quantum soliton is considered as the analogue of the classical soliton in quantum spin chain. The understanding about the quantum soliton is based on the following.

The quantum SG chain[31] is defined by the quantum version of the Hamiltonian given by Eq.(5.1.3)

$$H = Aaf^2 \int_{-\infty}^{\infty} dx \left[\frac{1}{2}\left(\frac{\partial \Phi}{\partial x}\right)^2 + \frac{\pi^2}{2} + \frac{m^2}{f^2}[1-\cos(f\Phi)] \right] \tag{5.2.15}$$

with

$$[\Phi(x), \pi(x')] = i\delta(x-x') \tag{5.2.16}$$

Comparing with the classical SG model,

$$\phi = f\,\Phi, \quad f^2 = (2A/JS^2)^{1/2}, \tag{5.2.17}$$

are introduced,[31] where f^2 is the coupling constant. The solutions of this Hamiltonian are quantum solitons. The practical importance of this quantum SG chain derives from the fact that realistic quantum spin chain Hamiltonian with broken planar symmetry can be approximately mapped to this quantum SG model, i.e., the quantum BM model can be map to quantum soliton model.

The quantum soliton also can be established by applying semiclassical quantization procedures to the soliton solution of the classical model. It follows from the semiclassical quantization results[36] that quantum solitons are linear superpositions of BMs.

Furthermore, there are recent efforts to describe the transition from quantum to classical soliton by varying the spin magnitude S.[37]

In summary, the relations between BMs and solitons (both classical and quantum) can be established through the way of quantum → classical and classical → quantum. It is important to emphasize that the BM effects are a consequence of the magnon interaction, or in other words, of inherent nonlinearities, which also gives rise to the soliton solutions in the continuum limit. In the classical limit, the origin of the BM effects may be identified as soliton features.

Through the correspondence between BMs and solitons, BM models have shown a new way of analyzing the relevance of solitons by first considering the problem quantum mechanically and then taking the classical limit.

3. Thermodynamics of Solitons and Bound Magnons

As discussed above, the BMs are a quantum feature and the solitons are a classical feature of the 1D Heisenberg ferromagnets. Both properties of the system are closely related. When experimental results are considered, it is often difficult to distinguish between classical and quantum features of the systems.

The theoretical free energy of *quantum* spin chains was found[38] to consist of two independent types of contributions, a classical part and a quantum part. The quantum free energy is described by magnons and BM contributions, which have been discussed in

Chapter 2. The classical free energy is described[38] by the SG soliton contribution in the case of an easy-plane Heisenberg ferromagnet, which is discussed below.

Characteristic of soliton contribution to thermodynamic properties is the activated temperature dependence. The easiest way to locate the soliton contribution is to use this temperature dependence quite generally. For the model of the SG Chain, the different approaches to the thermodynamics have lead to agreement for the final expression of the free energy by Sasaki and Tsuzuki,[39] at low temperature:

$$F_{sol} = - kTn_s ; \tag{5.3.1}$$

$$n_s = (8/\pi)^{1/2} mat^{-1/2} e^{-1/t}(1 - 7/8t - 59/128t^2 - ...), \tag{5.3.2}$$

where n_s is the soliton density (the number of solitons per unit length), $t = kT/E_s^0$, and $E_s^0 = 8S(2Jg\mu_B BS)^{1/2}$ is soliton creation energy. This expansion is believed to be fairly accurate up to t = 0.3.

The presence of a soliton is equivalent to a local deviation from the long-range order established by the external field. The magnetization density therefore decreases proportional to the soliton density. Quantitatively this decrease is calculated either phenomenologically or by differentiating the free energy with respect to field B. The decrease of the magnetization ΔM_{sol} and susceptibility $\Delta\chi_{sol}$ calculated from the expansion of the soliton free energy F_{sol} are[40]

$$\Delta M_{sol} = - \frac{\partial F}{\partial B} = - 4Ng\mu_B S(8/\pi)^{1/2} t^{-1/2} e^{-1/t}(1 - 19/8t - 3/128t^2 - 59/256t^3 - ..), \tag{5.3.3}$$

$$\Delta x_{sol} = \frac{\partial M}{\partial B} = -2Ng\mu_B S(8/\pi)^{1/2}(t/B)[(-t^{-3/2}e^{-1/t}/2 + t^{-5/2}e^{-1/t})(1 - 19/8t - 3/128t^2 - 59/256t^3 - ..) + t^{-1/2}e^{-1/t}(-19/8 - 3/64t - 177/256t^3 - ..)]. \quad (5.3.4)$$

The temperature depandence of Δx_{sol} and its comparison with x_{BM} and x_{SW} are shown in Fig.28. It shows that the decrease of the susceptibility caused by soliton excitations is negligible for the region $t < 0.09$, whereas it has a maximum at $t \approx 0.29$. It also can be seen that the temperature and field range of soliton effects on the suceptibility x_{sol} is close to that of the BM effects on the susceptibility x_{BM}.

The importantance of thermodynamics of the SG model in its application to the properties of soliton-bearing 1D magnets is extremely valuable for an understanding of experimentally observable nonlinear excitations in real spin chain systems.

4. Experiment

A. Sample

The 1D spin 1/2 Heisenberg ferromagnetic compound $[C_6H_{11}NH_3]CuBr_3$(CHAB) has been studied very extensively. Since the ferromagnetic intrachain exchange interaction in CHAB contains about 5% easy-plane anisotropy, this spin 1/2 system based on a quantum spin Hamiltonian was revealed to be fairly well described in terms of the classical SG model. This was accomplished by the early analysis of the field-dependent part of the heat capacity and spin-relaxation experiments[40]. Therefore, CHAB is a very good realization of

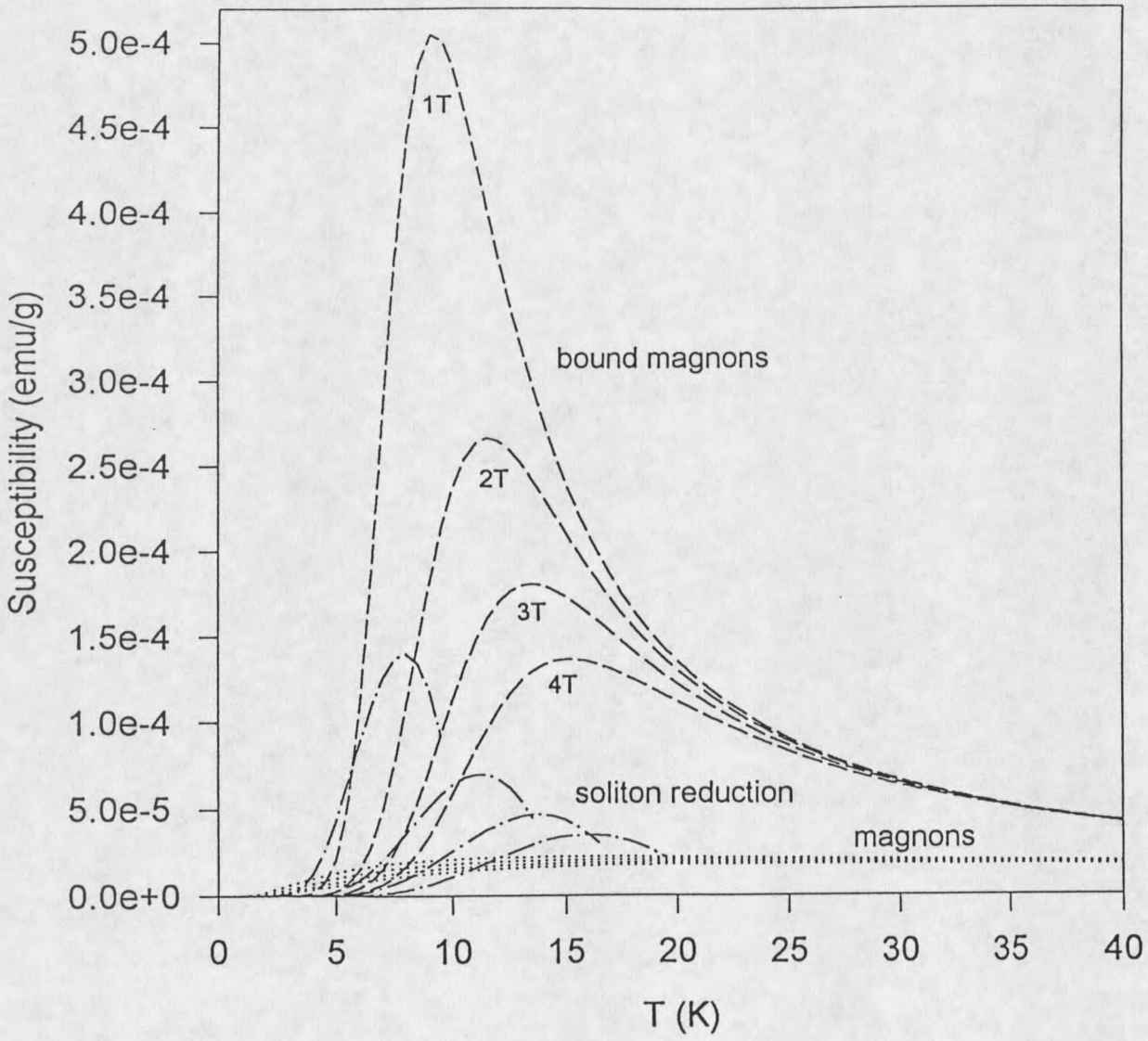


FIG. 28. Susceptibilities contributed from bound magnons, magnons and solitons.

theoretical model systems for the verification of the existence of both BM and soliton effects.

The crystallographic structure[20] of $[C_6H_{11}NH_3]CuBr_3$ (CHAB) is orthorhombic, space group $P2_12_12_1$, with a = 19.84A, b = 8.78A, and c = 6.44A. The compound is built up from bibridged linear chains of $CuBr_3^-$ ions running parallel to the *c* direction. The chains are effectively isolated in the *a* and *b* directions by the cyclohexylammonium complexes. The individual chains can be described by the Hamiltonian(5.2.5a) of 1D spin 1/2 easy-plane Heisenberg ferromagnet, with J/k = 50-70K and $1/\gamma \approx 0.95$. The exchange anisotropy results from the symmetry of the local environment of the Cu^{2+} ions. The interchain interactions are smaller than J/k by 3 orders of magnitude, give rise to a 3D long-range ordered state below $T_c = 1.50K$.

B. Experiment

The magnetic ac susceptibilities of the crystal sample of CHAB were measured from 4.2K to 35K in a ac field **h** = 10Oe, frequency f = 80Hz and dc magnetic fields **H** of 0, 1, 2, 3, 4, and 5 tesla. $\mathbf{B} = \mathbf{H} + \mathbf{h}\sin(2\pi ft)$ is in the xy-plane. The magnetizations M were measured as function of fields up to 5 tesla (H in the xy-plane) at several low temperatures between 4.2K and 10K. All measurements were performed on the LakeShore Model 7225 AC Susceptometer/DC magnetometer, which is described in Chapter 2.

C. Susceptibility

The temperature dependence of susceptibility of CHAB is shown in Fig.29. The rounded peaks at different temperature and field regions indicate that the linear magnon is certainly not the only excitation; nonlinear BMs seem to dominate the susceptibility. Using the Johnson and Bonner model which includes the susceptibtility contributed from BMs (mainly from heavy BMs, see Chapter 2) and magnons, data were fit. The best fitting resulted from parameters J/k = 65K, J'/k = -0.1K, $1/\gamma = 0.95$ and g = 2.04 is shown by dashed curves in Fig.29. As shown in Fig.29, however, JB model values are higher than experimental data in the regions of rounded peaks, and it indicates that in these ranges some other type of excitations must contribute to reduce susceptibility values. According to the discussion in Chapter 4, the spin canting effect is fairly small and not big enough to fit the susceptibility reduction in this system, although the compound CHAB was reported to exist certain spin canting.

Now we consider the soliton contribute to the susceptibility in addition to the quantum BM and magnon contributions. The expression Eq.(5.3.4) for the susceptibility reduction by solitons from the SG model is used. The result of the calculation with CHAB parameters ($\mathbf{S = 1/2, J/k = 65K, E_s^0/k = 10.95\sqrt{B}}$) are represented by the dashed-dotted curves in Fig.29. As can be seen in Fig.29, the decrease of susceptibility caused by solitons is negligible for $\mathbf{T/\sqrt{B}} < 1$ and in regions near $\mathbf{T/\sqrt{B}} \approx 3.2$ soliton effects are important. It is interesting to see that the temperature and field range of the soliton effect is close to that of the BM effect and the soliton effect lowers rounded peaks of BM effects. Together with BM and magnon contributions, total susceptibility is represented by solid curves in

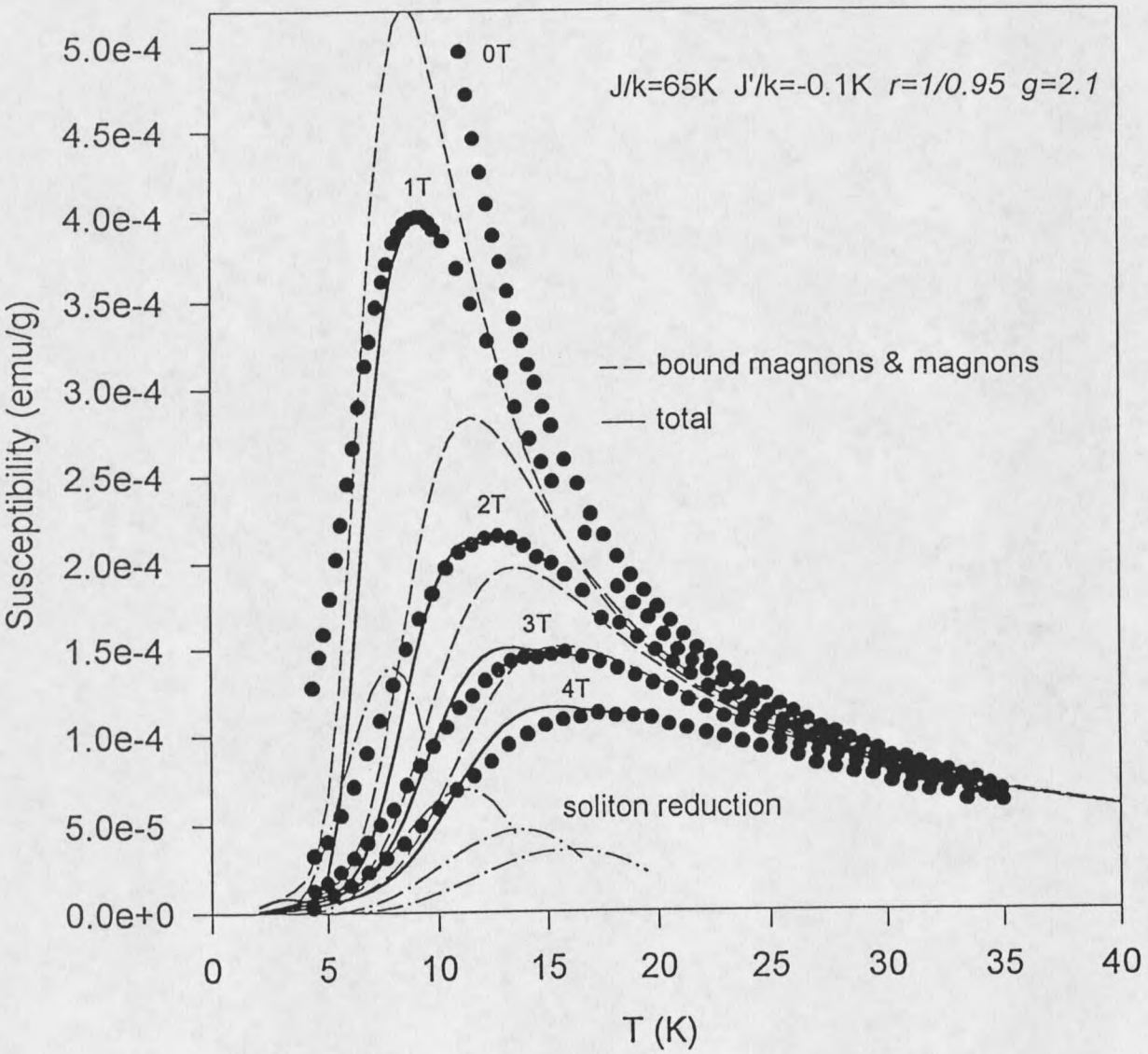


FIG. 29. Susceptibility of CHAB with soliton contribution.

Fig.29. We found that the experimental susceptibility of the system is a sum from the quantum contributions of BMs and magnons and the classical contribution of solitons. BMs dominate over magnons to raise the susceptibility and solitons reduce the susceptibility. The soliton reduction is about 25% of total susceptibility contributed from bound magnons and spin waves in the compound. It is obvious that this model yields a very good description of the data, especially since no adjustable parameters were used in the corresponding calculation of the soliton contribution.

A possible physical explanation of this good agreement between the theoretical model and the experimental data can be understood from the connection between BMs and solitons. Whereas BM contribution to the susceptibility is accounted mainly from heavy BMs (see chapter 2), in the classical limit the origin of these heavy BMs can be identified as immobile solitons. When immobile solitons excited, dynamic solitons should also be excited and contribute to the susceptibility. Thus, the nonlinear excitations of the system should include both stationary (immobile) and dynamic (mobile) excitations. The susceptibility thus is contributed from linear magnons, nonlinear stationary BMs, and dynamic solitons.

D. Magnetization

To comfirm above result, a comparison with the early reported result[40] of this compound is made. A set of magnetization curves[40] is shown in Fig.30. Triangles (Δ) represent reproduced data on the LakeShore Model 7225 DC magnetometer. Solid lines represent the result of the numerical quantum transfer matrix calculation[41], using the

parameters given in CHAB over the entire range of T and B for T > 2K. It is important to note that such a calculation includes all excitations (magnons, BMs, solitons, etc.) and the contribution of the linear and the nonlinear excitations cannot be separated. It can be seen that the experimental data are fit nearly perfectly by the numerical calculation.

In summary, while stationary quantum non-linear excitation BMs dominate the susceptibility over linear spin waves, dynamic classical non-linear excitation solitons are shown to appropriately decrease the susceptibility to give an excellent fit to data in 1D spin 1/2 Heisenberg easy-plane ferromagnets. The susceptibility can be decomposed into the separate contributions from magnons, BMs, and solitons. Comparing the numerical transfer matrix calculation, which included all excitations to fit data, now we successfully separate the effects of each of these excitations.

As shown, the model characterizing quantum spin chains by a quantum and a classical part, or a stationary and a dynamic part, provide much of our knowledge about quantum spin chains and form the starting point for an interpretation of experimental results in quantum spin chains.

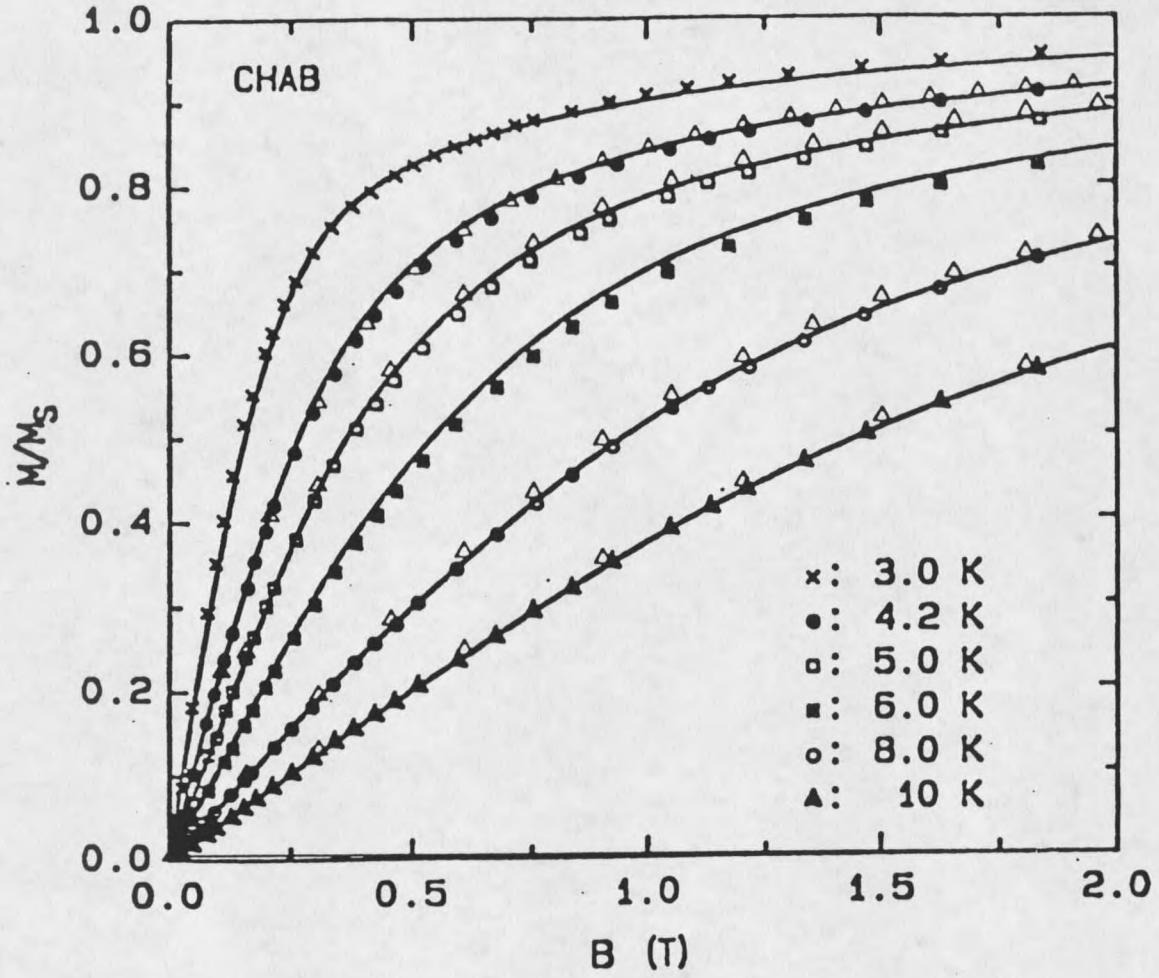


FIG. 30. Magnetization of CHAB at various temperatures.
Dots (except triangles ∇) represent earlier reported experimental data[21].
Solid curves denote the numerical transfer matrix results.[21]
Triangles ∇ represent reproduced data.

CHAPTER 6

CONCLUSIONS

Questions which were asked at the beginning of this thesis were open problems about BM. This thesis has attempted to answer these questions by studying each term of theoretical model Hamiltonian and testing them with experiments. In Chapter 2, thresholds of exchange coupling of intrachain and interchain for BM effects are theoretically predicted and experimentally confirmed to be $J_{threshold} < 10K$ and $(J'/J)_{threshold} > 10^{-1}$. In Chapter 4, the effects of spin canting on thermodynamic behaviors of the BM system is evaluated and our conclusion is that the thermodynamic function of the system are only affected by a factor change of anisotropy from γ to $1/\beta = J/(D^2+\gamma^2J^2)^{1/2}$ due to spin canting, i.e., spin canting effect is equivalent to changing exchange anisotropy of the system. Fitting the calculated model to the susceptibility data of CHAC shows that considering the spin canting effect in the system gives a better description of data.

As presented in Chapter 3, the degree and the type of anisotropies, arising from the anisotropic exchange and the single-ion anisotropy, play an important role on the susceptibility behavior of the BM systems. Experimental results on several good 1D spin 1/2 anisotropic Heisenberg ferromagnets from the Heisenberg to the Ising limit agree with theoretical expectations regarding the anisotropic exchange effect on BM dominance on susceptibility, and confirm that BMs exist and dominate susceptibility in the entire range of

exchange anisotropy γ and for fields up to 9 tesla. When considering single-ion anisotropy, the situation becomes complicated. Single-ion anisotropy gives rise to an new type of BM, called single-ion BM. Although the presence of single-ion BMs enhance the possibility of experimental observation of BM effects, single-ion BMs have not yet been clearly identified from the experimental data due to weak single-ion anisotropy in the compounds. Because of the complexities introduced by the single-ion anisotropy term in the Hamiltonian, completed single-ion BM spectrum and their effects upon low-temperature thermodynamic properties has not yet been solved, as far as the author knows. There is still a lot of interesting work to be done in this area by experimentalists as well as theorists. Experiments include ac susceptibility measurements and EPR measurement of the strength of the single-ion anisotropy on the 1D Heisenberg-Ising ferromagnetic compounds with the stronger single-ion anisotropy.

In Chapter 5, it is shown that while most of experiments in this thesis confirm that BMs dominate the susceptibility over linear spin waves, soliton excitations are found in the BM system and decrease the susceptibility of the system. The susceptibility is able to be decomposed into the separate contributions from bound magnons, magnons and solitons. (The soliton reduction is about 25% of total susceptibility contributed from bound magnons and spin waves, in the compound CHAB). The relations between BMs and solitons are summarized in the Ising limit and in the anisotropic Heisenberg case for the weak anisotropy and higher-n BM excitations, in order to better understand the description of experimental results.

In order to more completely understand BM excitations and their effects on thermodynamics, further experimental, theoretical and computational efforts would aim at the understanding the relations between BMs and solitons. For this, additional experimental work is particularly important, such as EPR line-width measurements on the 1D spin 1/2 ferromagnetic compounds in which BM existence is clearly identified. Also, possible investigations for the future are expected to clarify open questions such as the details of the physical picture of BM (structure of spin deviations).

From the present situation in the theoretical and experimental studies on 1D BMs, as discussed in this thesis, new directions for future studies of BMs may be seen. One such direction is the experimental and theoretical search for the BM effects in the 2D Heisenberg ferromagnets. Since increasing the dimensionality from 1 to 2 in the Heisenberg system is sufficient to prevent the onset of long range order at a non-zero temperature, the thermodynamics of the 2D Heisenberg model may therefore to a certain extent resemble the behavior found in the 1D chain model. The study of BM effects in 2D Heisenberg ferromagnets will remain attractive especially because of the theoretical prediction and experimental confirmation of that 2D solitons exist and dominate the thermodynamics in critical temperature range in a classical magnetic system[43].

REFERENCES

1. H. A. Bethe, Z. Phys. 71, 205 (1931).

2. M.Wortis, Phys.Rev. 132, 85 (1963).

3. J. Hanus, Phys. Rev. Lett. 11, 336 (1963).

4. R. Orbach, Phys. Rev. 112, 309 (1958).

5. R. P. Reklis and J. E. Drumheller, Phys. Rev. B9, 174 (1974).

6. I. G. Gochev, Sov. Phys. JETP. 34, 892 (1972).

7. G.I. Georgiev, Y.A. Kosevich, and V.M. Tsukernik,
Sov. Phys. JETP 48(6), 1095 (1978).

8. M.Gaudin, Phys. Rev. Lett. 26, 1301 (1971).

9. J. D. Johnson and J.C. Bonner, Phys. Rev. B22, 251(1980).

10. M. Takahashi and M. Yamada, J. Phys. Soc. Japan, 54, 2808 (1985).

11. P. Schlottmann, Phys. Rev.Lett. 56, 1618 (1986).

12. J.B. Torrance and M. Tinkham, Phys. Rev. 187, 595 (1969).

13. D. N. Haines and J. E. Drumheller, Phys. Rev. Lett. 58, 2702 (1987).

14. K. Ravindran, D. N. Haines, and J. E. Drumheller, J. Appl. Phys. 67, 5481 (1990).

15. D. N. Haines, K. Ravindran and J. E. Drumheller, J. Phys. Colloq. 49, C8-1483(1988).

16. D. N. Haines, K. Ravindran, and J. E. Drumheller, Phys. Rev. B45, 3122 (1992).

17. A. N. Goncharuk, V. N. Krivoruchko, and D. A. Yablonskii,
Sov. Phys. Solid State 27(8), 1464 (1985).

18. D. B. Losee, J. N. McElearny, A. Siegel, and R. L. Carlin,
Phys. Rev. B6, 4342 (1972).

19. D. D. Swank, C. P. Landee and R. D. willett, Phys. Rev. B20,2154 (1979).

20. C. P. Landee and R. D. Willett, Phys. Rev. Lett. 6, 463 (1979).

21. K. Kopinga, A. M. C. Tinus and W.J. de Jonge, Phys. Rev. B25, 4685 (1982);
and references therein.

22. T. Grigereit, Y. Liu, P. Zhou, J. E. Drumheller, and R. D. Willett,
J. Magn. Magn. Mater. 104-107, 831 (1992);

23. H. R. Jauslin and T.Schneider, Phys. Rev. B26, 5153 (1982).

24. R. Silberglitt and J. Torrance, Phys.Rev. B2, 772 (1970).

25. N. Papanicolaou and G.C. Psaltakis, Phys.Rev. B35, 342 (1987).

26. T. Moriya, Phys. Rev. 120 91 (1960).

27. D. Johnson and B. M. McCoy, Phys. Rev. A6, 1613 (1972).

28. V.N. Krivoruchko, Sov. J. Low.Temp. Phys. 12(8), 496 (1986).

29. O. Derzhko and A. Moina, preprint, ICMP-93-22E, L'viv, (1994).

30. T. Schneider, Phys.Rev. B24, 5327 (1981); and references therein.

31. H. J. Mikeska, Physica 120B, 235 (1983); and references therein.

32. B. A. Ivanov, Sov. J. Low Temp. Phys. 3, 505 (1977).

33. I. G. Gochev, Physics Lett., 89, 31 (1982).

34. A. M. Kesevich, B. A. Ivanov and A. S. Kovalev,

Sov. J. Low Temp. Phys., 3, 44 (1977).

35. M. M. Bogdan and A. M. Kosevich, Sov. Low Temp. Phys., 2, 794 (1976).

36. B. A. Ivanov and A.M. Kosevich, Sov. Phys. JETP 45(5), 1050 (1977).

37. H. J. Mikeska and S. Miyashita, preprint, University of Hannover, (1990).

38. L. F. Lemmens, K. Kopinga, and W. J. de Jonge, Phys. Rev. Lett. 63, 5 (1989).

39. K. Sasaki and T. Tsnguki, Solid State Commun., 41, 521 (1983).

40. K. Kopinga, A. M. Tinus, and W. J. de Jonge, Phys. Rev. B36, 5398 (1982).

41. K. Kopinga, T. Delica, and H. Leschke, Phys. Rev. B40, 7329 (1989).

42. R. A. Guyer and M. D. Miller, Phys. Rev. A17, 1205 (1976).

43. C. E. Zaspel, T. E. Grigereit, and J. E. Drumheller, Phys. Rev. Lett. 74, 4539 (1995).

MONTANA STATE UNIVERSITY LIBRARIES
3 1762 10246807 9